

**Assessing the compatibility of genotypes in the  
rice—*Magnaporthe oryzae* interaction by  
hyperspectral imaging**

**Dissertation**

zur Erlangung des Grades

Doktorin der Agrarwissenschaften (Dr. agr.)

der Landwirtschaftlichen Fakultät

der Rheinischen Friedrich-Wilhelms-Universität Bonn

von

**Angeline Wanjiku Maina**

aus

Trans-Nzoia, Kenia

Bonn 2024

**Referent: PD Dr. Erich-Christian Oerke**

**Korreferent: Professor Dr. Mathias Becker**

**Tag der mündlichen Prüfung: 13.06.2024**

**Angefertigt mit Genehmigung der Landwirtschaftlichen Fakultät der Universität Bonn**

## **Dedication**

I dedicate this dissertation to my beloved mother Pauline Wachera Maina, and to the cherished memory of my late father Albert Maina Njogu, with profound love and heartfelt appreciation.

## Acknowledgments

I would like to express my profound gratitude to PD. Dr. Erich-Christian Oerke for graciously agreeing to be my supervisor during my PhD studies. I count it a great privilege to have had the amazing guidance of such an incredibly, compassionate, and discerning mentor throughout my academic journey. His unwavering support and invaluable insights have been an anchor for me. I am particularly indebted to him for patiently addressing numerous queries that arose during my research.

In addition, I am also deeply grateful to Prof. Dr. Mathias Becker for agreeing to serve as my co-supervisor. Alongside PD. Dr. Erich-Christian Oerke, their mentorship and profound insights have played a pivotal role in my professional growth during my pursuit of this degree. I am also truly grateful to Jun. Prof. Dr. Janina Dierks for accepting my request to be a part of my committee, and to Prof. Dr. Claudia Knief, who chaired my doctoral committee.

Furthermore, my sincere gratitude goes out to PD. Dr. Ulrike Steiner for her invaluable contributions to my research, especially her expertise in microscopy and wise counsel. Similarly, Prof. Dr. Armin Djamei has been of immense help to my research, and I would like to thank him for generously granting me access to his laboratory.

Without mentioning my fellow graduate students—past and present—whose companionship and encouragement have been invaluable throughout this journey, I would be remiss. Similarly, the technical staff's consistent support with my experiments and the sense of community they created remains greatly appreciated. I am grateful for the knowledgeable advice I received in the laboratory from Kerstin Lange, Carolin Sichtermann, and Daniela Nowara. Dr. Mamoona Khan deserves a special mention for her assistance with confocal laser microscopy.

I would especially want to thank Josef Bauer, Jörg Nettekoven, Thomas Gerhardt and the rest of the hardworking team who keep the greenhouse running. A special thank you goes to Carolyn Mukiri Kambona for her invaluable assistance in data collection.

I am deeply appreciative of the support provided by the Deutscher Akademischer Austauschdienst (DAAD), for their financial and social support during my Ph.D. Undoubtedly, achieving my PhD ambition would have been a challenging endeavor without their financial assistance.

Finally, I extend my heartfelt thanks to my family for their unwavering prayers and encouragement. I reserve a special place in my heart for my late father, whose inspiration planted the seeds of my ambition, and my mother, whose immense sacrifices have paved the way for my academic achievements.

## **Publications included in this thesis**

### **Chapter 2 has been published:**

**Reprinted from Angeline W Maina** and Erich-Christian Oerke, 2023. Characterization of rice—*Magnaporthe oryzae* interactions by hyperspectral imaging. *Plant Disease*, 107(10), 3139-3147. <https://doi.org/10.1094/PDIS-10-22-2294-RE>

### **Chapter 3 has been published:**

**Angeline Wanjiku Maina**, Mathias Becker and Erich-Christian Oerke, 2024. Assessing interactions between nitrogen supply and leaf blast in rice by hyperspectral imaging. *Remote Sensing*, 16(6), 939. <https://doi.org/10.3390/rs16060939>

### **Chapter 4 has been published:**

**Angeline Wanjiku Maina** and Erich-Christian Oerke, 2024. Hyperspectral imaging for quantifying *Magnaporthe oryzae* sporulation on rice genotypes. *Plant Methods*, 20(1), 87. <https://doi.org/10.1186/s13007-024-01215-1>

## List of abbreviations

|        |  |
|--------|--|
| ANOVA  | Analysis of Variance   |
| AUDS   | Area Under Difference Spectrum                                     |
| BBCH   | Biologische Bundesanstalt, Bundessortenamt und Chemische Industrie |
| CNN    | Convolutional Neural Networks                                      |
| D.p.i. | Days Post Inoculation  |
| ETI    | Effector-Triggered Immunity  |
| FHB    | <i>Fusarium</i> Head Blight  |
| HSI    | Hyperspectral Imaging  |
| IH     | Invasive Hyphae  |
| IRRI   | International Rice Research Institute                              |
| KOH    | Potassium Hydroxide  |
| NIR    | Near-Infrared  |
| PAMPs  | Pathogen-Associated Molecular Patterns                             |
| PCA    | Principal Component Analysis                                       |
| PRRs   | Pattern Recognition Receptors                                      |
| QTLs   | Quantitative Trait Loci  |
| REIP   | Red Edge Inflection Point  |
| RGB    | Red Green Blue   |
| RH     | Relative Humidity  |
| ROIs   | Region Of Interests  |
| SAM    | Spectral Angle Mapper  |
| SDI    | Spectral Disease Indices   |
| SPAD   | Soil Plant Analysis Development                                    |
| SVIs   | Spectral Vegetation Indices  |
| SVM    | Support Vector Machine   |
| SWIR   | Short-Wave Infrared Range  |
| VIS    | Visible Range  |

## Table of contents

|   |             |
|---|-------------|
| <b>Dedication</b> .....   | <b>i</b>    |
| <b>Acknowledgments</b> .....  | <b>ii</b>   |
| <b>Publications included in this thesis</b> .....   | <b>iii</b>  |
| <b>List of abbreviations</b> .....  | <b>iv</b>   |
| <b>Table of contents</b> .....  | <b>v</b>    |
| <b>Abstract</b> .....   | <b>viii</b> |
| <b>Zusammenfassung</b> .....  | <b>ix</b>   |
| <b>1 Introduction</b> .....   | <b>1</b>    |
| 1.1 Rice cultivation .....  | 2           |
| 1.2 Rice blast.....   | 3           |
| 1.2.1 Taxonomy and host range of the rice blast fungus <i>Magnaporthe oryzae</i> .....                                | 5           |
| 1.2.2 Life cycle and pathogenesis of <i>M. oryzae</i> .....   | 5           |
| 1.2.3 Cellular and molecular processes during <i>M. oryzae</i> infection and colonization of the<br>leaf tissue ..... | 7           |
| 1.2.4 Phenotypic responses of rice to blast fungus <i>M. oryzae</i> .....   | 8           |
| 1.2.5 Mechanisms of rice resistance to blast fungus <i>M. oryzae</i> .....  | 9           |
| 1.2.6 Variability in the compatibility of rice— <i>M. oryzae</i> interaction.....                                     | 9           |
| 1.2.7 Influence of mineral N on susceptibility of rice to blast .....   | 10          |
| 1.3 The need for precise methods in phenotyping of plant disease .....  | 11          |
| 1.3.1 Advantages of sensor systems in sensing plant diseases .....  | 12          |
| 1.3.2 Sensor systems for disease sensing .....  | 12          |
| 1.3.3 Sensor platforms .....  | 13          |
| 1.3.4 Hyperspectral imaging and data structure .....  | 13          |
| 1.3.5 Workflow for disease sensing using hyperspectral imaging .....  | 14          |
| 1.3.6 Spectral reflectance properties of leaves .....   | 15          |
| 1.3.7 The influence of plant diseases on spectral reflectance properties of leaves.....                               | 16          |
| 1.4 Hyperspectral imaging for detecting plant diseases .....  | 17          |
| 1.4.1 Limitations of hyperspectral imaging in plant disease detection .....   | 18          |
| 1.4.2 Analysis of hyperspectral data .....  | 18          |
| 1.5 Objectives of the study.....  | 20          |
| <b>2 Characterization of rice—<i>Magnaporthe oryzae</i> interactions by hyperspectral imaging</b> <b>22</b>           |             |
| 2.1 Abstract .....  | 23          |
| 2.2 Introduction.....   | 23          |

|          |   |           |
|----------|---|-----------|
| 2.3      | Materials and Methods .....   | 25        |
| 2.3.1    | Plant material and fungal pathogen.....   | 25        |
| 2.3.2    | Plant cultivation, inoculum preparation and inoculation .....   | 26        |
| 2.3.3    | Visual assessment of disease severity.....  | 26        |
| 2.3.4    | HSI .....   | 27        |
| 2.3.5    | Preprocessing of hyperspectral images .....   | 27        |
| 2.3.6    | Analysis of hyperspectral images.....   | 27        |
| 2.3.7    | Statistical analysis .....  | 28        |
| 2.4      | Results .....   | 28        |
| 2.4.1    | Effects of genotypes on blast symptom development .....   | 28        |
| 2.4.2    | Effects of host and pathogen genotypes on disease severity.....   | 29        |
| 2.4.3    | Symptom types in the interactions of rice and <i>M. oryzae</i> genotypes .....                              | 30        |
| 2.4.4    | Spectral signatures of healthy and diseased rice tissue .....   | 31        |
| 2.4.5    | Spatio-temporal dynamics of spectral patterns during <i>M. oryzae</i> pathogenesis.....                     | 33        |
| 2.4.6    | Quantification of subareas of blast symptom types .....   | 34        |
| 2.5      | Discussion .....  | 35        |
| 2.6      | Literature Cited.....   | 40        |
| 2.7      | Supplementary Data.....   | 45        |
| <b>3</b> | <b>Assessing interactions between nitrogen supply and leaf blast in rice by hyperspectral imaging .....</b> | <b>50</b> |
| 3.1      | Abstract .....  | 51        |
| 3.2      | Introduction.....   | 51        |
| 3.3      | Materials and Methods .....   | 53        |
| 3.3.1    | Origin and cultivation of rice and blast isolates.....  | 53        |
| 3.3.2    | Measurements of leaf chlorophyll and N content .....  | 54        |
| 3.3.3    | Measurement of leaf reflectance of spectral information .....   | 55        |
| 3.3.4    | Pre-processing of hyperspectral images .....  | 55        |
| 3.3.5    | Analysis of hyperspectral data .....  | 56        |
| 3.3.6    | Assessment of blast symptoms in RGB images.....   | 57        |
| 3.3.7    | Statistical analysis .....  | 57        |
| 3.4      | Results .....   | 57        |
| 3.4.1    | Rice plant response to increased mineral N supply .....   | 57        |
| 3.4.2    | Effect of mineral N supply on the spectral signature of healthy leaves .....                                | 58        |
| 3.4.3    | Effects of mineral N supply on the expression of leaf blast symptoms .....                                  | 61        |
| 3.4.4    | Effects of mineral N supply on rice blast intensity.....  | 62        |

|          |  |            |
|----------|--|------------|
| 3.4.5    | Effect of mineral N supply on leaf blast symptom types of rice genotypes .....                             | 63         |
| 3.4.6    | Variability of spectral signatures of blast symptom types as affected by mineral N supply .....            | 64         |
| 3.5      | Discussion .....   | 67         |
| 3.6      | Conclusions.....   | 70         |
| 3.7      | References.....  | 70         |
| 3.8      | Supplementary Materials .....  | 76         |
| <b>4</b> | <b>Hyperspectral imaging for quantifying <i>Magnaporthe oryzae</i> sporulation on rice genotypes .....</b> | <b>80</b>  |
| 4.1      | Abstract .....   | 81         |
| 4.2      | Background.....  | 81         |
| 4.3      | Materials and Methods .....  | 84         |
| 4.3.1    | Plant material.....  | 84         |
| 4.3.2    | Pathogen and inoculation .....   | 84         |
| 4.3.3    | Measurement of conidia production .....  | 85         |
| 4.3.4    | Microscopy.....  | 85         |
| 4.3.5    | Hyperspectral measurements and image analysis.....   | 85         |
| 4.3.6    | Spectral quantification of <i>M. oryzae</i> sporulation .....  | 86         |
| 4.3.7    | Statistical analysis .....   | 86         |
| 4.4      | Results .....  | 88         |
| 4.4.1    | Effect of rice genotypes on the intensity of <i>M. oryzae</i> sporulation.....                             | 88         |
| 4.4.2    | Morphological characteristics of sporulating lesions, conidiophores, and conidia.....                      | 89         |
| 4.4.3    | Phenotypes of typical blast symptom types during conidia production .....                                  | 90         |
| 4.4.4    | Spectral assessment of blast symptom subareas .....  | 90         |
| 4.4.5    | Effects of <i>M. oryzae</i> sporulation on reflectance spectra of blast lesions .....                      | 93         |
| 4.5      | Discussion .....   | 97         |
| 4.6      | References .....   | 101        |
| 4.7      | Supplementary Material.....  | 105        |
| <b>5</b> | <b>General discussion and conclusions .....</b>  | <b>108</b> |
| <b>6</b> | <b>References .....</b>  | <b>118</b> |

## Abstract

The optical properties of plants are valuable indicators of their health and can be used to detect, monitor, and characterize both biotic and abiotic stresses. Spectral techniques like hyperspectral imaging (HSI), have gained attention in plant phenotyping due to their ability to capture distinct spectral signatures associated with disease symptoms and nutrient stress. Understanding the complex interactions between host plants, pathogen and plant nutritional status is pivotal for effective disease assessment and management. Here the feasibility of HSI in the visible/near-infrared range in assessing the compatibility of genotypes in the rice (*Oryza sativa*)—*Magnaporthe oryzae* pathosystem has been investigated. The potential of HSI as a tool for assessing the sporulation of *M. oryzae* isolates on resistant and susceptible rice genotypes was examined as well as the effect of varying rates of mineral nitrogen (N) supply on the complex host-pathogen interactions. Hyperspectral data were analyzed by using the spectral angle mapper (SAM) algorithm for supervised classification. Spectral signatures differed between healthy and diseased tissue of rice genotypes varying in susceptibility to *M. oryzae*. Gene-for-gene-specific interactions between rice and *M. oryzae* resulted in diverse blast symptom types, enabling the grading of host-pathogen interactions. Time-series imaging of symptoms revealed significant differences in the manifestation and progression of blast symptom subareas. Distinct spectral signatures of these symptom subareas enabled their differentiation and classification by SAM algorithm with higher accuracy than visual assessments. The influence of mineral N supply on chlorophyll content, blast severity, lesion size, and number of lesions depended on the genotypes of rice. Analysis of reflectance spectra of healthy leaves and disease symptoms spectra revealed significant effects of mineral N supply, particularly in the visible and red-edge range of spectra, and interactions with rice genotypes and blast symptom subareas. The red edge inflection point was linked to the rate of mineral N supply. Among rice genotypes infected with *M. oryzae*, blast symptoms significantly differed in conidia production. Spectral signatures associated with grey tissue – corresponding to the sporulating area of *M. oryzae* lesions - differed between rice genotypes and a significant, positive correlation was identified between the area under the difference spectrum, representing spectral changes due to sporulation and the number of conidia per lesion and per lesion area. This study demonstrates the efficiency of HSI in assessing the compatibility of rice genotypes to *M. oryzae* interactions, thereby promoting the phenotyping process, and supporting plant breeding for disease resistance.

## Zusammenfassung

Die optischen Eigenschaften von Pflanzen sind wichtige Indikatoren für deren Gesundheitszustand und können zur Detektion, Überwachung und Charakterisierung von biotisch und abiotisch bedingtem Stress verwendet werden. Spektrale Verfahren wie abbildende Hyperspektralsensoren (AHS) haben aufgrund ihrer Fähigkeit zur Erfassung verschiedener spektraler Signaturen von Pflanzenkrankheiten und Nährstoffeffekten bei der Phänotypisierung von Pflanzen Bedeutung erlangt. Für eine effektive Erfassung und Bekämpfung von Krankheiten ist das Verständnis der komplexen Wechselwirkungen zwischen Wirtspflanze, Pathogen und Ernährungszustand ganz entscheidend. In dieser Arbeit wurde die Anwendbarkeit eines AHS-Systems im sichtbaren und nahinfraroten Bereich für die Bewertung der Kompatibilität zwischen den Genotypen im Wirt-Pathogen-System Reis (*Oryza sativa*) und *Magnaporthe oryzae* untersucht. Das Potential des AHS zur Erfassung der Sporulation von *M. oryzae* auf resistenten und anfälligen Reisgenotypen wurde ebenso erfasst wie der Effekt von unterschiedlichen Mengen von mineralischem Stickstoff (N) auf die komplexen Wirt-Pathogen-Interaktionen. Die hyperspektralen Daten wurden mit dem Spectral Angle Mapper (SAM)-Algorithmus für eine überwachte Klassifikation ausgewertet. Die spektralen Signaturen von gesundem und befallenem Blattgewebe der Reisgenotypen mit unterschiedlicher Krankheitsanfälligkeit gegenüber dem Reisblattbrand waren verschieden. Gen-für-Gen-spezifische Interaktionen zwischen Reis und *M. oryzae* führten zu unterschiedlichen Symptomtypen, die eine Bewertung der Kompatibilität der Wirt-Pathogen-Interaktionen ermöglichten. Aufnahmen des zeitlichen Verlaufs der Symptomentwicklung zeigten Unterschiede im Auftreten und in der Entwicklung der Symptom-Teilregionen auf. Unterschiedliche spektrale Signaturen dieser Teilgebiete ermöglichten ihre Differenzierung und Klassifizierung mittels SAM mit einer höheren Genauigkeit als visuelle Bewertungen. Die Wirkung des mineralischen N auf Chlorophyllgehalt, Intensität des Reisblattbrandes, Größe und Anzahl von Läsionen wurde durch den Reisgenotyp modifiziert. Die Einflüsse der N-Versorgung auf die spektralen Eigenschaften von gesundem Reisgewebe und Krankheitssymptomen waren insbesondere im Bereich des sichtbaren Lichtes und des Anstiegs zum Nahinfrarot ausgeprägt und wurden durch die Interaktionen zwischen den Genotypen von Wirt und Pathogen modifiziert. Die Lage des Wendepunktes dieses Anstiegs kennzeichnete die N-Versorgung der Pflanzen. Die Konidienbildung von *M. oryzae* auf den Blattsymptomen wurde durch den Reisgenotyp beeinflusst. Die spektrale Signatur der grauen Symptombereiche - sie entsprechen der sporulierenden Fläche der Symptome - war bei den Reisgenotypen unterschiedlich und wurde durch die Konidienbildung verändert. Zwischen der Fläche der Differenzspektren und der Anzahl Konidien pro Läsion bzw. pro Läsionsfläche bestand eine positive Korrelation. Die Studie belegt das Potential von AHS zur Bewertung der Kompatibilität der Interaktionen zwischen Genotypen von Wirt und Pathogen, sodass diese Technologie in der Züchtung auf Krankheitsresistenz für Phänotypisierungen der Genotyp-spezifischen Reaktion genutzt werden kann.

## 1 Introduction

Enhancement of disease resistance in crops can significantly increase productivity by preventing substantial losses attributed to plant pathogens (Nelson et al., 2018; Deng et al., 2020). A disease is a harmful deviation from the normal physiological functions or structure of a plant caused by biotic factors including fungi, bacteria, viruses, nematodes, and abiotic factors (Agrios, 2005). It has been estimated that about 7 to 15 % of global crop production is lost because of the activity of a wide range of plant pathogens (Oerke and Dehne, 2004). Use of fungicides to combat fungal diseases has led to the development of fungicide-resistant strains, making it even more challenging to manage plant diseases (Younas et al., 2023). Furthermore, the constantly evolving and dynamic nature of host-pathogen interactions implies that virulent pathogens can emerge and overcome genetic resistance of previously resistant crop varieties particularly when such resistance is conferred by major genes (Mundt, 2014; Nelson et al., 2018; Deng et al., 2020).

Breeding for long-lasting and broad-spectrum disease resistance is a key strategy for sustainably managing plant diseases caused by fungal pathogens (Mundt, 2014; Tanner et al., 2022). The identification of the genetic basis for resistance and its linkage to the phenotype represents a pivotal step in breeding for disease resistance in plants (Li et al., 2014). Advancements in molecular methods such as marker-assisted selection, genome analysis, and deeper knowledge of genomes and associated genes have greatly enhanced genotyping techniques in breeding for disease resistance (Ashkani et al., 2015). However, the detection and identification of pathogen-resistant plant genotypes by molecular methods (genotyping) is only the first step which has to be validated under different environmental conditions to account for genotype  $\times$  environment interactions (Li et al., 2014). This phenotyping approach is time-consuming and expensive, limiting the breeding process. Additionally, the molecular or analytical methods are destructive limiting the possibility of conducting time-series assessments of plants' response to pathogen attack (Kuska et al., 2015; Bock et al., 2020).

During the host-pathogen interactions, various physiological and biochemical changes take place in plants (Tanner et al., 2022). The highly individualized interactions between the genotypes of the host plants and pathogens further complicate the phenotyping process (Mahlein et al., 2019). Characterization of the plant responses to pathogen attacks and their spatial pattern of occurrences is essential for understanding plant-pathogen interactions (Leucker et al., 2016). This knowledge is also valuable in breeding programs aimed at developing disease-resistant cultivars (Nelson et al., 2018). Therefore, there is a need for the development of more specific and objective phenotyping techniques to enhance breeding for quantitative disease resistance (Mahlein et al., 2019).

In this thesis the potential of hyperspectral imaging (HSI) in the visible (VIS) and near-infrared (NIR) ranges of the electromagnetic spectrum to characterize the compatibility of plant-pathogen interactions has been investigated. The work focused on investigating both resistant and susceptible interactions involving various genotypes of rice (*Oryza sativa* L.) and the pathogen *Magnaporthe oryzae*. In rice—*M. oryzae* interaction, leaf blast symptoms exhibit variations, ranging from tiny necrotic spots to enlarged lesions differing in tissue coloration. The study aimed to establish a link between spectral changes and different types of blast symptom and/or symptom subareas, to characterize various types of resistance/susceptibility reactions of tissue subjected to *M. oryzae* infection and to grade the host pathogen compatibility. The influence of mineral nitrogen (N) nutrition on blast susceptibility was also examined in the rice—*M. oryzae* interaction. Despite N being crucial for optimizing rice growth and yield, it influences the susceptibility of rice plants to *M. oryzae*. This study thus aimed to provide an understanding of the interaction between host, pathogen and mineral N application and investigate the effect of nutritional status of rice plants on their susceptibility to blast and the spectral signature of all components involved in the interaction.

Further studies involved the assessment of pathogen sporulation on both susceptible and resistant rice genotypes. Sporulation plays a critical role in initiating new infections, facilitating the dissemination of the disease, and serves as a key factor in the development of disease epidemics. Assessment of blast lesion phenotypes using HSI, in relation to sporulation, was done to identify plant genotype differences in disease resistance. Quantification of *M. oryzae* sporulation was achieved through the calculation of the area under the difference spectrum (AUDS) using HSI data metrics. This approach aimed at providing a deeper understanding of the complex dynamics underlying host-pathogen interactions and pathogen reproduction. HSI data were analyzed by using the spectral angle mapper (SAM) algorithm for supervised classification. The effectiveness of HSI in assessing the complex dynamics in the rice—*M. oryzae* interaction was demonstrated. This technology is beneficial for disease phenotyping in basic research and has potential for application in disease sensing under field conditions.

### 1.1 Rice cultivation

Rice, one of the most important cultivated cereal crops serves as a source of 23 % of calories and nutrition for over half of the global human population (Wilson and Talbot, 2009). More than 92 % of rice cultivation occurs in Asia, providing up to 50 % of the dietary caloric supply (Sharma et al., 2012). Rice cultivation mostly takes place in warm, humid sub-tropics/tropics, warm sub-humid tropics, and cool humid subtropics regions of the world (Ou, 1985). Fig. 1.1 illustrates worldwide rice production. The projected global rice production for the year 2023 was 518.14 million tons (milled

basis) (USDA, 2023). In the Asian region, rice production accounted for 471.5 million tons. Latin America and the Caribbean expected a 2.2 % reduction, while the United States anticipated a 20.2 % increase in production. Sub-Saharan Africa's overall harvest was forecasted to increase by 5.3 %, reaching a new peak of 25.8 million tons (FAO, 2023a).

There are two primary rice species, *Oryza sativa* - originally cultivated in Southeast Asia and now globally distributed, and *O. glaberrima*, exclusive to the African continent but gradually being replaced by *O. sativa*. *Oryza sativa* is further categorized into *O. sativa* ssp. *indica* which is adapted to the tropics and *O. sativa* ssp. *japonica*, adapted to the temperate regions and sub-tropical uplands (Sharma et al., 2012). The aus rice derived from the hybridization between indica and local wild populations is mainly distributed across South Asia (Zhou et al., 2022).

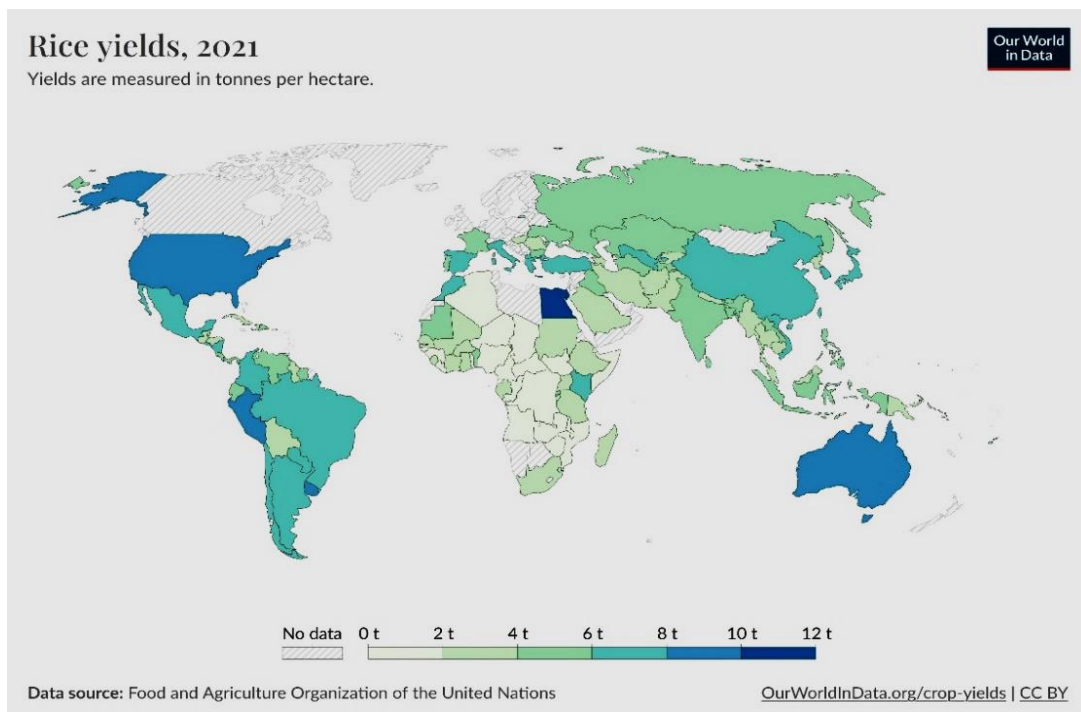


**Fig. 1.1:** Global rice production in tonnes per hectare (FAO, 2023b processed by Our World in Data).

## 1.2 Rice blast

Rice blast, one of the most important foliar diseases of rice (*O. sativa* L.), is caused by the haploid, filamentous ascomycetous fungus *Magnaporthe oryzae* B.C. Couch (anamorph *Pyricularia oryzae*) (Couch and Kohn, 2002; Talbot, 2003). Blast has the potential to cause damage to rice crops at every stage of their growth including seedlings, vegetative, and reproductive stages (Wilson and Talbot, 2009). Leaf blast occurrence and intensity can vary significantly based on geographic location, time, prevailing environmental conditions, management practices, and the presence of susceptible rice host tissue (Ou, 1985). Blast thrives in warm and humid climates, including rain-fed uplands, and

irrigated lowlands where conditions are favorable for the growth, multiplication, and spread of the pathogen (Khush and Jena, 2009). To date, rice blast is found in nearly 85 countries worldwide where rice is cultivated (Fig.1.2, Wang et al., 2014). Blast causes an annual yield loss of about 10 to 30 % of rice, culminating in estimated losses of a staggering \$66 billion worldwide (Nalley et al., 2016; Valent, 2021). This significant economic impact not only jeopardizes the livelihoods of farmers, but also poses a potential threat to the food supply of approximately 60 million people worldwide (Sharma et al., 2012; Valent, 2021).

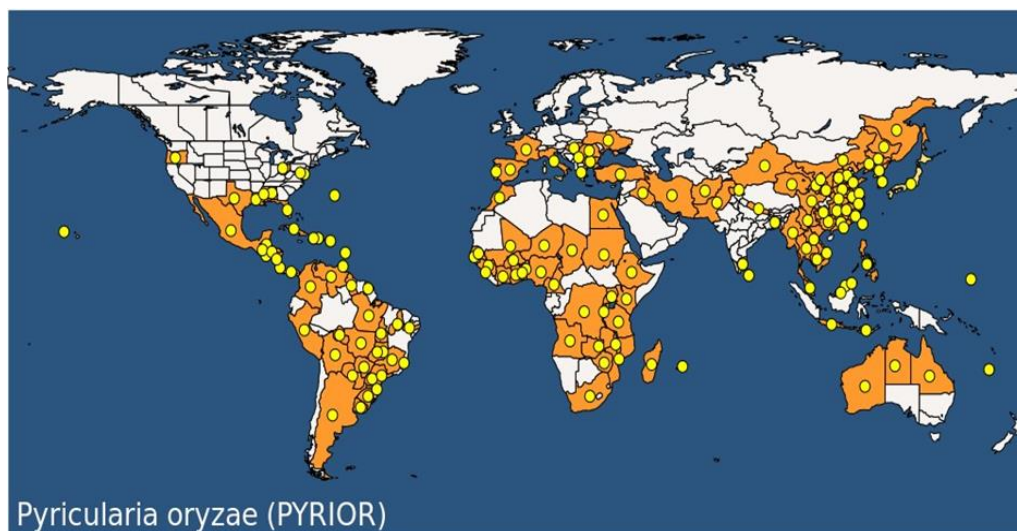


**Fig. 1.2:** Global distribution of *M. oryzae* (EPPO, 2023).

The impact of rice blast on global rice production is substantial, leading to significant losses reported in various regions. Notable instances include the 1993 rice blast epidemic in Southern China, which resulted in an estimated loss of 1.1 million tons of rice (Khush and Jena, 2009). In 2003, rice blast was responsible for yield losses of more than 2.6 million tons in India, which was about 0.8 % of the total yield (Rachel, 2022). Rice blast outbreaks in the southern states of the USA, such as Arkansas, Louisiana, and Texas, have led to yield losses ranging from 10 to 50 % (Nalley et al., 2016). In Sub-Saharan Africa, rice blast outbreaks in countries like Ghana, Gambia, Nigeria, Burkina Faso, Sierra Leone, and Kenya have caused yield losses ranging from >20 to 100 % affecting the livelihoods of rice farmers in the region (Nutsugah et al., 2005; Séré et al., 2011; Kihoro et al., 2013).

The rice blast pathosystem is of significant interest, not only due to its widespread impact on global rice agricultural productivity but also the study of *M. oryzae* as model organisms for plant pathogenic ascomycetes with its host plant rice has revealed important concepts associated with plant-fungal interaction (Ebbole, 2007; Jain et al., 2017). The whole genome sequence of *M. oryzae* provides more information into the genetic adaptations necessary for the pathogen to cause disease (Dean et al., 2005). The high adaptability of *M. oryzae* to its primary host plant species rice, as well as

the genetic diversity of the pathogen and the complex nature of blast disease, underscores the importance of employing advanced experimental approaches in investigating the compatible and incompatible interactions between rice and *M. oryzae*.

### 1.2.1 Taxonomy and host range of the rice blast fungus *Magnaporthe oryzae*

*Magnaporthe oryzae* B.C. Couch 2002 is the name of the teleomorph of a fungus belonging to the phylum Ascomycota, class Sordariomycetes, order Magnaporthales, family Magnaporthaceae. The name of the anamorph is *Pyricularia oryzae* Cavara 1892 (Couch and Kohn, 2002).

*Magnaporthe oryzae* is a heterothallic fungus possessing a single mating-type gene locus that produces two alleles, MAT1-1 and MAT1-2 (TeBeest et al., 2007; Saleh et al., 2012). While sexual reproduction is predominantly observed in the center of its origin, the ability of *M. oryzae* to reproduce sexually was lost during its spread to other regions of the world. Nevertheless, certain strains can reproduce sexually in vitro when two opposite mating types come into contact. In such cases, at least one of the strains must be a female-fertile strain capable of forming sexual structures, including perithecia, asci, and ascospores (Tharreau et al., 2009; Saleh et al., 2012). As perithecia have not yet been identified under field conditions, the role of ascospores in promoting genetic diversity and facilitating the dissemination of the pathogen continues to be elusive (Saleh et al., 2012). As a result, the sexual stage may not play a significant role in disease epidemics.

The pathogen *M. oryzae* has a relatively narrow host range, primarily limited to members of the grass family (*Poaceae*) (Ou, 1985; Couch et al., 2005). Although its primary and economically significant host is rice, *M. oryzae* can also infect other cultivated and wild grass species, including barley, wheat, pearl millet, and finger millet (Couch and Kohn, 2002; Couch et al., 2005). Phylogenetic studies have distinguished *M. oryzae* pathogenic to rice, millet and other grasses from *M. grisea* strains isolated from *Digitaria* (e.g. crabgrass and fingergrass) based on distinct genetic differences and the absence of the ability to interbreed between the two groups (Couch and Kohn, 2002).

### 1.2.2 Life cycle and pathogenesis of *M. oryzae*

The rice blast fungus exhibits a hemibiotrophic lifestyle, characterized by two distinct phases of development during its life cycle (Kankanala et al., 2007; Fernandez and Orth, 2018). Initially, the fungus grows actively in living plant tissue (biotrophic phase) but later transitions to a necrotrophic phase in which it induces plant cell death and relies on nutrients released from these dead cells to facilitate sporulation on necrotic disease lesions (Fernandez and Orth, 2018). The disease cycle is initiated by the hyaline asexual conidia (Fig. 1.3). The conidia measuring approximately 20 to 22 × 10

to 12  $\mu\text{m}$ , are characterized by having three cells with a single, identical nucleus per cell (Ou, 1985; TeBeest et al., 2007; Valent, 2021).

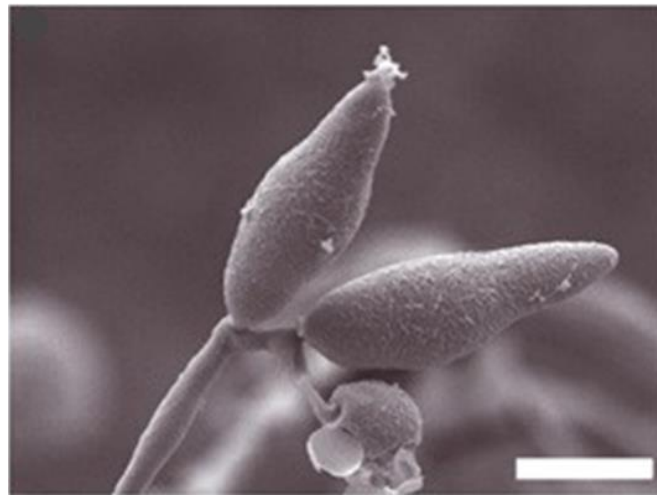


**Fig. 1.3:** Morphology of hyaline conidia of *M. oryzae* attached on a conidiophore as observed under a scanning electron microscope. Scale bar represents 10  $\mu\text{m}$  (modified from Wilson and Talbot, 2009).

*Magnaporthe oryzae* begins its infection cycle with the deposition of three-celled, pyriform-shaped conidia onto the hydrophobic surface of rice leaves, which subsequently adhere to the cuticle (Fig. 1.4a). A dome-shaped infection structure called appressorium forms at the tip of a germ tube emerging from a conidium. As the appressorium matures, a thick layer of melanin deposition forms on the inner side of the appressorium cell wall which provides an impermeable barrier to prevent the efflux of comparable solutes. The three-celled conidium collapses and dies in a programmed process that requires autophagy and the contents of conidium are recycled into the appressorium (Fernandez and Orth, 2018). The appressorium builds up enormous internal turgor pressure (up to 8 MPa) through the accumulation of large concentrations of glycerol (Fernandez and Orth, 2018). The pressure is transformed into a mechanical force exerted at the base of the appressorium, resulting in the formation of a penetration peg that ruptures the plant's cuticle and gains entry to the host tissue (Martin-Urdiroz et al., 2016).

Once inside the host, the pathogen forms primary invasive hyphae (IH), which develop into bulbous intracellular IH that spread through the plant tissue via plasmodesmata (Fig. 1.4a, 1.4b). IH invaginate the plant membrane forming the plant-derived extra-invasive hyphal membrane compartment, a characteristic of biotrophy (Jones et al., 2021). Upon penetration, a plant membrane-rich structure known as the biotrophic interface complex appears adjacent to the tips of the primary IH, but later localizes subapically to bulbous IH as disease develops (Kankanala et al., 2007). As fungal infection progresses within rice cells, the initially infected cells lose their viability, characterized by

host vacuole shrinkage and subsequent rupture (Jones et al., 2021). The IH aggressively continues to move from cell to cell for a few days until the fungus switches to the necrotrophy lifestyle, causing the death of the cell. The formation of disease lesions on leaves occurs 3 to 4 days after infection (Talbot, 2003; Wilson and Talbot, 2009).

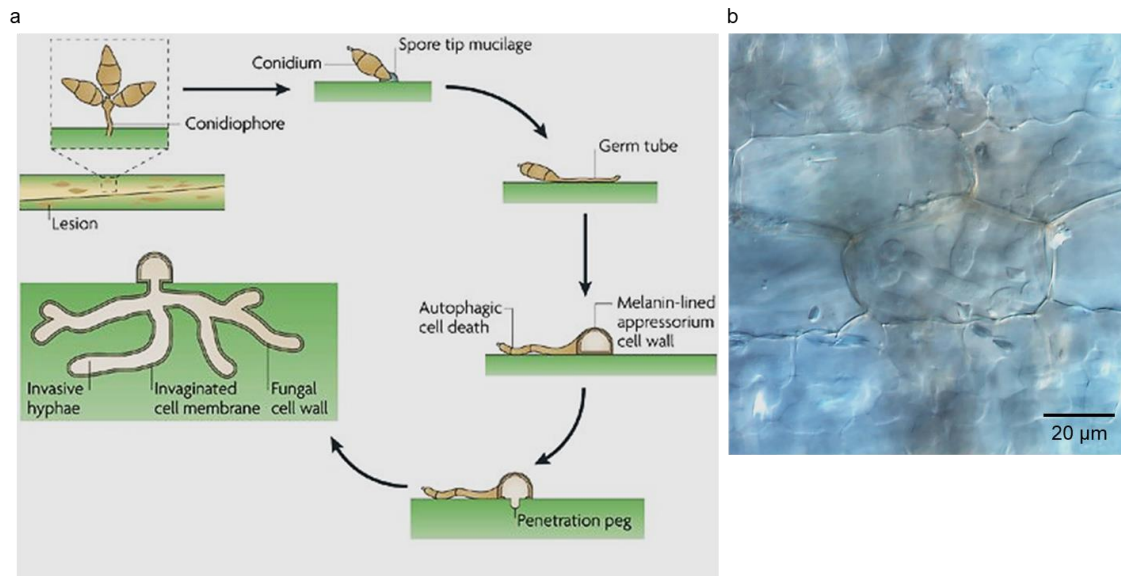


**Fig. 1.4:** (a) The disease infection cycle of *M. oryzae* (adapted from Wilson and Talbot, 2009); (b) growth of bulbous invasive hyphae *M. oryzae* within leaf tissue as observed in bright field microscopy (KOH-aniline blue staining; own image).

Under humid conditions, high RH > 90 %, and moderate temperatures of about 24°C (Wang et al., 2014), the fungus produces large numbers of conidia from aerial conidiophores that protrude from disease lesions (Ebbole, 2007; Wilson and Talbot, 2009). The sporulation capacity of an individual lesion depends on the relative area of the grey center where sporulation occurs (Valent, 2021). Blast infections exhibit a polycyclic nature, characterized by recurrent cycles of spore proliferation, spread, and infection during a growing season (Couch et al., 2005).

### 1.2.3 Cellular and molecular processes during *M. oryzae* infection and colonization of the leaf tissue

*Magnaporthe oryzae* has evolved more elaborate mechanisms for initial attachment, entry, and subsequent infection of their hosts. Processes such as perception of environmental cues (Fernandez and Orth, 2018), activation of signaling transduction pathways (Wilson and Talbot, 2009; Ryder and Talbot, 2015), generation of turgor pressure and control of cell cycle checkpoints (Fernandez and Orth, 2018) which regulate development of the appressorium during infection have been studied extensively. The pathogen also secretes enzymes e.g., cutinases that interact with hydrophobins to

provide a means for very tight adhesion of the conidia to the cuticle (Skamnioti and Gurr, 2007). To successfully establish infections, *M. oryzae* must overcome the plant's immune response. The initial layer involves the recognition of pathogen-associated molecular patterns (PAMPs) by plant cell surface pattern recognition receptors (PRRs), followed by intracellular host resistance genes (*R*) that identify pathogen effectors (*AVR*), triggering effector-triggered immunity (ETI) (Wang et al., 2014). To achieve this, the fungus secretes fungal effectors into the host cell that manipulate and suppress the host plant immunity, facilitating rapid colonization of plant tissues (Kankanala et al., 2007). Additionally, *M. oryzae* can modulate hormonal activity to create a more favorable environment for their growth and survival (Ryder and Talbot, 2015).

#### 1.2.4 Phenotypic responses of rice to blast fungus *M. oryzae*

Various rice genotypes show different types of reaction patterns (infection types) in response to infection by *M. oryzae* (IRRI, 2013). The infection types can range from low to high, depending on the compatibility of host and pathogen (Fig. 1.5). The typical progression of leaf blast symptoms begins with small brown necrotic lesions, which evolve into short, round or elliptic shaped lesions (intermediate reactions) to larger elliptical, spindle-shaped, or diamond-shaped lesions (susceptible reactions) characterized by whitish to grey centers, and brown borders that are surrounded by a yellow or chlorotic halo (TeBeest et al., 2007). Older lesions commonly exhibit a pale tan color with necrotic edges (Wang et al., 2014). As lesions enlarge, they coalesce causing extensive damage to leaf tissue and in severe cases, result in the complete death of the entire plant (TeBeest et al., 2007). Resistant cultivars typically exhibit small, brown spots, indicating a hypersensitive response (TeBeest et al., 2007; IRRI, 2013).

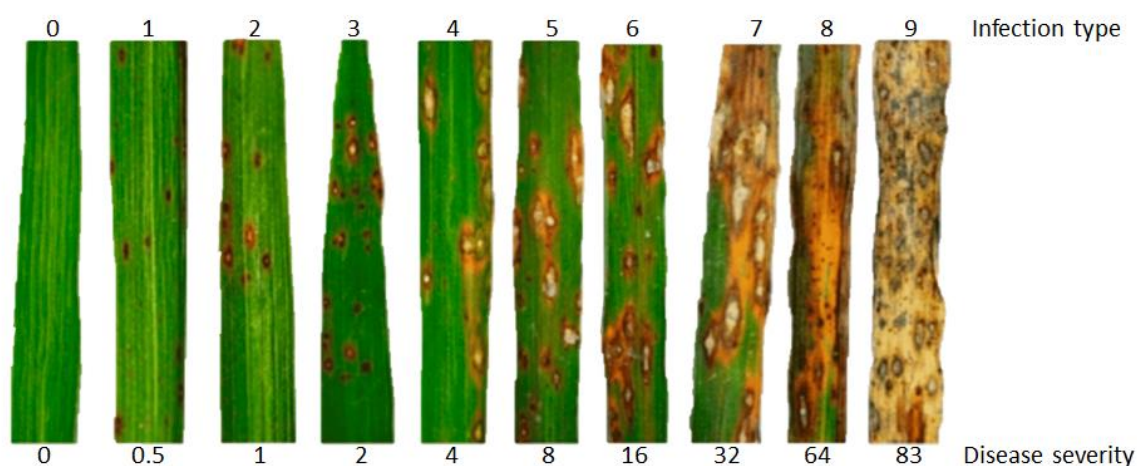


**Fig. 1.5:** Infection types and disease severity on rice leaves differing in susceptibility to blast (adapted from Jalalifar et al., 2023).

### 1.2.5 Mechanisms of rice resistance to blast fungus *M. oryzae*

Rice blast resistance can be classified into complete or partial resistance (Wang et al., 2014). Complete resistance of rice to blast is typically qualitative, with a cultivar classified as either resistant or susceptible based on lesion types. These lesion types or infection types result from specific genetic interactions between host plants and pathogens (Ou, 1980; Talukder et al., 2004). This type of resistance is race specific as a single major resistance (*R*) gene in the host interacts specifically with a corresponding dominant avirulence (*AVR*) gene in the pathogen (Younas et al., 2023). *Magnaporthe oryzae* avirulence (*Avr*) genes and their corresponding *R* genes such as *AvrPita /Pita* (Orbach et al., 2000), *Avr-Pia /Pia*, *AVR-Pii /Pii* (Yoshida et al., 2009), *AvrPi54/Pi54* (Sharma et al., 2012) and *AVR-Pi9/Pi9* (Wu et al., 2015) have been documented. However, complete resistance is not stable as it is rapidly overcome by the pathogen (Mundt, 2014).

Quantitative (partial) resistance of rice to *M. oryzae* is race non-specific and controlled by minor *R*-genes or polygenes referred to as quantitative trait loci (QTLs) (Talukder et al., 2004; Wang et al., 2014). Each of these genes make a relatively small contribution to overall resistance (Wang et al., 2014) resulting in decreased selection pressure against the pathogen (Fukuoka et al., 2014). QTLs are effective against a wide spectrum of pathogen races and the robust nature of partial resistance makes it challenging to break (Wang et al., 2014). Over 350 QTLs resistant to blast have been mapped including but not limited to *Pi35*, *Pi21* and *qBR4-2* (Fukuoka et al., 2012, 2014).

### 1.2.6 Variability in the compatibility of rice—*M. oryzae* interaction

The interaction between rice cultivars and blast fungal pathogens is complex and characterized by a significant dimension of variability. This variability can be observed in several aspects including the genetic diversity of both rice cultivars and *M. oryzae* isolates, and the influence of environmental conditions on their ability to adapt and respond to each other's presence (Ou, 1980; Gallet et al., 2014). Understanding the patterns of infection depends on variations in the rice resistance to *M. oryzae*, the growth capacity of the fungal pathogen in the host tissue, and its infectivity (Gallet et al., 2014).

Rice cultivars display a wide range of quantitative (partial) reactions to different strains of *M. oryzae* (Ou, 1980; Roumen, 1992; Gallet et al., 2014). It is common to observe a mixture of different types of leaf blast symptoms ranging from resistant, moderately resistant or susceptible, and susceptible blast lesion types. These different types of lesions appear in close proximity to each other along with significant variation in the proportion of affected tissue, the number and size of lesions within a leaf and among leaves of different rice cultivars. The interaction between multiple resistance genes in the host and many virulence genes in the pathogen often results in a continuous spectrum of

symptom expression (Hubballi et al., 2022). According to Ou (1980), the diversity in lesion types observed on the same leaf can be attributed to genetic variations among spores derived from a single conidial culture and that a one-grade difference in the host reaction to the pathogen often occurs.

Beyond rice × *M. oryzae* interactions, differential interactions have been reported in barley—*Puccinia hordei* pathosystem suggesting minor-gene-for-minor-gene specific interactions between the host and pathogen (Marcel et al., 2008). In the interaction between *Arabidopsis thaliana* and the bacterial pathogen *Pseudomonas syringae* pv. *maculicola*, the control of partial resistance appeared to involve multiple genes, as no clear separation into distinct classes of more resistant and more susceptible individuals was observed (Rant et al., 2013). Ashourloo et al. (2014) observed that different types of leaf rust symptoms including yellow, orange, dark brown, and dry leaf of variable sizes, simultaneously occurred in various parts of a wheat leaf. These studies suggest that instead of a single gene conferring resistance or susceptibility, multiple genes in both the host plant and the pathogen interact in a coordinated manner, collectively influencing the plants response to pathogen attack.

Environmental conditions such as temperature, prolonged periods of leaf wetness, and high relative humidity (Greer and Webster, 2001) as well as mineral N fertilizer (Huang et al., 2017) can further diversify resistance expression and significantly influence the outcome of the rice—*M. oryzae* interactions (Wang et al., 2014).

### 1.2.7 Influence of mineral N on susceptibility of rice to blast

The nutritional status of a plant plays a role in its predisposition to invading pathogens (Walters and Bingham, 2007). Mineral nutrients e.g., nitrogen (N), phosphorus (P), potassium (K), sulfur (S), magnesium (Mg), manganese (Mn), and silicon (Si), influence disease severity (Sun et al., 2020). However, the relationship between mineral N supply and plant pathogen infection is complex (Maywald et al., 2023). Nitrogen is an essential element in numerous metabolic pathways, contributing to the synthesis of enzymes, coenzymes, amino acids, proteins, as well as in plant photosynthesis (Sun et al., 2020). As a major yield-limiting nutrient, mineral N not only promotes the growth and development of rice plants but also influences plant susceptibility or resistance to pathogens (Huang et al., 2017).

The relationship between mineral N and plant diseases depends on the lifestyle of the pathogens (Sun et al., 2020). High mineral N fertilizer application has been documented to increase plant susceptibility to infection by biotrophic pathogens and decrease that of necrotrophic pathogens (Hoffland et al., 2000; Krupinsky et al., 2007; Dordas, 2008). However, the impact of N supply on the susceptibility of plants to necrotrophic fungus such as *Botrytis cinerea* has been shown to rely on the

virulence of the specific strain (Lecompte et al., 2010). This suggests that disease susceptibility is influenced by mineral N supply, and the effect of N on susceptibility of plants varies depending on the pathogen. Other nutritional elements differ to mineral N and may be used to compensate for the promotional effect of N to diseases (Dordas, 2008).

The effect of N on blast can be opposite depending on the compatibility of rice—*M. oryzae* interaction (Maywald et al., 2023). An excessive or high mineral N level can result in abundant vegetative growth, making rice plants more attractive to fungal proliferation thus increasing their susceptibility to blast (Long et al., 2000; Talukder et al., 2005). The increased susceptibility of rice plants to blast has also been attributed to an increased nutrient supply to the fungus due to the elevated concentrations of specific amino acids, such as glutamine and alanine in plants subjected to high mineral N supply (Huang et al., 2017). Many modern high-yielding plant cultivars tend to be more susceptible to blast when exposed to high N fertilizer inputs (Talukder et al., 2005; Deng et al., 2020). *Magnaporthe oryzae* infection of rice tissue may also decrease or remain unaffected with increasing mineral N levels (Maywald et al., 2023). On the other hand, a high mineral N supply can stimulate the expression of plant defense genes during infection. However, the ability of rice plants to counteract increased fungal pathogenicity at high N levels is limited, resulting in increased blast susceptibility (Huang et al., 2017). N-starved conditions have also been reported to increase rice susceptibility to blast (Talbot et al., 1993).

Maintaining a balanced mineral N nutrition and implementing precise, well-informed nutrient management practices are crucial for effectively managing and controlling rice blast. This includes choosing the right dosage, proper timing for mineral N application, and selecting appropriate N sources (Long et al., 2000; Maywald et al., 2023). Additionally, the development of blast-resistant rice varieties that perform well under varying mineral N conditions can mitigate the disease impact and ensure sustainable rice production.

### **1.3 The need for precise methods in phenotyping of plant disease**

Phenotyping disease resistance and the development of effective cultivars within breeding programs demand the application of precise, objective, and automated optical methods. These methods are critical for disease symptom detection in the initial stages of pathogenicity, tracking disease progress, and characterization of the resistance reactions of crops to pathogens (Tanner et al., 2022). Moreover, understanding the complex host-pathogen interactions is essential, alongside continuous monitoring of crop nutritional status. These combined efforts are instrumental in developing and implementing successful disease management strategies and disease resistance breeding systems thereby reducing the risk of crop diseases.

### 1.3.1 Advantages of sensor systems in sensing plant diseases

The use of objective, non-invasive optical sensor systems in automated processes offers an alternative to the subjective, labor-intensive, and costly visual assessment of plant diseases (Lowe et al., 2017; Zhang et al., 2020). These sensor systems have the ability to non-destructively capture the spatially distributed spectral information about plant diseases, making them valuable for time-series experiments (Mishra et al., 2017; Bock et al., 2020). In the field, farmers need sensors to make informed decisions for disease control by employing site-specific application of plant protection measures e.g., fungicides to patches of crop diseases (West et al., 2010). In breeding for disease resistance, sensors are utilized to phenotype the reactions of plant genotypes to pathogen attacks (Kuska et al., 2015). Additionally, sensors play a crucial role in assessing the health and quality of food (Pu et al., 2019), as well as fruits and vegetables (Li et al., 2018).

### 1.3.2 Sensor systems for disease sensing

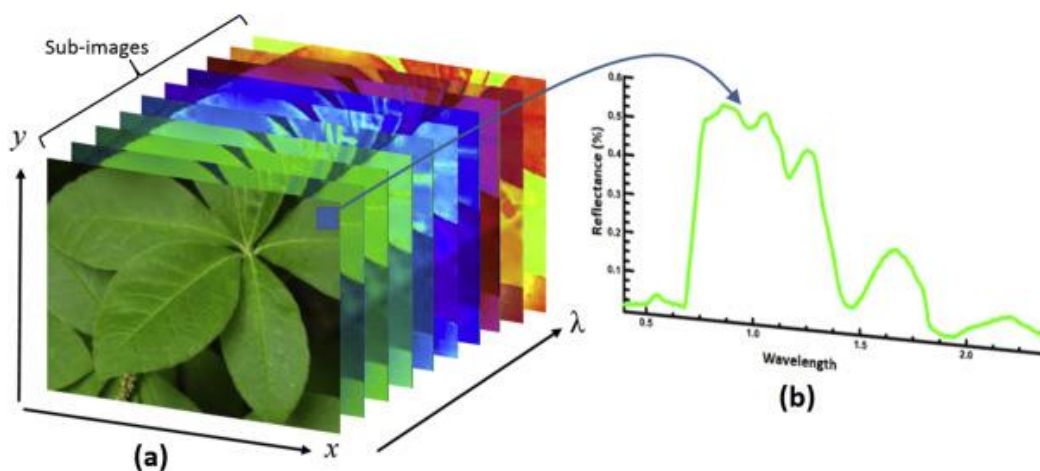
Optical sensors can be classified according to their spectral resolution (the number and widths of measurement bands), spectral scale (ultraviolet, visible, near-infrared, shortwave infrared), or measuring principle (imaging or non-imaging) (Thomas et al., 2018; Oerke, 2020). Non-imaging sensors (e.g. spectroradiometers) average spectral information over a given field of view without storing spatial information (West et al., 2010). On the other hand, imaging sensors vary in spatial resolutions and include RGB imaging (red, green, and blue bands), multi- and hyperspectral imaging, infrared thermography, and chlorophyll fluorescence imaging (Mahlein, 2016). Multispectral sensors measure spectral data in a few bands in RGB and additional wavebands in the near-infrared (NIR) (< 20 spectral bands). These sensors are often lightweight and cost-effective. Hyperspectral sensors record narrow spectral bands across a continuous spectral range, with spectral resolutions < 1 nm (Oerke, 2020). HSI contains more detailed spatial and spectral information than RGB and multi spectral sensors, as each pixel is a vector with the dimensionality of the number of wavebands recorded (Mishra et al., 2017). HSI systems provide high sensitivity and suitability for disease sensing, however, are heavier, more expensive and the measurement process takes more time (Thomas et al., 2018). The large amount of data generated by HSI poses a challenge in terms of storage, processing, and analysis due to its higher dimensionality requiring sophisticated computational techniques and algorithms (Pu et al., 2019). Additionally, in practical agricultural settings in the field, farmers often require simpler and more robust sensors, which is not the case for HSI, limiting their applicability to basic research.

### 1.3.3 Sensor platforms

Optical sensor technologies offer a means to phenotype plant diseases on a scale both in space and time, that was previously unattainable (Oerke, 2020; Gold, 2021). They bridge the gap between labor-intensive field measurements and genomic characterization (Li et al., 2014; Kuska et al., 2015), enabling more effective disease detection and informed decision-making regarding pathogen control (Li et al., 2014). Sensor systems in laboratory settings provide detailed observations of pure pixels of pathogens, tissues, or organs (Zhang et al., 2020). At the leaf level, imaging sensors, allows for a detailed examination of physiological and biochemical changes occurring in response to biotic and abiotic stresses and an understanding of the biological processes influencing disease expression (Gold, 2021).

### 1.3.4 Hyperspectral imaging and data structure

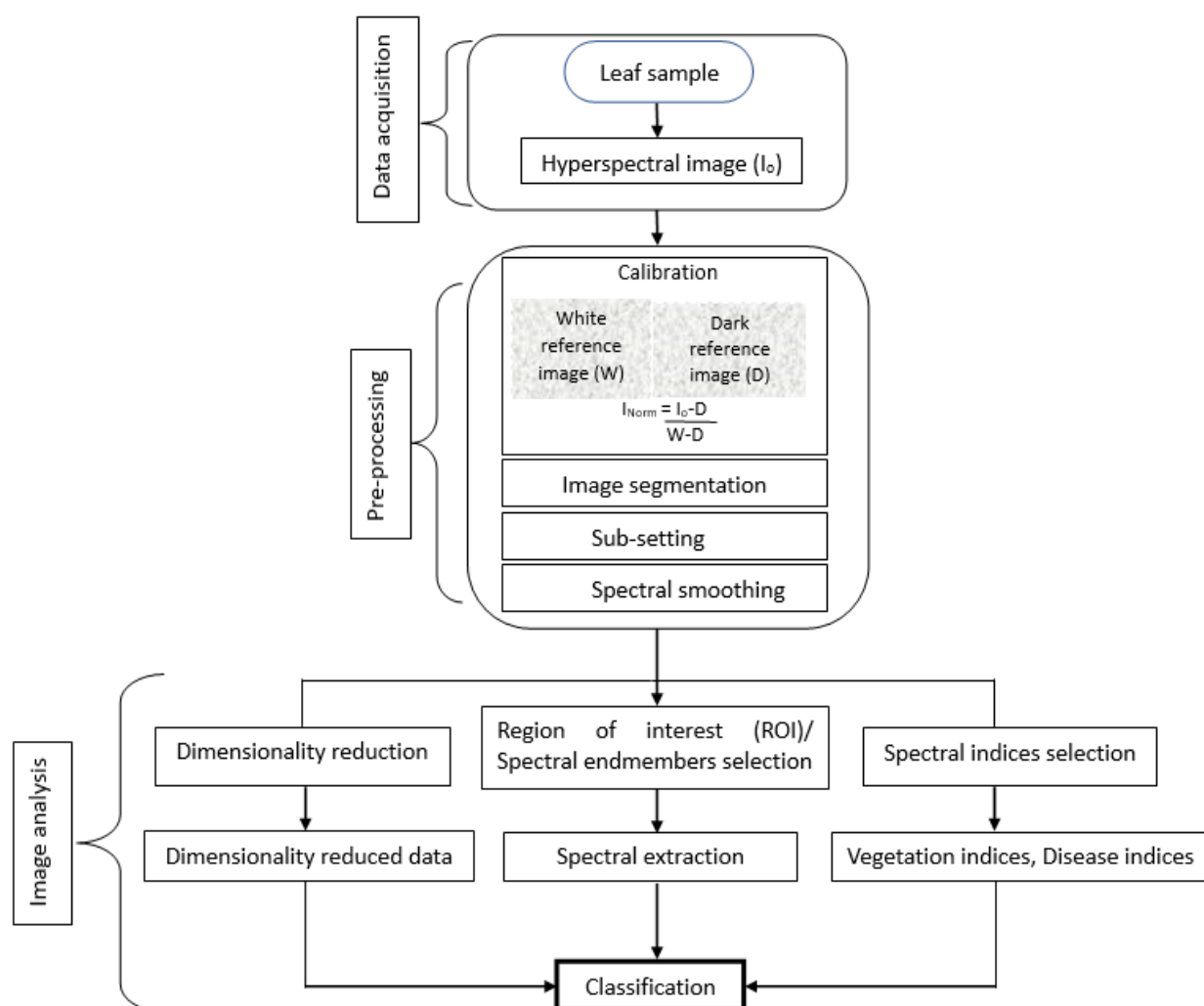
Hyperspectral imaging (HSI) is an important technique that provides objective, non-destructive, and precise analysis of plant disease phenotypes as well as time-series measurements (Lowe et al., 2017). Image acquisition using HSI can be done using different approaches- the push broom (line scanner), the filter-based, and whisk broom (point scanning) set-ups. Line scanning is the most used method due to its capability to continuously scan in one direction (Paulus and Mahlein, 2020). HSI captures the reflectance spectrum at numerous narrow and contiguous wavelengths across the electromagnetic spectrum, extending beyond the visible range, thus providing detailed spectral information for each pixel in an image (Mishra et al., 2017). HSI simultaneously acquires both spatial and spectral information resulting in a three-dimensional data cube, with two spatial dimensions ( $x$  and  $y$ ) and a spectral dimension ( $\lambda$ , wavelength) (Fig. 1.6).



**Fig. 1.6:** A hyperspectral image of a green leaf (a) a stack of narrow band sub-images that form a three-dimensional hypercube; (b) reflectance signature of a particular pixel at a specific location on the leaf's surface (adapted from Mishra et al., 2017).

### 1.3.5 Workflow for disease sensing using hyperspectral imaging

Disease sensing involves a multi-step process, including data/image acquisition, preprocessing, feature extraction, and image analysis (Fig. 1.7). Depending on the sensor system, data acquisition can involve either non-imaging (spectral data only, Mahlein et al., 2013) or imaging (spatial and spectral data) techniques (Lowe et al., 2017). For non-imaging sensors, data acquisition involves averaging over wavelengths to smooth the spectrum or reduce the number of wavelengths (Li et al., 2018). After image acquisition, the initial pre-processing stage involves spectral calibration of the data according to the maximum and minimum reflectance intensity. This normalization process corrects the significant signal variations caused by the non-uniformity of the illumination and removes random noise signals (Mishra et al., 2017; Cheshkova, 2022). The step calibrates the raw intensity values using black and white reference images back to relative reflectance (Paulus and Mahlein, 2020).



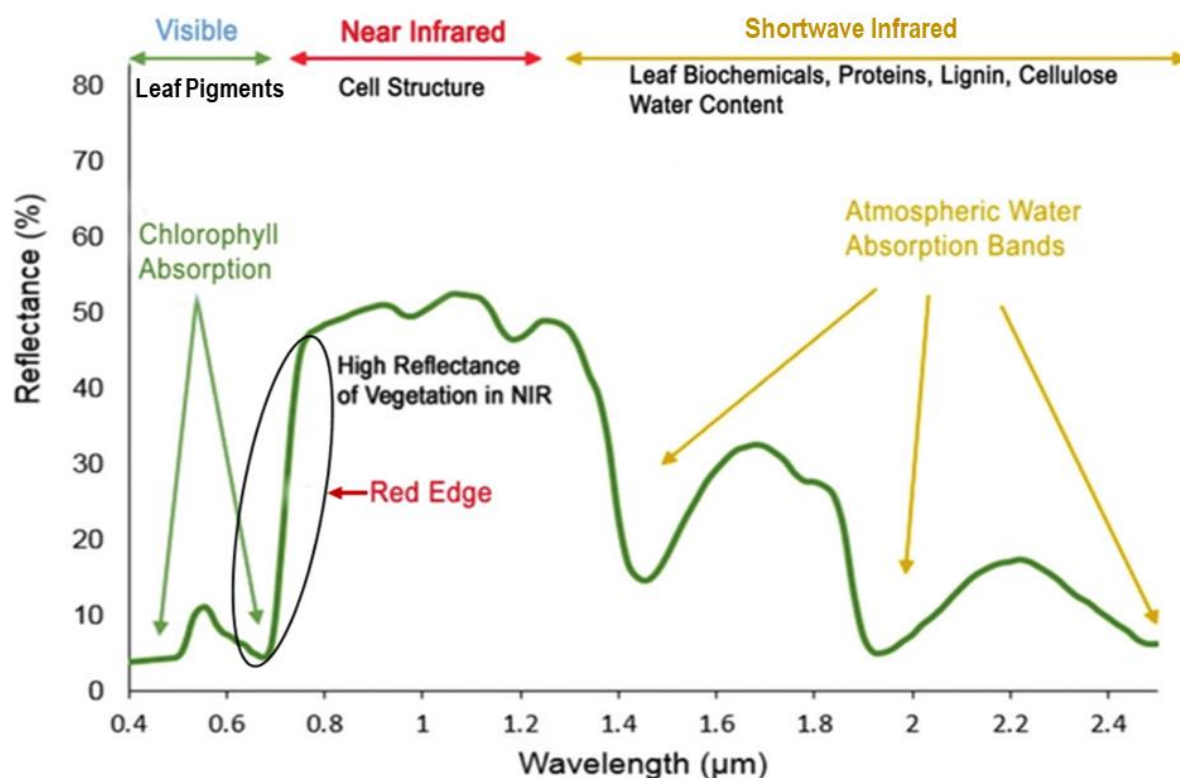
**Fig. 1.7:** Workflow for hyperspectral imaging (modified from Cheshkova, 2022).

Image segmentation is done to extract area(s) of interest from the background for subsequent spectral analysis (Cheshkova, 2022). Spectral sub-setting is then employed to select desired wavebands, reducing image complexity for further analysis. To mitigate high-frequency noise in raw spectral data and enhance the spectral signal-to-noise ratio, noise removal techniques such as Savitzky–Golay filter are applied (Savitzky and Golay, 1964). A region of interests (ROIs) tool is then used to create a mask on the image, isolating and delineating pure spectral endmembers e.g., healthy tissue and the diseased area (Mahlein et al., 2012). Subsequently, feature extraction identifies and extracts relevant spectral information from the ROIs. Dimension reduction methods such as principal component analysis (PCA) may be employed in feature extraction to achieve efficient data handling (Li et al., 2018; Cheshkova, 2022). Spectral vegetation indices (SVI) or spectral disease indices (SDI) can also be used as features (Ashourloo et al., 2014; Cheshkova, 2022). Finally, classification techniques are applied to categorize pixels containing spectrally distinct characteristics (Mishra et al., 2017) based on subset features and/or the full range of spectral data (Zhang et al., 2020).

### 1.3.6 Spectral reflectance properties of leaves

When light strikes a leaf surface, it can be absorbed, transmitted, or reflected. Unlike reflection, a phenomenon where light bounces off the surface, the spectral reflectance of leaves is a quantitative measure of the amount of light that is reflected by a leaf to that of the illuminated light at various wavelengths across the electromagnetic spectrum (Li et al., 2014; Ustin and Jacquemoud, 2020). These wavelengths include the visible (VIS, 400 – 700 nm), near-infrared (NIR, 700 – 1000 nm), and shortwave infrared (SWIR, 1000 – 2500 nm) spectral regions (Lowe et al., 2017; Ustin and Jacquemoud, 2020). Each wavelength provides unique information about the leaf's biochemical properties, structure and composition (Fig. 1.8).

In the visible region, reflectance is generally low due to the absorption by photoactive pigments such as chlorophyll, carotenoids, and non-photosynthetic pigments like anthocyanin (Sims and Gamon, 2002; Mishra et al., 2017). In the NIR wavebands, leaves exhibit high reflectance due to multiple scattering of light at the air-cell interfaces within the leaf tissue or direct reflection from the leaf surface (Ustin and Jacquemoud, 2020). The NIR also exhibits two bands of water absorption around 970 and 1200 nm (Sims and Gamon, 2002). In the SWIR region, strong water absorption occurs at 1200, 1400, 1940, and 2400 nm wavebands, resulting in low reflectance (Zhang and Guo, 2006). Additionally, structural compounds such as proteins, and other carbon components like cellulose, lignin, and starch, absorb in the SWIR range (Ustin and Jacquemoud, 2020).



**Fig. 1.8:** Characteristic spectral reflectance signature of a green leaf in the visible, near-infrared, and shortwave infrared ranges. For each wavelength range, the biochemical and structural components that influence reflection are indicated (modified from Roman and Ursu, 2016).

### 1.3.7 The influence of plant diseases on spectral reflectance properties of leaves

The interactions between plants and pathogens cause structural and metabolic modifications that manifest as visible disease symptoms and/ or the physical presence of pathogens such as hyphae and conidia, altering the spectral characteristics of leaves (Tanner et al., 2022). Pathogens that induce the degradation of photosynthetic pigments cause chlorotic lesions that alter the reflectance in the VIS (West et al., 2010). Modifications in the NIR reflect the influence of pathogens on plant cellular structures (Mahlein, 2016). Necrotrophic pathogens induce tissue degradation through their toxins or enzymes, leading to necrosis which causes changes in plant water content reflected by increased reflectance at 1400 and 1930 nm in the SWR (Tanner et al., 2022). Alternatively, visible colonies on leaves produced by biotrophic pathogens like powdery mildews and rust fungi indicate the presence of the pathogen itself which influences the optical properties of the plants (Mahlein, 2016; Bohnenkamp et al., 2021). Therefore, modification in plant physiology during pathogenesis can be linked to hyperspectral data by attributing specific changes of spectral reflectance pattern to known physiological processes (Tanner et al., 2022).

### 1.4 Hyperspectral imaging for detecting plant diseases

To effectively detect, identify, and quantify plant diseases, HSI needs to be sensitive to biophysical and biochemical abnormalities caused by fungal attacks and the diseases resulting from pathogen invasion and tissue colonization (Oerke, 2020). These effects on leaf reflection can be utilized to detect minor variations in plants' reaction to pathogen attacks, which serves as the foundation for spectral investigations of disease phenotypes (Kuska et al., 2015). Non-imaging sensors cannot differentiate healthy and specific disease tissue and the tissue spectrum averaging limits the sensitivity of the system (Mahlein et al., 2012). Moreover, precise spectral differences can be detected only at higher disease severities (Oerke, 2020). The combination of high spatial resolution and sensitivity of HSI, in contrast, enables the detection of diseases at even very low levels of severity making it suitable for decision-making in disease control (Lowe et al., 2017; Oerke, 2020). The connection between pathogenesis processes and the resistance of host plants to pathogens, as indicated by changes in spectral signatures, highlights the potential of HSI-based phenotyping to enhance and accelerate the assessment of plant disease resistance (Kuska et al., 2017). This technology significantly reduces the time and cost associated with traditional visual rating methods (Lowe et al., 2017; Bock et al., 2020).

HSI has been widely used in controlled and field settings to assess and characterize plant responses to both abiotic and biotic stresses, extending beyond rice and its associated diseases. It has been used to monitor water stress (Elvanidi et al., 2018), pigments and nutrient status (Jain et al., 2007; Zhao et al., 2016). In plant pathogen interaction, non-imaging sensors were used to assess diseases such as apple scab caused by *Venturia inaequalis* (Delalieux et al., 2007), to discriminate fungal infection levels in rice panicles (Liu et al., 2010), and powdery mildew of winter wheat caused by *Blumeria graminis* (Zhang et al., 2012). Whetton et al. (2018) used a hyperspectral line imager to measure yellow rust and *Fusarium* head blight in wheat and barley in the field. Using both laboratory and field HSI systems, citrus canker was detected at several disease development stages, i.e., asymptomatic, early, and late symptoms (Abdulridha et al., 2019). HSI has also been used to detect powdery mildew (*Erysiphe necator*) in grapevine (Pérez-Roncal et al., 2020).

HSI enabled the characterization of the spatial, spectral, and temporal changes of disease symptoms in various host-pathogen systems (Mahlein et al., 2012). In rice, HSI has been used to grade the host-pathogen compatibility and phenotyping of leaf blast symptoms (Zheng et al., 2013). HSI has also proven successful in assessing the sporulation rate of *Cercospora beticola* in sugar beet (Oerke et al., 2019).

### 1.4.1 Limitations of hyperspectral imaging in plant disease detection

The use of HSI in the study of plant-pathogen interactions has shown to be feasible, but specific findings can vary based on the unique characteristics of the host, pathogen, and environmental conditions. HSI has its limitations, including high equipment costs, data complexity, longer measurement time, limited field of view, low throughput, and suitability variations for different crops and diseases (Martinelli et al., 2015).

HSI measurements are influenced by environmental conditions. Controlled settings such as laboratories and greenhouses minimize the impact of external factors, such as variations in weather conditions, ensuring accurate and reproducible measurements (Bock et al., 2020). In contrast disease detection in the field is influenced by disturbances like wind which can lead to plant movement, obscuring spectral images, causing blurred spatial information (Bock et al., 2020; Cheshkova, 2022). Changing illumination conditions due to clouds can render data uninterpretable. The 3D structure of plants, including leaf architecture also affects the spectral signal (Bohnenkamp et al., 2019). The presence of diseases on lower plant leaf levels can lead to a decreased reflected signal, posing a challenge for accurate disease detection (Bock et al., 2020). Additionally, using detached leaves in a greenhouse is not an automated process for disease detection due to its invasive nature which limits time series measurements (Kuska et al., 2015). Therefore, the choice of using this method should be guided by specific research needs and the availability of resources.

### 1.4.2 Analysis of hyperspectral data

The primary drawback of employing HSI in plant disease phenotyping is the complexity of the data. Spectral techniques, such as spectral vegetation indices (SVIs), work by computing ratios of two (or more) bands within the electromagnetic spectrum, effectively reducing the complexity of hyperspectral data (dimensionality reduction) which results in reduced computational time. SVIs play a crucial role in assessing and monitoring biochemical and biophysical plant parameters, serving as valuable indicators of plant health and vigor (Gitelson et al., 2002). Disease-specific spectral disease indices (SDI) have also been developed for detection of various diseases of different crop plants. These SDIs have been used to detect diseases such as sugar beet rust and *Cercospora* leaf spot (Mahlein et al., 2013) and brown rust (Ashourloo et al., 2014).

Image classification in hyperspectral data analysis involves categorizing individual pixels within an image into groups or classes based on their unique spectral signatures (Cheshkova, 2022). These spectral signatures of leaves represent the reflected light at different wavelengths associated with each pixel (Li et al., 2014). This classification process can be either unsupervised (automatically group pixels into clusters or classes based on spectral similarity without prior knowledge) or supervised

(classify pixels based on a priori knowledge of spectral characteristics associated with predefined classes). In the context of plant disease detection, supervised classification is commonly used and relies on methods like the support vector machine (SVM), and spectral angle mapper (SAM) algorithm, which enables simultaneous pixel classification (Mewes et al., 2011). Additionally, deep learning methods such as Convolutional Neural Networks (CNN) have proven effective in identifying and classifying subtle symptoms of diseases (Shoaib et al., 2023).

In particular, SAM offers the advantage of having predefined classes for analysis, ensuring precision in the types of classes considered. Furthermore, its insensitivity to variation in illumination makes it a robust choice for spectral analysis (Kruse et al., 1993). To employ SAM effectively, a spectral library is created using spectral information obtained from manually labeled (annotated) regions of interest (ROIs). These ROIs represent spectrally unique signatures of pure image components or endmembers within the image. SAM then compares the spectral angle (= spectral similarity) between a reference spectrum from the spectral library and the spectrum of each pixel in the hyperspectral image (Fig. 1.9; Kruse et al., 1993; Luc et al., 2005).

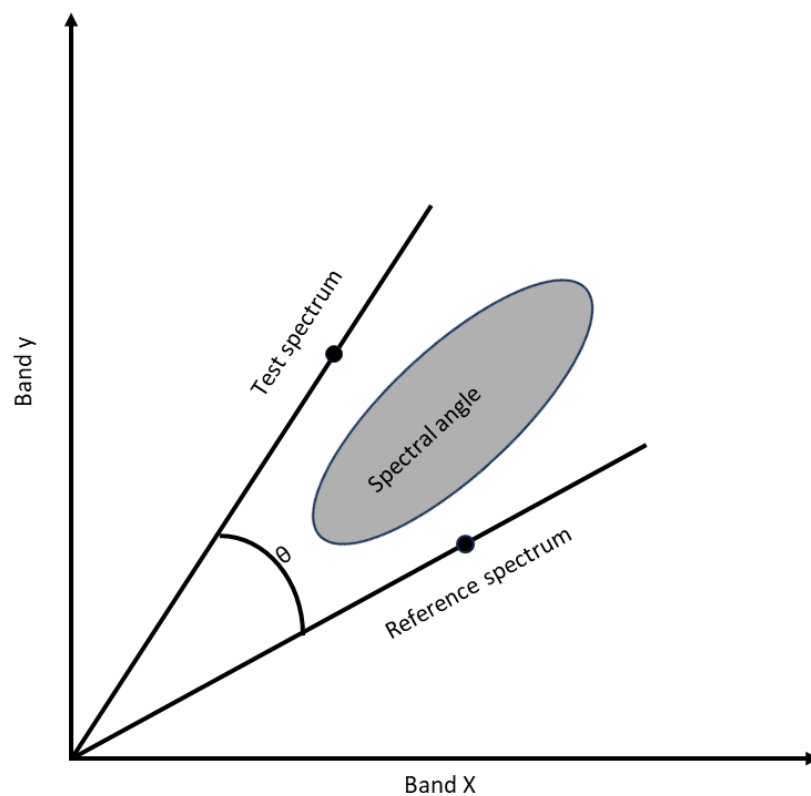


**Fig. 1.9:** A visual representation of the spectral angle mapper plot displaying a test spectrum and reference spectrum. The angle  $\theta$  between these two vectors represents the spectral similarity between them (modified from Kruse et al., 1993).

Smaller spectral angles indicate higher similarity, while larger angles indicate less similarity. SAM has found extensive application in detecting and quantifying disease-specific symptoms (Mahlein et al., 2012). In evaluating the accuracy of SAM algorithms, classification results are commonly compared to actual disease data (ground truth information), which may include RGB images. However, it is important to acknowledge that the accuracy and effectiveness of SAM can be influenced by factors like data quality, parameter selection, and the specific application context (Girouard et al., 2004; Kuching, 2007). Careful consideration of these factors is essential for reliable disease detection and classification using HSI.

### 1.5 Objectives of the study

This study aimed at investigating the optical properties of rice—*M. oryzae* interactions and the host reaction to blast disease in different rice genotype × pathogen genotype interactions using HSI under controlled conditions. To achieve this goal, different incompatible and compatible interactions of rice and *M. oryzae* were studied.

The first part of the study dealt with an investigation of the diverse reactions exhibited by various rice genotypes differing in susceptibility to different *M. oryzae* isolates using HSI. Furthermore, genotype-dependent variations in the manifestation of symptoms associated with rice blast were examined (Chapter 2). In rice—*M. oryzae* interactions, large symptom variability exists ranging from no lesion- incompatible (highly resistant) to large diamond shaped lesions - fully compatible (highly susceptible) interactions. The variability of lesions in size, shape, colour and number between and even within a single leaf reflects the gene-for-gene interactions between rice genotypes and *M. oryzae*. This study investigated whether during pathogenesis, different tissue types (symptom subareas) develop in a coordinated way to a specific blast symptom and how the proportion of each tissue type vary within a leaf and among leaves. The lesion variability was investigated in detail to know whether blast lesion types are related to genotypic disease resistance and how they influence the grading of host-pathogen compatibility, which could potentially serve as a valuable tool in screening for disease resistance within breeding programs.

The effectiveness of HSI in detecting and characterizing the complex interactions among three mineral N rates, different *M. oryzae* isolates, and selected rice genotypes with varying susceptibility to blast was assessed. The effects of mineral N application on the expression of leaf blast symptoms and the intensity of blast and on the spectral variability of healthy and diseased tissue were examined (Chapter 3). Mineral N application affects plant susceptibility to blast fungus *M. oryzae*. Studying the influence of N nutrition on rice blast using HSI was expected to obtain a comprehensive understanding of the complex interplay between nutrient availability, plant growth, and disease dynamics and the

effect of gene-for gene interaction. As N-nutrition is important to farmers and crop breeders, this knowledge is crucial for developing strategies to optimize nutrient management practices in rice cultivation, to get high yields, and improve disease resistance in high-input production systems.

The capability of hyperspectral imaging as a tool for quantifying *M. oryzae* sporulation on rice genotypes was assessed in chapter 4. This aspect of the study involved investigations of *M. oryzae* sporulation on both resistant and susceptible rice genotypes and the use of spectral data to quantify pathogen sporulation. In rice, slow-blasting or partial resistance indicates that the plant exhibits some degree of resistance to the pathogen, revealing how minor genes in host genotypes and pathogen isolates operate. The sporulation of *M. oryzae* was investigated by HSI, offering a quantitative approach for assessing fungal sporulation dynamics, shedding light on a critical aspect of the plant-pathogen interaction. The assessment of this epidemiologically relevant parameter may improve the phenotyping of crops in breeding for disease resistance.

## 2 Characterization of rice–*Magnaporthe oryzae* interactions by hyperspectral imaging

Chapter 2 has been published:

**Reprinted from Angeline W. Maina** and Erich-Christian Oerke\*, 2023. Characterization of Rice–*Magnaporthe oryzae* Interactions by Hyperspectral Imaging. *Plant Disease*, 107(10), 3139-3147. <https://doi.org/10.1094/PDIS-10-22-2294-RE>

Institute for Crop Science and Resource Conservation (INRES) - Plant Pathology, Rheinische Friedrich-Wilhelms University of Bonn, Germany

### Author contributions

**A.W.M.** and E.-C.O. designed the study and interpreted the data. **A.W.M.** performed the experiments, carried out the hyper- spectral measurements and the statistical analysis, and drafted the manuscript. All authors read, revised, and approved the final manuscript.

## 2.1 Abstract

Hyperspectral imaging has the potential to detect, characterize and quantify plant diseases objectively and non-destructively to improve phenotyping in breeding for disease resistance. In this study, leaf spectral reflectance characteristics of five rice genotypes diseased with blast caused by three *Magnaporthe oryzae* isolates differing in virulence were compared with visual disease ratings under greenhouse conditions. Spectral information (140 wavebands, range 450 to 850 nm) of infected leaves was recorded with a hyperspectral imaging microscope at 3, 5 and 7 days postinoculation to examine differences in symptom phenotypes and to characterize the compatibility of host-pathogen interactions. Depending on the rice genotype  $\times$  *M. oryzae* genotype interaction, blast symptoms varied from tiny necrosis to enlarged lesions with symptom subareas differing in tissue coloration and indicated gene-for-gene-specific interactions. The blast symptom types were differentiated based on their spectral characteristics in the visible/near-infrared range. Symptom-specific spectral signatures and differences in the composition of leaf blast symptom type(s) resulted in unique spectral and spatial patterns of the rice–*M. oryzae* interactions based on the size, shape and color of the symptom subarea. Spectral angle mapper classification of spectra enabled (i) discrimination between healthy (green) and diseased tissue of rice genotypes, (ii) classification and quantification of different blast symptom subareas, and (iii) grading of the host-pathogen compatibility (low – intermediate – high). Hyperspectral imaging was more sensitive to small changes in disease resistance than visual disease assessment and enabled the characterization of various types of resistance/susceptibility reactions of tissue subjected to *M. oryzae* infection.

**Key words:** Blast, host-pathogen compatibility, hyperspectral imaging, rice, symptom types

## 2.2 Introduction

Blast is one of the most important fungal diseases of rice (*Oryza sativa*) caused by the filamentous, ascomycetous, hemibiotrophic fungus *Magnaporthe oryzae* (anamorph *Pyricularia oryzae*) (Couch and Kohn 2002; Talbot et al. 1993). The disease causes yield losses of up to 80% when epidemics occur (Boddy 2016; Ou 1985). Rice genotypes infected by *M. oryzae* exhibit variation in leaf blast phenotypes depending on their genetically fixed degree of susceptibility or resistance, their growth stage, and the environmental conditions (Agbowuro et al. 2020; Ou 1985; Ribot et al. 2008). Symptoms range from tiny necrotic spots (on resistant genotypes), roundish lesions with small gray centers and brown margins (intermediate), and spindle shaped lesions with large gray centers and brown margins (on susceptible genotypes) (Boddy 2016; IRRI 2002; Ou 1980). Assessment of rice blast is commonly done visually by human raters (Bock et al. 2010, 2020; Feng et al. 2020; Kobayashi et al. 2001; Zhao et al. 2022). The method is time consuming, laborious, and subjective, which makes it

difficult to assess rice × *M. oryzae* interactions that result in various disease phenotypes. In contrast, imaging techniques such as hyperspectral imaging (HSI) allow precise and automatic measurement of crop diseases as they are objective and significantly reduce the amount of work in comparison with visual rating methods (Bock et al. 2010; Lowe et al. 2017). HSI measures large quantities of samples faster than visual rating methods, which requires trained personnel to visually inspect each plant individually and record the observations manually (Bock et al. 2010; Thomas et al. 2018).

Disease symptoms result from physiological changes in plant metabolism caused by pathogen activities. These changes alter the spectral characteristics of plant tissue, which provide the basis for spectral investigation of disease phenotypes by HSI (Arens et al. 2016; Mutka and Bart 2014; Oerke et al. 2016). A pixel-wise extraction of spectral reflectance permitted the differentiation of *Cercospora* leaf spot (CLS) symptoms of sugar beet genotypes into subareas (Leucker et al. 2016). HSI is nondestructive and may be used in time series experiments on the same plants and can detect single symptoms and assess disease severity (Kuska et al. 2015; Oerke et al. 2016).

The reflectance spectrum resulting from multiple interactions between irradiation and the plants' biophysical (e.g., leaf surface and tissue structure) and biochemical properties (e.g., content of pigments and water; Blackburn 2007; Mishra et al. 2020; Tanner et al. 2022) can be measured for all pixels of an image. Structural and metabolic changes caused by the plant-pathogen interaction lead to modifications of spectral reflectance pattern in the visible (VIS, 400 to 700 nm) and near-infrared (NIR, 700 to 1,000 nm) that can be detected by HSI with high spatial resolution (Bauriegel et al. 2011; Leucker et al. 2016; Mahlein et al. 2018). Analysis of the modified spectra enables the detection of fungal diseases (Mahlein 2016; Zhou et al. 2018). Use of HSI to characterize the spatio-temporal dynamics of plant diseases is key to understand important processes during pathogenesis (Bendel et al. 2020; Mahlein et al. 2012; Oerke et al. 2016).

Differentiation between healthy and diseased leaf tissue using HSI is rather easy and has been described several times. Differentiation between symptoms of diseases which may be very similar is more challenging and has been shown for diseases of sugar beet (Mahlein et al. 2010, 2012), wheat (Alisaac et al. 2019; Bauriegel et al. 2011), and others (Bendel et al. 2020; Zhou et al. 2018). Leucker et al. (2016) were able to distinguish between symptom types of CLS of sugar beet genotypes differing in nonrace-specific resistance to *Cercospora beticola*. HSI has been used to detect rice blast caused by *M. oryzae* (Kobayashi et al. 2016; Zhang et al. 2022a, b; Zhao et al. 2022; Zheng et al. 2013), quantify disease severity (Bock et al. 2020; Zhang et al. 2022a, b), and to grade the host-pathogen compatibility (low – intermediate – high; Huang et al. 2015; Zheng et al. 2013).

The expression of different leaf blast symptom type(s) results from genetically controlled interactions between genotypes of the host plant and the pathogen (Ou 1980; Takabayashi et al. 2002). Gene for-gene-specific interaction implies that the outcome of the interaction (= the degree of compatibility) depends on the specific combination of resistance and virulence genes, an aspect which has not yet been investigated in rice × *M. oryzae* interaction using HSI. The identification and characterization of plants' resistance reactions to fungal pathogens could be useful for plant breeding to screen for new genotypes that are disease resistant (Kuska et al. 2017; Tanner et al. 2022). Sensors for disease assessment, therefore, ought to be adaptable to changes in the variability of host plant tissue, pathogen genotypes causing different host reactions, disease symptoms, and different symptoms on different parts of a plant, such as rice blast on leaves, necks, and panicles (Oerke 2020).

To obtain more comprehensive information on disease phenotype, analysis of the entire spectrum in the VIS and NIR range is important. Spectral angle mapper (SAM) algorithm (Kruse et al. 1993) was used for supervised classification of hyperspectral data. The algorithm is insensitive to differences in illumination and allows the definition of classes (reference spectra) which can be derived from RGB images and compared with their details. SAM utilizes the spectral angle as a measure of similarity between two spectra, which makes it very sensitive to small variations in spectral reflectance (Kruse et al. 1993; Kuching 2007).

In this study, five rice genotypes (CO 39, IR64, Koshihikari, Kusabue, and Nipponbare), known to vary in the level of resistance to *M. oryzae* isolates Guy 11, Li1497 and TH6772, were used to investigate whether HSI is suitable for differentiating the host genotypes' response(s) to *M. oryzae* attack and the host genotype-dependent development of blast symptom types. The specific objectives were: (i) to describe the spectral characteristics of healthy (green) rice leaves and those infected by *M. oryzae*; (ii) to describe the spectral characterization of different subareas of blast symptoms; (iii) to assess the spectral variability of blast symptom types at early (3 days postinoculation [d.p.i.]), middle (5 d.p.i.), and late (7 d.p.i.) stages of pathogenesis; and (iv) to use the spectral information for grading the host-pathogen compatibility depending on the rice genotype × pathogen genotype interactions.

## 2.3 Materials and Methods

### 2.3.1 Plant material and fungal pathogen

Five cultivars of rice (*O. sativa*) were used in this study. Cultivar CO 39 (accession number IRGC 51231) was obtained from IRRI, the Philippines, and cultivar Kusabue, cultivar Koshihikari, and cultivars Nipponbare and IR64 were kindly provided by Ulrich Schaffrath, Aachen University

(Germany); by BASF SE, Limburgerhof; and by Michael Frei, Department for Plant Nutrition, University of Bonn, respectively. The genotypes were selected based on the rice type and their reaction to *M. oryzae* as reported from literature and from researchers who provided plant and pathogen material for this study. The genotypes CO 39 (susceptible) and IR64 (resistant) are *O. sativa* indica type, and cultivars Koshihikari, Kusabue, and Nipponbare (susceptible) are *O. sativa* japonica type.

The *M. oryzae* isolate TH6772 was obtained from Ulrich Schaffrath, Aachen University; isolate Guy 11 was kindly supplied by Didier Tharreau (CIRAD, Montpellier, France); and isolate Li1497 was obtained from BASF SE (Limburgerhof, Germany).

### 2.3.2 Plant cultivation, inoculum preparation and inoculation

Rice seeds were sown directly in loamy soil in 9-cm-diameter pots. For each genotype, four seeds per pot were sown with four technical replications. The pots were placed in plastic trays filled with water. Two weeks after sowing, N-P-K fertilizer (NovaTec Classic, COMPO EXPERT GmbH, Germany), with a ratio of 12-8-16 (+3+trace elements), was applied at the rate of 0.4 g/pot. Plants were grown in a greenhouse facility at the University of Bonn under controlled conditions, simulating a minimum 12 h-photoperiod, a temperature of 25/22°C day/night, and 60% relative humidity (RH; every 15 min, spells of 1 min misting the air to increase RH).

*M. oryzae* isolates Guy 11, Li1497, and TH6772 were cultivated on rice leaf agar (50 g blended fresh rice leaves, 15 g agar, 10 g soluble starch, and 2 g brewer's yeast in 1,000 ml water). The cultures were incubated under UV light (16/8 h day/night) at 25°C for 14 days to induce sporulation. Conidia of *M. oryzae* were harvested by scraping off the mycelia using tap water with a droplet of Tween 20 and 0.4% gelatin which was strained through a double layer of cheese cloth. For each genotype, rice plants at the three leaf stage (BBCH 13, 18-day-old seedlings) were inoculated by spraying with conidial suspensions ( $10^5$  conidia/ml) using a hand sprayer. The inoculated plants were kept in a dark moist incubation chamber at 25°C and >95% RH for 24 h, and they were taken back to the greenhouse afterward. The experiments were conducted three times in a completely randomized design.

### 2.3.3 Visual assessment of disease severity

The third leaf of each plant was assessed for disease severity (a total of 16 leaves per genotype). The severity of leaf blast was assessed by visually approximating the percentage of diseased leaf area at 3, 5, and 7 d.p.i. using the standard evaluation system for rice leaf blast (IRRI 2002, 2013). The percentage of diseased leaf area relative to the total area was estimated with a visual scale for scoring of blast severity, with 0 representing 0% diseased leaf area (highly resistant), 1 = <1% diseased leaf area (resistant), 3 = <4% diseased leaf area (moderately resistant), 5 = blast lesions infecting 4 to 10%

of leaf area (moderately susceptible), 7 = blast lesions infecting 26 to 50% of leaf area (susceptible), and 9 = blast lesions infecting >75% of leaf area (highly susceptible; IRRI 2002, 2013).

#### **2.3.4 HSI**

Spectral reflectance of rice leaves was recorded under controlled conditions using ImSpector V10E HSI systems (Spectral Imaging Ltd., Oulu, Finland) mounted on a stereo microscope foreoptic (Z6 APO, Leica, Wetzlar, Germany) covering the visible and NIR spectral wavelength range from 400 to 1,000 nm with 2.8 nm spectral resolution. It consists of a lens (OLE-23) fixed on an imaging spectrograph (V10E-QE, Specim, Finland) attached on a positioning XY-motorized table (H105/2/0 ProScan Upright Stage, Prior Scientific, Jena, Germany) and two linear light emitters (Dual Line Lightlines, Schott, Mainz, Germany) that provide constant artificial illumination intensity throughout measurements. The HSI data were obtained by line scanning using a camera (C8484–05, Hamamatsu City, Japan) integrated within the spectrograph. The system was switched on 1 h before taking the images to ensure constant illumination. Images for healthy and infected leaf samples were taken in a dark room to realize optimal illumination and constant measurement conditions. To monitor the disease progress, the inoculated leaves were scanned at 3, 5, and 7 d.p.i., respectively, and were immediately put back into the greenhouse after each data acquisition. Four hyperspectral images per sample were taken: (i) an image of the object area of interest with optimized time of exposure; (ii) a dark current image of the object; (iii) an image of a white reference bar; and (iv) a dark current image of the white reference bar. Hyperspectral images were acquired by using the Lumo software, which produced spectral data cubes (Spectral Imaging Ltd.).

#### **2.3.5 Preprocessing of hyperspectral images**

The reflectance of samples was calculated by normalizing the images in relation to the white reference spectra and the dark current measurements by use of ENVI 5.3 + IDL 8.3 software (ITT Visual Information Solutions, U.S.A.). Due to the large noise at both ends of the spectra, only the wavelengths between 450 and 850 nm (140 wavebands) were selected. The Savitzky-Golay filter was subsequently applied to smooth the resultant reflectance data (Savitzky and Golay 1964).

#### **2.3.6 Analysis of hyperspectral images**

The preprocessed images were further analyzed using the ENVI + IDL software. The spectral information of image pixels for rice leaves was analyzed by the SAM algorithm for supervised classification (Kruse et al. 1993). For each time of image recording, a hyperspectral library of spectral information of different blast symptom subareas was created. These reference spectra of blast symptom subareas were used in the SAM classification of different blast symptom types. SAM

calculates the spectral similarity of the pixels of interest and all reference spectra selected in an  $n$ -dimensional space depending on the number of spectral bands. The algorithm assigns all pixels to the reference components or leaves them unclassified and illustrates the classification result in a false-colour image. The SAM method was performed using the software ENVI 5.3 + IDL 8.3 to discriminate between healthy and diseased rice tissue, to assess the different stages of blast pathogenesis, and to quantify various blast symptom types of resistance/susceptibility reactions of tissue subjected to *M. oryzae* attack.

### 2.3.7 Statistical analysis

The statistical analysis was performed using R studio statistical software (Gelfond et al. 2018). For normally distributed data, a standard analysis of variance was performed. Tukey's HSD test at ( $P = 0.05$ ) was done to detect significant differences in disease severity of *M. oryzae*-inoculated plants. Correlation between percentage diseased area and blast symptom types was done using Pearson's correlation coefficient with the significance threshold set at  $P \leq 0.05$ . The Kruskal-Wallis test was used to assess pixel classification frequency (%) of the symptom subareas for each rice genotype  $\times$  pathogen interaction. Dunn's test for multiple comparisons at  $P \leq 0.05$  was done to test the significance differences of blast symptom subareas.

## 2.4 Results

### 2.4.1 Effects of genotypes on blast symptom development

Phenotypes of rice blast symptom types were assessed 3, 5, and 7 d.p.i. (Fig. 2.1). Symptoms differed among pathogen isolate  $\times$  rice genotype interactions, which were revealed to be gene-for-genes specific. On resistant genotypes (e.g., IR64), small, dark brown symptoms appeared 3 d.p.i. and did not increase neither in size nor number until 7 d.p.i. On rice genotype CO 39 infected with isolate TH6772, dark brown symptoms slightly larger than the lesions in IR64 were observed during pathogenesis. On rice genotype CO 39, which is highly susceptible to isolates Guy 11 and Li1497, initial symptoms of small dark brown spots and gray-green patches occurred 3 d.p.i. The symptoms enlarged, rapidly coalesced, and developed a white and/or gray center surrounded by gray-green tissue with a brown margin and chlorotic tissues at 5 and 7 d.p.i. Light brown tissue was also observed 7 d.p.i. Rice genotype Koshihikari, which is highly susceptible to isolate Li1497, produced small brown and chlorotic areas at 3 d.p.i. The lesions subsequently expanded, coalesced, and developed a white or gray center surrounded by either chlorotic tissue or brown margin at 5 and 7 d.p.i. Isolate TH6772 caused small brown spots on leaves of rice genotypes Kusabue and Nipponbare within 3 d.p.i. At 5

d.p.i., gray tissue surrounded by dark green tissue was observed. As symptoms expanded further, gray tissue coalesced, and chlorotic areas appeared on genotype Kusabue 7 d.p.i. (Fig. 2.1).

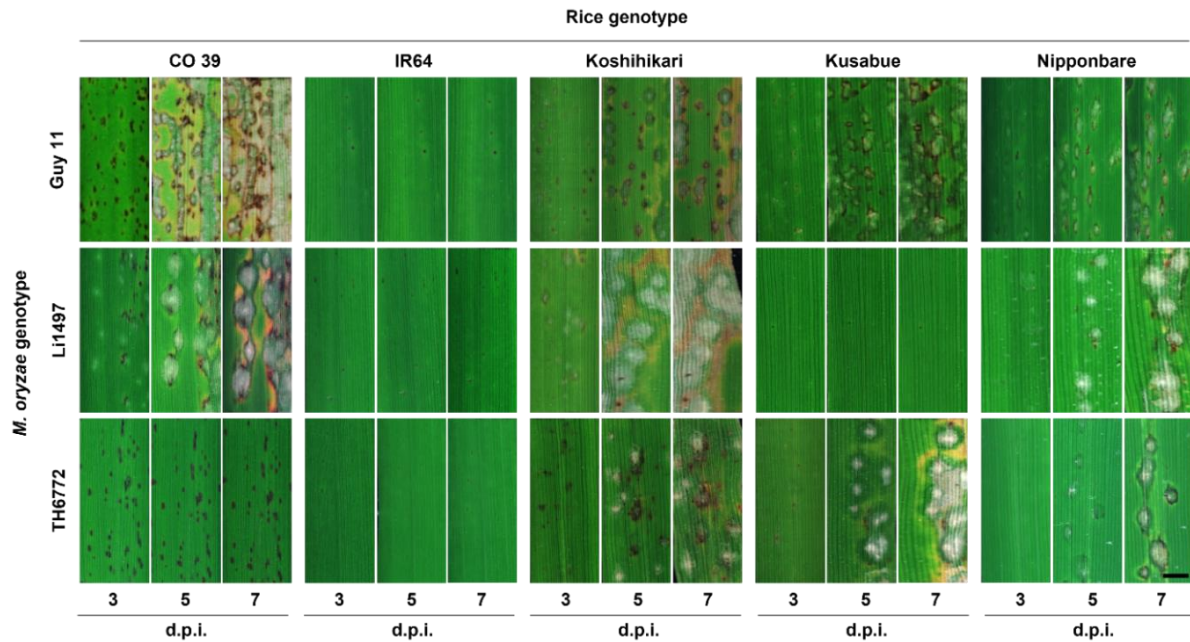


**Fig. 2.1.** Phenotypes of blast symptoms and their progression during pathogenesis on leaves of five rice genotypes infected by three isolates of *Magnaporthe oryzae* 3, 5, and 7 days postinoculation (d.p.i.). Leaf blast symptoms for each rice genotype differed depending on the compatibility of rice × *M. oryzae* interactions (RGB images of representative leaf parts; bar size = 5 mm).

#### 2.4.2 Effects of host and pathogen genotypes on disease severity

The severity of blast on rice leaves was visually assessed 3, 5 and 7 d.p.i. (Supplementary Table S2.1; Fig. 2.2). The interaction of rice × *M. oryzae* genotypes was characterized by highly significant variation ( $P < 0.05$ ) in blast severity ranging from low (1%) to high (73.4%) disease intensity 7 d.p.i., when symptoms had fully developed. Disease severity significantly varied ( $P < 0.01$ ) among the *M. oryzae* isolates as well as among the susceptibility levels of different rice genotypes (Supplementary Table S2.2). No significant variation ( $P < 0.05$ ) in blast severity was observed in ‘IR64’ (resistant) and ‘Nipponbare’ (susceptible). The other three host genotypes varied significantly in their reaction to the pathogens, indicating the mechanism of gene-for-gene-specific interaction (Fig. 2.2).

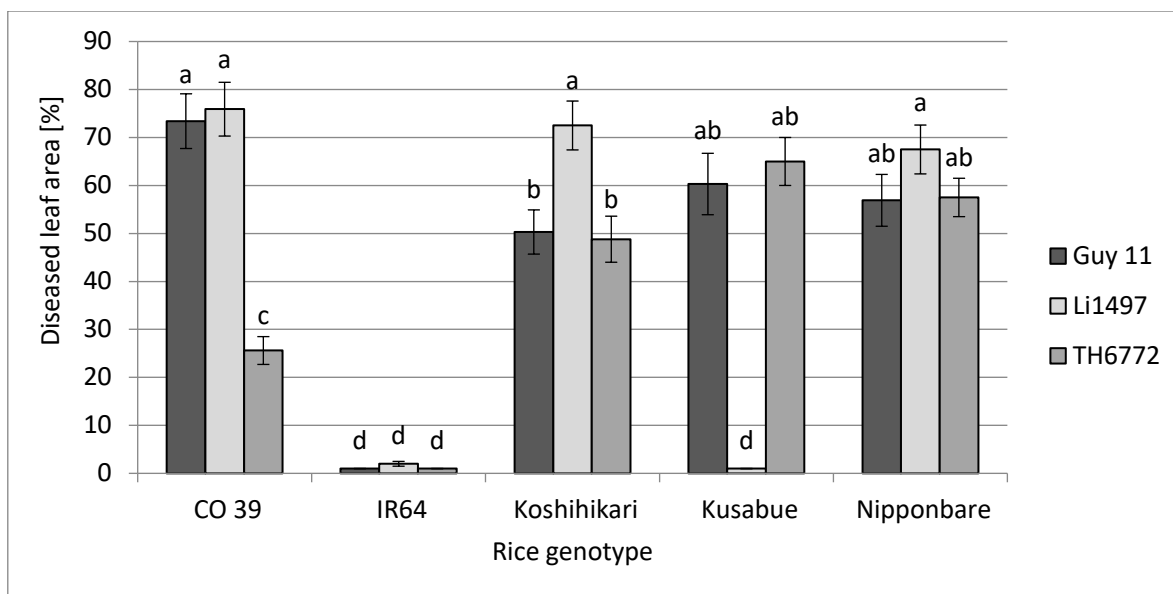


**Fig. 2.2.** Visual assessment of rice blast severity on five rice genotypes infected with three genotypes of *Magnaporthe oryzae* 7 days postinoculation. Observations are based on a representative of three independent experiments using 16 plants per genotype. Letters denote statistically significant differences according to Tukey's HSD test ( $P = 0.05$ ).

### 2.4.3 Symptom types in the interactions of rice and *M. oryzae* genotypes

Considering the reaction of host genotypes to the isolates of the blast pathogen, the interactions of rice  $\times$  *M. oryzae* were classified into five levels of compatibility. They included highly susceptible, susceptible, moderately susceptible, moderately resistant, and resistant host reactions (Fig. 2.3). Due to limited variability of symptom types within the interactions among leaves and within single leaves of rice genotypes, the symptom types varied  $\pm 1$  category. This enabled the classification of the host-pathogen interactions according to the visual symptom assessment (Table 2.1). The symptom type of rice  $\times$  *M. oryzae* interactions was positively correlated to disease severity as assessed visually 7 d.p.i. (Fig. 2.4). This correlation was significant or highly significant for all isolates and had an overall coefficient of determination of  $R^2 = 0.862$  (linear) and 0.951 (exponential equation).

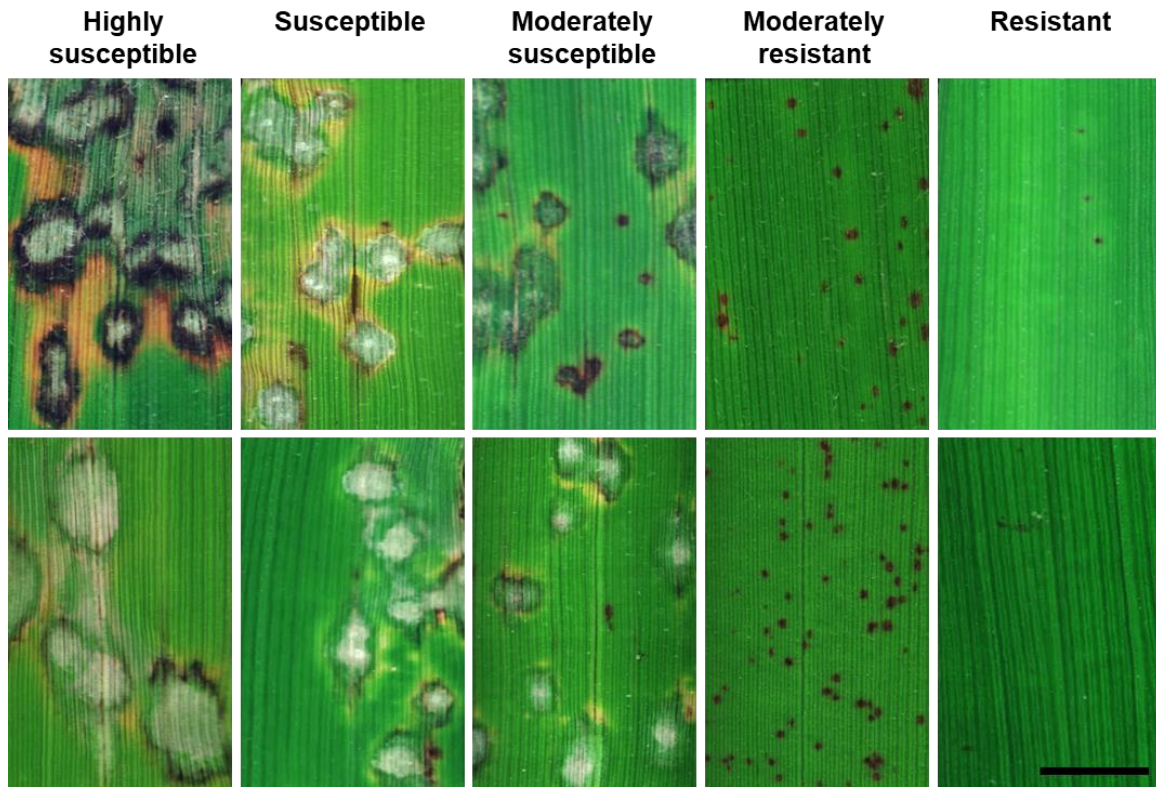


**Fig. 2.3.** Phenotypes of typical leaf blast symptom types demonstrating the compatibility between genotypes of rice and *Magnaporthe oryzae* 7 days postinoculation. Two images per category demonstrate the variability within each category (bar size = 10 mm).

**Table 2.1.** Matrix of the rice–*Magnaporthe oryzae* interactions representing different disease reaction types for five rice genotypes inoculated with three isolates of *M. oryzae*<sup>2</sup>

| <i>M. oryzae</i> isolate | Rice genotype |      |             |         |            |
|--------------------------|---------------|------|-------------|---------|------------|
|                          | CO 39         | IR64 | Koshihikari | Kusabue | Nipponbare |
| Guy 11                   | HS            | R    | MS          | S       | MS         |
| Li1497                   | HS            | R    | HS          | R       | S          |
| TH6772                   | MR            | R    | MS          | S       | MS         |

<sup>2</sup>R = resistant, MR = moderately resistant, MS = moderately susceptible, S = susceptible, and HS = highly susceptible.

#### 2.4.4 Spectral signatures of healthy and diseased rice tissue

The spectral characteristics of healthy tissue and tissue infected by the three isolates of *M. oryzae* were assessed for the five rice genotypes at 7 d.p.i. As demonstrated for rice genotypes IR64 and CO 39, the spectral signatures of healthy and diseased leaf tissue differing in compatibility to *M.*

*oryzae* genotypes were distinct (Fig. 2.5). The spectral reflectance of mature blast symptom subareas differed significantly depending on the color (and structure) of the tissue. Higher compatibility of interactions was linked to more complexity of blast symptoms and an increased number of symptom subareas.

In incompatible interactions, reflectance of dark brown tissue slightly decreased in the VIS and in the NIR range as compared with healthy tissue (Fig. 2.5). In compatible interactions, spectra of dark brown tissue had decreased reflectance in VIS and NIR regions, while gray tissue was characterized by a strong increase in reflectance throughout the spectrum. Spectral reflectance of chlorotic and gray-green leaf tissue increased in both VIS and NIR regions in genotype CO 39 infected with Li1497 (Fig. 2.5). Spectral reflectance of light brown tissue was characterized by a slight decrease in the VIS and NIR in rice genotype CO 39 infected with isolates Guy 11 and Li1497, respectively (Fig. 2.5).

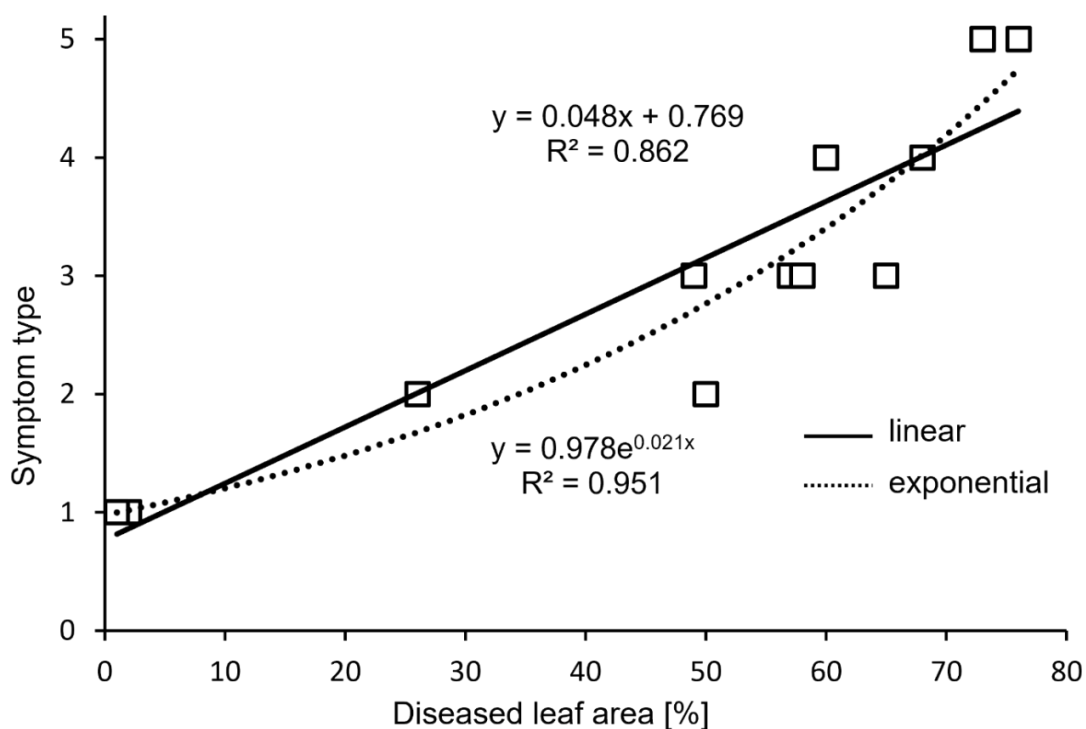


**Fig. 2.4.** Correlation between disease severity and blast symptom type for *Magnaporthe oryzae* isolates Guy 11, Li1497, and TH6772 on five rice genotypes (Pearson’s correlation method,  $P < 0.05$ ). Symptom types: 1 = resistant, 2 = moderately resistant, 3 = moderately susceptible, 4 = susceptible, and 5 = highly susceptible.

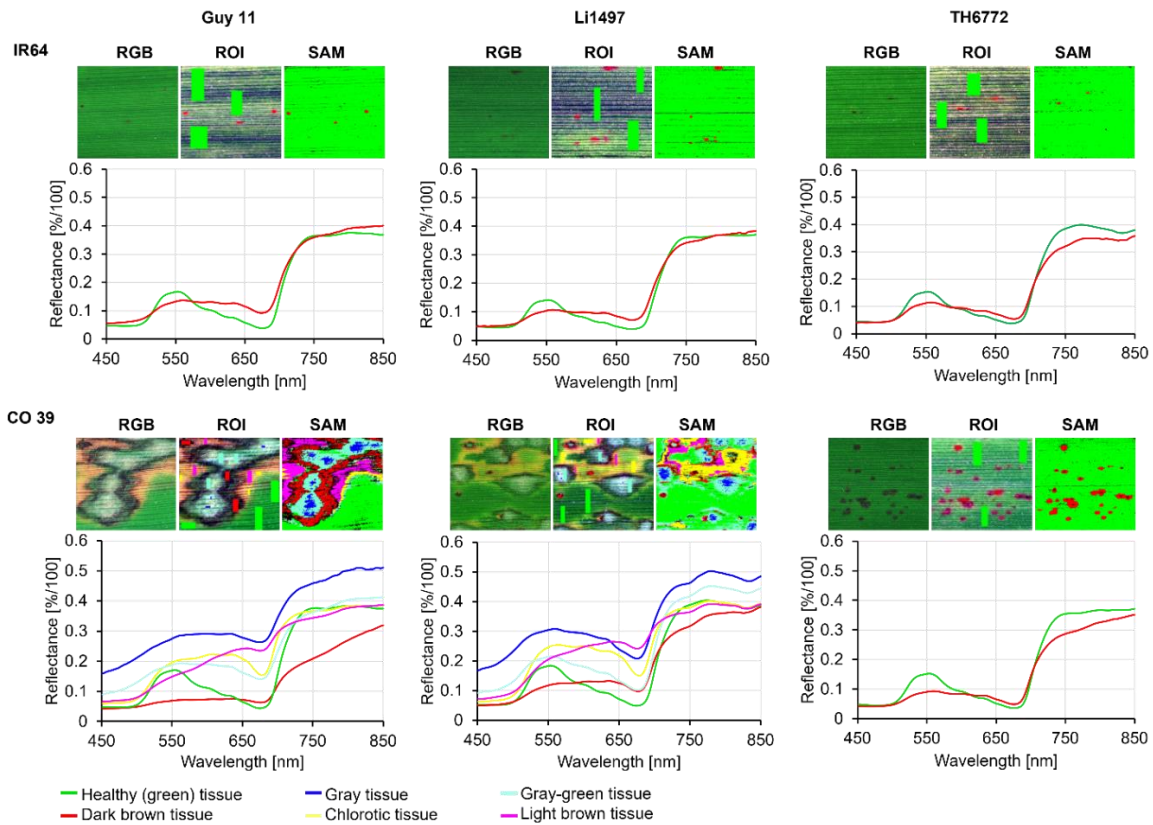


**Fig. 2.5.** Spectral characterization of different subareas of blast symptoms depending on host-pathogen compatibility: images illustrate RGB image, the choice of region of interest (ROI) for producing representative reflection spectra (endmembers), and spectral angle mapper (SAM) classification results, respectively. Rice genotype IR64 was resistant to isolates Guy 11, Li1497, and TH6772; genotype CO 39 was moderately resistant to isolate TH6772 but highly susceptible to isolates Guy 11 and Li1497.

#### 2.4.5 Spatio-temporal dynamics of spectral patterns during *M. oryzae* pathogenesis

The development of blast symptom types on rice leaves was examined during pathogenesis depending on host-pathogen compatibility using reflectance spectra at 3, 5, and 7 d.p.i. for SAM classification. In resistant interactions (e.g., IR64 infected with Guy 11 [Fig. 2.6], Li1497 [Supplementary Fig. S2.1], and TH6772 [Supplementary Fig. S2.2]), two classes, healthy and dark brown tissue types, were defined at 3, 5, and 7 d.p.i. In compatible rice  $\times$  *M. oryzae* interactions, the number and size of diseased tissue types increased as the disease progressed from 3 d.p.i. through 5 to 7 d.p.i. As demonstrated for ‘Nipponbare’ infected with Guy 11, the number of classes increased from two (healthy tissue and dark brown tissue) to four classes (healthy tissue, dark brown tissue, gray tissue, and gray-green tissue) 5 d.p.i. The complex ‘Nipponbare’  $\times$  *M. oryzae* interaction finally resulted in six classes (additional chlorotic and light brown tissues) (Fig. 2.6). For rice genotype CO 39, which is highly susceptible to isolate Guy 11, six classes were also defined at 7 d.p.i. Spectral signatures of

different subareas of typical leaf blast symptoms significantly differed from healthy rice tissue as well as from each other for the respective rice genotypes over time (Fig. 2.7; Supplementary Figs. S2.3 and S2.4). For the susceptible genotype CO 39, there was a change in tissue from one symptom type (= spectral class) to another with time. Each blast subarea corresponded to specific spectral signatures at distinct developmental stages in pathogenesis (Fig. 2.7).

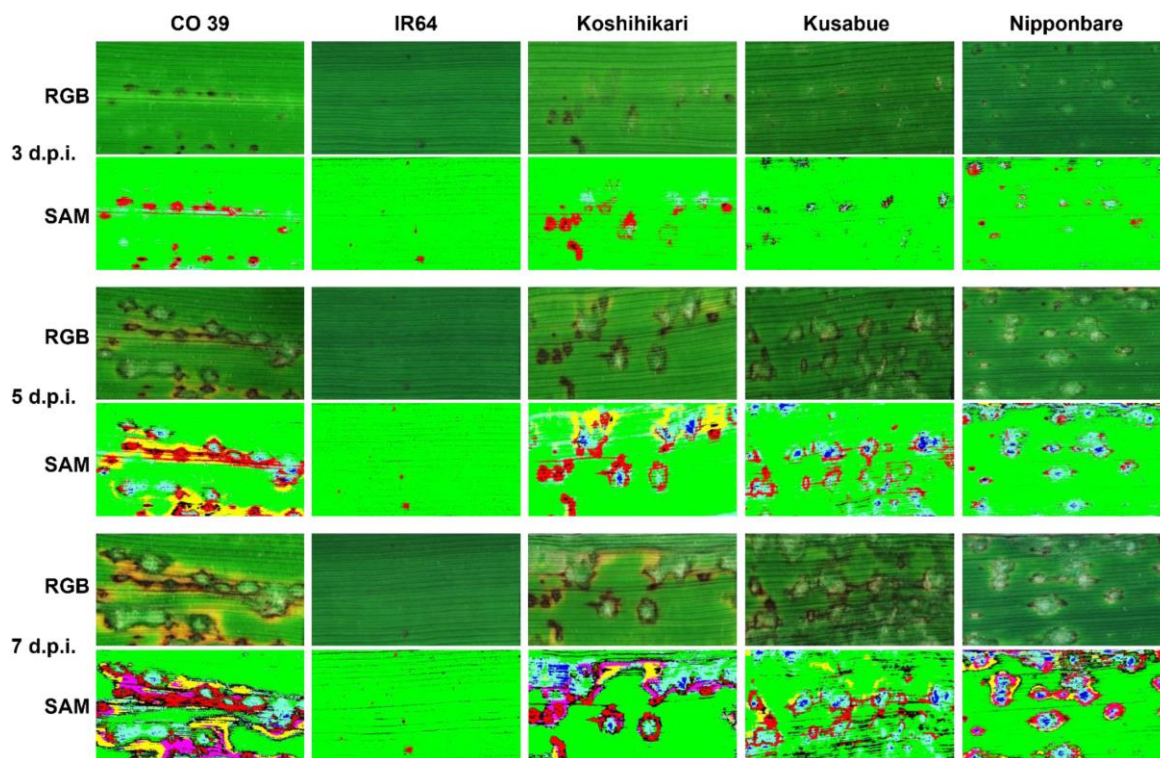


**Fig. 2.6.** Dynamics of blast symptom development and hyperspectral classification of reflectance according to spectral angle mapper (SAM) at different stages of pathogenesis for five rice genotypes inoculated with *Magnaporthe oryzae* isolate Guy 11. Different subareas of blast symptom types were classified in supervised classification by a SAM algorithm at 3, 5, and 7 days postinoculation (d.p.i.).

#### 2.4.6 Quantification of subareas of blast symptom types

Results of the image classification allowed for quantification of the subareas of blast symptom types according to their spectral characteristics (Table 2.2). Longitudinal measurements on the same leaf region demonstrated an increase in the size of leaf blast subareas during pathogenesis. For the resistant genotype IR64, the frequency of pixels in class ‘healthy’ was >95% at 7 d.p.i., the pathogenesis stage with mature blast symptoms. The high frequency of healthy tissue indicated high resistance to *M. oryzae* infection. For genotype CO 39, which was highly susceptible to isolate Guy 11, pixels of healthy tissue had a frequency <35% at 7 d.p.i., indicating high disease severity, a high frequency of pixels representing diseased tissue, and a high number of different tissue classes (Table

2.2). This number of symptom subareas increased with the compatibility of the host-pathogen interaction from one (resistant) to five (highly susceptible reaction). Significant differences ( $P < 0.05$ ) of blast symptom subareas for individual rice genotype  $\times$  *M. oryzae* interactions were observed (Table 2.2).

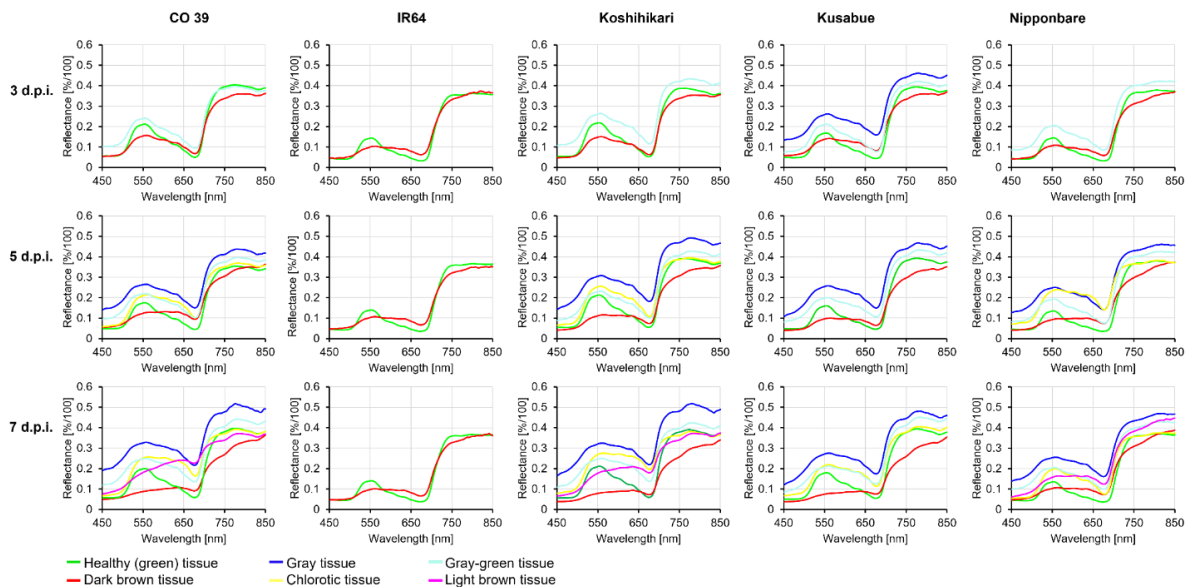


**Fig. 2.7.** Spectral signatures of healthy (green) and infected leaf tissue of five rice genotypes, CO 39, IR64, Koshihikari, Kusabue, and Nipponbare, inoculated with *Magnaporthe oryzae* isolate Guy 11 at 3, 5, and 7 days postinoculation (d.p.i.). For genotype IR64 (resistant), two classes were defined at all stages of pathogenesis. For the highly susceptible genotype CO 39, three, five, and six classes of blast symptom subareas were defined 3, 5, and 7 d.p.i., respectively.

## 2.5 Discussion

The pathogenesis of leaf blast on different rice genotypes was characterized on the tissue level using a HSI microscope. The gene-for-gene-specific interactions between genotypes of rice and isolates of *M. oryzae* resulted in large variation of leaf blast phenotypes (= symptom types). This is optimal as a database for disease phenotyping to be used in the screening of rice genotypes for disease resistance within breeding programs. Roumen (1992) reported on differential responses of 10 rice genotypes to leaf blast. Khadka et al. (2013) observed different blast reaction patterns among finger millet cultivars. In this study, initial necrotic lesions on resistant genotypes did not increase in size during pathogenesis and remained small and separate. The emergence of necrotic lesions due to the hypersensitive reaction (HR) and other defense responses inhibits tissue colonization on resistant rice genotypes (Campos-Soriano et al. 2013). In susceptible rice genotypes, initial necrotic spots on leaves were observed to increase to numerous, large, gray or whitish, and partly merging lesions due to rapid

fungal growth within the leaf tissue. This led to complex blast symptom types that covered a large area of the leaf surface, confirming earlier reports (Ribot et al. 2008; Roumen 1992; Talbot et al. 1993).

**Table 2.2.** Quantitative assessment of the compatibility in the interactions of five rice genotypes × three *Magnaporthe oryzae* isolates from hyperspectral imaging<sup>z</sup>

| <i>M. oryzae</i> isolate | Symptom sub-area       | Rice genotype (Mean ± SD) |                         |                           |                          |                          |
|--------------------------|------------------------|---------------------------|-------------------------|---------------------------|--------------------------|--------------------------|
|                          |                        | CO 39                     | IR64                    | Koshihikari               | Kusabue                  | Nipponbare               |
| Guy 11                   | Healthy (green) tissue | 30.2 <sup>a</sup> ± 6.3   | 97.8 <sup>a</sup> ± 0.5 | 72.4.0 <sup>a</sup> ± 6.3 | 53.2 <sup>a</sup> ± 9.3  | 67.2 <sup>a</sup> ± 4.4  |
|                          | Dark brown tissue      | 9.2 <sup>c</sup> ± 3.1    | 0.2 <sup>c</sup> ± 0.5  | 4.4 <sup>c</sup> ± 1.7    | 10.0 <sup>ab</sup> ± 2.9 | 6.0 <sup>bc</sup> ± 1.9  |
|                          | Gray tissue            | 2.4 <sup>d</sup> ± 1.5    | 0.0                     | 1.2 <sup>d</sup> ± 0.8    | 2.0 <sup>c</sup> ± 1.0   | 1.0 <sup>d</sup> ± 0.0   |
|                          | Chlorotic tissue       | 7.4 <sup>cd</sup> ± 3.2   | 0.0                     | 4.2 <sup>c</sup> ± 2.1    | 10.6 <sup>ab</sup> ± 6.5 | 6.1 <sup>bc</sup> ± 3.3  |
|                          | Gray-green tissue      | 18.2 <sup>ab</sup> ± 3.4  | 0.0                     | 10.6 <sup>ab</sup> ± 2.7  | 15.8 <sup>ab</sup> ± 3.9 | 10.8 <sup>ab</sup> ± 1.9 |
|                          | Light brown tissue     | 11.2 <sup>bc</sup> ± 5.7  | 0.0                     | 2.7 <sup>cd</sup> ± 0.6   | 2.0 <sup>c</sup> ± 0.0   | 3.0 <sup>cd</sup> ± 1.6  |
|                          | unclassified           | 21.0 <sup>a</sup> ± 3.9   | 1.6 <sup>b</sup> ± 0.6  | 6.40 <sup>bc</sup> ± 2.6  | 8.4 <sup>bc</sup> ± 3.9  | 5.6 <sup>c</sup> ± 2.5   |
| Li1497                   | Healthy (green) tissue | 32.8 <sup>a</sup> ± 10.0  | 97.0 <sup>a</sup> ± 0.7 | 46.2 <sup>a</sup> ± 6.9   | 97.6 <sup>a</sup> ± 1.1  | 58.2 <sup>a</sup> ± 10.2 |
|                          | Dark brown tissue      | 8.4 <sup>bc</sup> ± 2.9   | 1.4 <sup>b</sup> ± 0.6  | 6.0 <sup>de</sup> ± 2.5   | 1.0 <sup>b</sup> ± 0.7   | 6.8 <sup>bc</sup> ± 6.8  |
|                          | Gray tissue            | 2.0 <sup>d</sup> ± 1.0    | 0.0                     | 3.2 <sup>e</sup> ± 2.2    | 0.0                      | 3.2 <sup>c</sup> ± 3.3   |
|                          | Chlorotic tissue       | 7.4 <sup>bc</sup> ± 3.8   | 0.0                     | 6.8 <sup>cd</sup> ± 3.9   | 0.0                      | 7.8 <sup>bc</sup> ± 4.5  |
|                          | Gray-green tissue      | 30.4 <sup>a</sup> ± 11.0  | 0.0                     | 21.6 <sup>a</sup> ± 8.3   | 0.0                      | 14.8 <sup>ab</sup> ± 6.4 |
|                          | Light brown tissue     | 4.6 <sup>cd</sup> ± 3.1   | 0.0                     | 5.4 <sup>de</sup> ± 4.6   | 0.0                      | 1.0 <sup>c</sup> ± 0.0   |
|                          | unclassified           | 14.6 <sup>ab</sup> ± 8.0  | 2.2 <sup>b</sup> ± 0.8  | 11.2 <sup>bc</sup> ± 2.8  | 1.2 <sup>b</sup> ± 0.5   | 11.0 <sup>b</sup> ± 3.6  |
| TH6772                   | Healthy (green) tissue | 91.4 <sup>a</sup> ± 2.5   | 98.0 <sup>a</sup> ± 0.7 | 77.6 <sup>a</sup> ± 6.7   | 61.8 <sup>a</sup> ± 9.5  | 74.8 <sup>a</sup> ± 3.3  |
|                          | Dark brown tissue      | 5.2 <sup>b</sup> ± 1.6    | 0.2 <sup>b</sup> ± 0.5  | 5.0 <sup>bc</sup> ± 2.0   | 9.8 <sup>bc</sup> ± 5.4  | 4.4 <sup>bc</sup> ± 3.6  |
|                          | Gray tissue            | 0.0                       | 0.0                     | 0.8 <sup>d</sup> ± 0.5    | 3.8 <sup>c</sup> ± 1.5   | 1.1 <sup>c</sup> ± 0.6   |
|                          | Chlorotic tissue       | 0.0                       | 0.0                     | 1.8 <sup>d</sup> ± 2.4    | 8.0 <sup>bc</sup> ± 8.5  | 5 <sup>ab</sup> ± 3.3    |
|                          | Gray-green tissue      | 0.0                       | 0.0                     | 9.6 <sup>ab</sup> ± 3.2   | 14 <sup>ab</sup> ± 6.0   | 5 <sup>ab</sup> ± 1.2    |
|                          | Light brown tissue     | 0.0                       | 0.0                     | 1.5 <sup>cd</sup> ± 0.7   | 0.0                      | 0.0                      |
|                          | unclassified           | 3.4 <sup>b</sup> ± 0.9    | 1.4 <sup>b</sup> ± 0.6  | 4.6 <sup>bc</sup> ± 2.7   | 4.4 <sup>bc</sup> ± 3.3  | 9.2 <sup>ab</sup> ± 1.9  |

<sup>z</sup> Means followed by the same superscript letter in the same column for each *M. oryzae* isolate are not significantly different ( $P < 0.05$ ; Kruskal-Wallis test followed by Dunn’s multiple pairwise comparison test). SD = standard deviation. Pixel classification frequency (%) of different subareas of rice blast symptoms by spectral angle mapper (SAM) classification 7 days postinoculation (n = 5).

The rice genotypes differing in resistance to *M. oryzae* exhibited various blast phenotypes which resulted also in differences in disease severity (i.e., percentage diseased leaf area). The positive

correlation between disease severity and the blast symptom types was independent of the genotypes of the host and pathogen. Therefore, it should be possible to characterize the compatibility between (new) rice genotypes and *M. oryzae* isolates either by assessing the severity of leaf blast or the infection type of the specific rice × *M. oryzae* system. Because of the gene-for-gene-specific relationship in this host-pathogen system, screening approaches for blast resistance require the inoculation of several pathogen isolates differing in virulence. The resulting increased number of plots/plants makes automated disease scoring even more beneficial for the selection of appropriate rice accessions. Previous studies have reported the potential of HSI not only to detect diseases but also to differentiate among disease symptoms caused by various pathogen species that occur simultaneously on the same host plant species and among host cultivar reactions to pathogen attack (Leucker et al. 2016; Rumpf et al. 2010). In this study, HSI was suitable to distinguish rice × *M. oryzae* interactions differing in compatibility resulting from complex gene-for-gene interactions between host and pathogen genotypes. Among infection types, the variability of spectral characteristics was higher (= more informative) than the visual assessment of blast severity and symptom types. Infection types may differ from low to high even in quantitative resistance (of wheat and barley) to races of rust fungi (Kolmer 1996). In compatible interactions, the blast symptom types changed with the time of pathogenesis and reached a high complexity of mature symptoms. Therefore, early stages of pathogenesis were not suitable for rating of disease susceptibility/compatibility. In later stages, a mixture of blast symptom types occurred on leaves of a specific host-pathogen combination. However, limited variation ( $\pm 1$  type) in the reaction of plant tissue to the pathogen enabled the classification of rice genotypes into five levels of susceptibility/resistance. Thus, the ability to distinguish these differences in the reaction to *M. oryzae* may facilitate rice genotype selection in breeding for blast resistance.

The dynamics of spectral signatures between healthy and diseased rice leaf tissue differed. Noninfected leaf tissue displayed a typical low reflectance from 400 to 700 nm, a peak at 500 to 570 nm, a sharp reflectance increase at the red edge point, and a high reflectance plateau in the NIR (Kobayashi et al. 2001; Lowe et al. 2017; Zhou et al. 2018). In infected leaf tissue, the spectral reflectance in the visible range increased consistently, except for the dark brown tissue, which decreased reflectance compared with nondiseased tissue. The increase of reflectance in the VIS range results from the reduced absorption by photosynthetic pigments such as chlorophyll due to pigment degradation and decreased photosynthetic activity (Blackburn 2007; Mishra et al. 2020). A decrease in dry mass and changes in tissue structure causes an increased reflectance in the NIR region (Kobayashi et al. 2003; Tanner et al. 2022). Modifications in the NIR range related to structural

discontinuities indicate a higher degree of damage to the tissue due to successful colonization by the pathogen.

The progress of blast symptoms in rice leaves differed among the five host genotypes studied. The subareas of blast symptoms were associated with significant changes in reflectance over the full wavelength range. Our results confirm that it is possible to visualize and differentiate the development of lesions at different stages of pathogenesis. However, mature symptoms proved to be more complex and typical for host-pathogen compatibility than early stages with rather unspecific symptoms. Reflectance spectra of rice infected with panicle blast at different stages of grain development also showed differing spectral characteristics (from nonimaging hyperspectral measurements) over the developmental period (Kobayashi et al. 2001). Similarly, sugar beet diseases differed in their temporal and spatial development (Mahlein et al. 2012), and the influence on the spectral signatures was correlated to the intensity of physiological changes and the extent of the symptom expansion (Mahlein et al. 2010, 2012). Due to the progress of pathogenesis from early lesion to mature leaf blast symptoms, rating of the host-plant reaction to pathogen attack should focus on mature, more specific symptoms.

In susceptible genotypes, progress of blast symptoms during pathogenesis resulted from an increase in the number and in the size of leaf tissue types and a shift from one symptom type to the other. Blast lesions on rice enlarge due to the rapid growth and expansion of *M. oryzae* hyphae in the leaf tissue (Agbowuro et al. 2020; Boddy 2016). The spectral reflectance signatures of blast symptom subareas on rice genotypes differed even among stages of pathogenesis. Similarly, Mahlein et al. (2012) were able to investigate spatial patterns of discrete symptoms of CLS and other sugar beet diseases by pixel-wise assignment of spectral signatures. The hyperspectral reflectance pattern of CLS symptoms revealed different subareas depending on the genotype of the sugar beet and was linked to susceptibility, resistance, or tolerance (Mahlein et al. 2019). Changes in the spectral signature of diseased tissue indicate not only the manifestation of various disease phenotypes but may also provide information on the stage of pathogenesis.

Since SAM is a robust method that can handle complex spectral signatures, we used it to classify the various blast symptom type(s). The SAM classification algorithm uses the average spectrum of each endmember class (e.g., healthy tissue and different symptom characteristics) (Mahlein et al. 2012; Oerke et al. 2016). In this study, data were analyzed by using spectral libraries produced specifically for each time of image recording. Highly effective resistance (= low compatibility) resulted only in dark brown sites of infection. This class was also present in compatible interactions, which included additional tissue types that should be related to (rapid) fungal growth and spread in host tissue. Statistically, the correlation between disease severity and symptom type could be described by

an exponential equation better than by a linear equation, which reflects the higher diversity of symptoms in highly compatible interactions. The higher the number of classes, the higher the susceptibility of host genotype to pathogen genotype, while the lower the number of classes, the easier the classification.

The number of symptom classes alone was not suitable for precise classification and differentiation of rice × *M. oryzae* interactions, especially for highly susceptible, susceptible, and moderately susceptible genotypes. In case of two or more classes of diseased tissue, the overall percentage of leaf area with symptoms and the percentages of specific tissue types enabled classification of the compatibility level of host-pathogen interactions and the level of resistance of rice genotypes. The parameters and threshold levels indicated in Table 2.3 were suitable for rating the disease reaction of genotypes under the chosen experimental conditions. In practical plant breeding experiments, they have to be adjusted to (i) virulence of the pathogen isolate(s), (ii) inoculum density, (iii) developmental stage of plants at the time of inoculation influencing disease susceptibility, (iv) environmental conditions, and (v) the time of disease assessment. Moreover, application of HSI for disease phenotyping will enable symptom types to be assessed automatically using only a few plants. Standardization of the experimental conditions is crucial for the reliability of results of phenotyping experiments for resistance breeding, which have to be carried out under various environmental conditions (Mahlein 2016). When expanding the use of the sensor system to other host-pathogen systems, the parameters should be adapted to the symptom types which depend also on the lifestyle of the pathogens.

**Table 2.3.** Criteria for the classification of rice × *Magnaporthe oryzae* interactions by using information from hyperspectral images processed by the spectral angle mapper (SAM) algorithm

| Compatibility level    | Number of classes | Percent leaf area classified as |           |            |            |
|------------------------|-------------------|---------------------------------|-----------|------------|------------|
|                        |                   | Green                           | Chlorotic | Dark brown | Gray-green |
| Highly susceptible     | 5                 | <45                             | 6 – 7     | 6 – 9      | >15        |
| Susceptible            | 4 – 5             | 45 – 60                         | 8 – 11    | 7 – 10     | 10 – 15    |
| Moderately susceptible | 5                 | 60 – 85                         | 2 – 8     | 4 – 6      | 6 - 15     |
| Moderately resistant   | 1                 | 85 – 95                         | 0         | 2 – 8      | 0          |
| Resistant              | 1                 | >95                             | 0         | <2         | 0          |

HSI may be used to characterize disease symptoms by overall mean spectra of the respective tissue area affected (e.g., Bohnenkamp et al. 2021; Kuska et al. 2015). This approach requires a high amount of manual segmentation depending on the different symptom sizes and neglects the coalescing of symptoms. The diversity in symptom composition and size makes it impossible to derive symptom-specific spectral signatures (i.e., one spectrum per blast symptom [type]). The highly diverse symptoms (i.e., irregular shape and size of blast lesions varying from <1 mm to >10 mm in at least one dimension) are not suitable for identification by symptom type-specific signatures, but symptoms have to be classified and quantified by using the symptoms' details. However, quantification of typical blast subareas makes the method independent of the size and shape of symptoms and requires near-range imaging hardly suitable for in-field measurements.

Our study demonstrates the necessity to use several pathogen isolates in screening approaches for improved horizontal resistance of rice to *M. oryzae* (or mixture of isolates differing in virulence genes). Further investigations are required to establish the link between spectral characteristics and changes in tissue structure, pigmentation, and pathogen growth. The possibility of establishing a general hyperspectral library containing data corresponding to all different rice blast symptom types should be investigated because such system would be very beneficial for practical breeding for disease resistance.

## 2.6 Literature Cited

- Agbowuro, G. O., Afolabi, M. S., Olamiriki, E. F., and Awoyemi, S. O. 2020. Rice blast disease (*Magnaporthe oryzae*): A menace to rice production and humanity. Intern. J. Path. Res. 4:32-39.
- Alisaac, E., Behmann, J., Rathgeb, A., Karlovsky, P., Dehne, H.-W., and Mahlein, A.-K. 2019. Assessment of *Fusarium* infection and mycotoxin contamination of wheat kernels and flour using hyperspectral imaging. Toxins 11:556.
- Arens, N., Backhaus, A., Döll, S., Fischer, S., Seiffert, U., and Mock, H.-P. 2016. Non-invasive presymptomatic detection of *Cercospora beticola* infection and identification of early metabolic responses in sugar beet. Front. Plant Sci. 7: 1377.
- Bauriegel, E., Giebel, A., Geyer, M., Schmidt, U., and Herppich, W. B. 2011. Early detection of *Fusarium* infection in wheat using hyper-spectral imaging. Comput. Electron. Agric. 75:304-312.
- Bendel, N., Kicherer, A., Backhaus, A., Köckerling, J., Maixner, M., Bleser, E., Klück, H.-C., Seiffert, U., Voegelé, R. T., and Töpfer, R. 2020. Detection of grapevine leafroll-associated virus 1 and 3 in white and red grapevine cultivars using hyperspectral imaging. Remote Sens. 12:1693.
- Blackburn, G. A. 2007. Hyperspectral remote sensing of plant pigments. J. Exp. Bot. 58:855-867.

- Bock, C. H., Barbedo, J. G. A., Del Ponte, E. M., Bohnenkamp, D., and Mahlein, A.-K. 2020. From visual estimates to fully automated sensor-based measurements of plant disease severity: Status and challenges for improving accuracy. *Phytopathol. Res.* 2:9.
- Bock, C. H., Poole, G. H., Parker, P. E., and Gottwald, T. R. 2010. Plant disease severity estimated visually, by digital photography and image analysis, and by hyperspectral imaging. *Crit. Rev. Plant Sci.* 29:59-107.
- Boddy, L. 2016. Pathogens of autotrophs. Pages 245-292 in: *The Fungi*, 3rd ed. Elsevier Inc, Amsterdam, the Netherlands.
- Bohnenkamp, D., Behmann, J., Paulus, S., Steiner, U., and Mahlein, A.-K. 2021. A hyperspectral library of foliar diseases of wheat. *Phytopathology* 111: 1583-1593.
- Campos-Soriano, L., Val'e, G., Lupotto, E., and San Segundo, B. 2013. Investigation of rice blast development in susceptible and resistant rice cultivars using a *gfp* expressing *Magnaporthe oryzae* isolate. *Plant Path.* 62:1030-1037.
- Couch, B. C., and Kohn, L. M. 2002. A multilocus gene genealogy concordant with host preference indicates segregation of a new species, *Magnaporthe oryzae*, from *M. grisea*. *Mycologia* 94:683-693.
- Feng, L., Wu, B., Zhu, S., Wang, J., Su, Z., Liu, F., He, Y., and Zhang, C. 2020. Investigation on data fusion of multisource spectral data for rice leaf diseases identification using machine learning methods. *Front. Plant Sci.* 11:577063.
- Gelfond, J., Goros, M., Hernandez, B., and Bokov, A. F. 2018. A system for an accountable data analysis process in R. *R J.* 10:6-21.
- Huang, S., Qi, L., Ma, X., Xue, K., Wang, W., and Zhu, X. 2015. Hyperspectral image analysis based on BoSW model for rice panicle blast grading. *Comput. Electron. Agric.* 118:167-178.
- IRRI. 2002. Page 56 in: *Standard Evaluation System for Rice (SES)*. International Rice Research Institute, Manila, Philippines.
- IRRI. 2013. *Standard Evaluation System for Rice (SES)*, 5th ed. International Rice Research Institute, Manila, Philippines. [http://www.clrri.org/ver2/uploads/SES\\_5th\\_edition.pdf](http://www.clrri.org/ver2/uploads/SES_5th_edition.pdf)
- Khadka, R. B., Shrestha, S. M., and Manandhar, H. K. 2013. Pathogenic variability and differential interaction of blast fungus (*Pyricularia grisea* SACC.) isolates with finger millet lines in Nepal. *Nepal J. Sci. Tech.* 14:17-24.

- Kobayashi, T., Kanda, E., Kitada, K., Ishiguro, K., and Torigoe, Y. 2001. Detection of rice panicle blast with multispectral radiometer and the potential of using airborne multispectral scanners. *Phytopathology* 91:316-323.
- Kobayashi, T., Kanda, E., Naito, S., Nakajima, T., Arakawa, I., Nemoto, K., Honma, M., Toujyou, H., Ishiguro, K., Kitada, K., and Torigoe, Y. 2003. Ratio of rice reflectance for estimating leaf blast severity with a multispectral radiometer. *J. Gen. Plant Path.* 69:17-22.
- Kobayashi, T., Sasahara, M., Kanda, E., Ishiguro, K., Hase, S., and Torigoe, Y. 2016. Assessment of rice panicle blast disease using airborne hyperspectral imagery. *Open Agric. J.* 10:28-34.
- Kolmer, J. A. 1996. Genetics of resistance to wheat leaf rust. *Ann. Rev. Phytopathol.* 34:435-455.
- Kruse, F. A., Lefkoff, A. B., Boardman, J. W., Heidebrecht, K. B., Shapiro, A. T., Barloon, P. J., and Goetz, A. F. H. 1993. The spectral image processing system (SIPS)—interactive visualization and analysis of imaging spectrometer data. *Remote Sens. Environ.* 44:145-163.
- Kuching, S. 2007. The performance of maximum likelihood, spectral angle mapper, neural network and decision tree classifiers in hyperspectral image analysis. *J. Comp. Sci.* 3:419-423.
- Kuska, M., Wahabzada, M., Leucker, M., Dehne, H.-W., Kersting, K., Oerke, E.-C., Steiner, U., and Mahlein, A.-K. 2015. Hyperspectral phenotyping on the microscopic scale: Towards automated characterization of plant-pathogen interactions. *Plant Meth.* 11:28.
- Kuska, M. T., Brugger, A., Thomas, S., Wahabzada, M., Kersting, K., Oerke, E.-C., Steiner, U., and Mahlein, A.-K. 2017. Spectral patterns reveal early resistance reactions of barley against *Blumeria graminis* f. sp. *hordei*. *Phytopathology* 107:1388-1398.
- Leucker, M., Mahlein, A.-K., Steiner, U., and Oerke, E.-C. 2016. Improvement of lesion phenotyping in *Cercospora beticola*-sugar beet interaction by hyperspectral imaging. *Phytopathology* 106:177-184.
- Lowe, A., Harrison, N., and French, A. P. 2017. Hyperspectral image analysis techniques for the detection and classification of the early onset of plant disease and stress. *Plant Meth.* 13:80.
- Mahlein, A.-K. 2016. Plant disease detection by imaging sensors – parallels and specific demands for precision agriculture and plant phenotyping. *Plant Dis.* 100:241-251.
- Mahlein, A.-K., Kuska, M. T., Behmann, J., Polder, G., and Walter, A. 2018. Hyperspectral sensors and imaging technologies in phytopathology: State of the art. *Annu. Rev. Phytopathol.* 56:535-558.
- Mahlein, A.-K., Kuska, M. T., Thomas, S., Wahabzada, M., Behmann, J., Rascher, U., and Kersting, K. 2019. Quantitative and qualitative phenotyping of disease resistance of crops by hyperspectral

- sensors: Seamless interlocking of phytopathology, sensors, and machine learning is needed. *Curr. Opin. Plant Bio.* 50:156-162.
- Mahlein, A.-K., Steiner, U., Dehne, H.-W., and Oerke, E.-C. 2010. Spectral signatures of sugar beet leaves for the detection and differentiation of diseases. *Prec. Agric.* 11:413-431.
- Mahlein, A.-K., Steiner, U., Hillnhütter, C., Dehne, H.-W., and Oerke, E.-C. 2012. Hyperspectral imaging for small-scale analysis of symptoms caused by different sugar beet diseases. *Plant Meth.* 8:3-13.
- Mishra, P., Polder, G., and Vilfan, N. 2020. Close range spectral imaging for disease detection in plants using autonomous platforms: A review on recent studies. *Curr. Robot. Rep.* 1:43-48.
- Mutka, A. M., and Bart, R. S. 2014. Image-based phenotyping of plant disease symptoms. *Front. Plant Sci.* 5:734.
- Oerke, E.-C. 2020. Remote sensing of diseases. *Ann. Rev. Phytopath.* 58:225-252.
- Oerke, E.-C., Herzog, K., and Toepfer, R. 2016. Hyperspectral phenotyping of the reaction of grapevine genotypes to *Plasmopara viticola*. *J. Exp. Bot.* 67:5529-5543.
- Ou, S. H. 1980. Pathogen variability and host resistance in rice blast disease. *Ann. Rev. Phytopathol.* 18:167-187.
- Ou, S. H. 1985. *Rice Diseases*, 2nd ed. Commonwealth Mycological Institute, Kew, U.K.
- Ribot, C., Hirsch, J., Balzergue, S., Tharreau, D., Nott´eghem, J.-L., Lebrun, M.-H., and Morel, J.-B. 2008. Susceptibility of rice to the blast fungus, *Magnaporthe grisea*. *J. Plant Physiol.* 165:114-124.
- Roumen, E. C. 1992. Effect of leaf age on components of partial resistance in rice to leaf blast. *Euphytica* 63:271-279.
- Rumpf, T., Mahlein, A. K., Steiner, U., Oerke, E. C., Dehne, H. W., and Plümer, L. 2010. Early detection and classification of plant diseases with support vector machines based on hyperspectral reflectance. *Comp. Electron. Agric.* 74:91-99.
- Savitzky, A., and Golay, M. J. E. 1964. Smoothing and differentiation of data by simplified least squares procedures. *Analy. Chem.* 36:1627-1639.
- Takabayashi, N., Tosa, Y., Oh, H. S., and Mayama, S. 2002. A gene-for-gene relationship underlying the species-specific parasitism of *Avena/Triticum* isolates of *Magnaporthe grisea* on wheat cultivars. *Phytopathology* 92:1182-1188.
- Talbot, N. J., Ebbole, D. J., and Hamer, J. E. 1993. Identification and characterization of *MPG1*, a gene involved in pathogenicity from the rice blast fungus *Magnaporthe grisea*. *Plant Cell* 5:1575-1590.

- Tanner, F., Tonn, S., de Wit, J., Van den Ackerveken, G., Berger, B., and Plett, D. 2022. Sensor-based phenotyping of above-ground plant-pathogen interactions. *Plant Meth.* 18:35.
- Thomas, S., Kuska, M. T., Bohnenkamp, D., Brugger, A., Alisaac, E., Wahabzada, M., Behmann, J., and Mahlein, A. K. 2018. Benefits of hyperspectral imaging for plant disease detection and plant protection: A technical perspective. *J. Plant Dis. Prot.* 125:5-20.
- Zhang, G., Xu, T., and Tian, Y. 2022a. Hyperspectral imaging-based classification of rice leaf blast severity over multiple growth stages. *Plant Meth.* 18:123.
- Zhang, G., Xu, T., Tian, Y., Feng, S., Zhao, D., and Guo, Z. 2022b. Classification of rice leaf blast severity using hyperspectral imaging. *Sci. Rep.* 12:19757.
- Zhao, D., Feng, S., Cao, Y., Yu, F., Guan, Q., Li, J., Zhang, G., and Xu, T. 2022. Study on the classification method of rice leaf blast levels based on fusion features and adaptive-weight immune particle swarm optimization extreme learning machine algorithm. *Front. Plant Sci.* 13:879668.
- Zheng, Z., Qi, L., Ma, X., Zhu, X., and Wang, W. 2013. Grading method of rice leaf blast using hyperspectral imaging technology. *Trans. Chin. Soc. Agric. Eng.* 29:138-144.
- Zhou, R.-Q., Jin, J.-J., Li, Q.-M., Su, Z.-Z., Yu, X.-J., Tang, Y., Luo, S.-M., He, Y., and Li, X.-L. 2018. Early detection of *Magnaporthe oryzae*-infected barley leaves and lesion visualization based on hyperspectral imaging. *Front. Plant Sci.* 9:1962.

2.7 Supplementary Data

**Table S2.1:** Visual assessment of rice blast severity on 5 rice genotypes infected with 3 genotypes of *M. oryzae* 3, 5 and 7 days post inoculation (d.p.i.).

| <i>M. oryzae</i> isolates | Rice genotypes | Days post inoculation (Mean ± SEM) |                           |                          |
|---------------------------|----------------|------------------------------------|---------------------------|--------------------------|
|                           |                | 3                                  | 5                         | 7                        |
| Guy 11                    | CO 39          | 15.0 <sup>a</sup> ± 2.5            | 47.5 <sup>a</sup> ± 5.4   | 73.4 <sup>a</sup> ± 5.7  |
|                           | IR64           | 1.0 <sup>b</sup> ± 0               | 1.0 <sup>e</sup> ± 0      | 1.0 <sup>d</sup> ± 0     |
|                           | Koshihikari    | 2.9 <sup>b</sup> ± 0.6             | 30.6 <sup>abc</sup> ± 4.3 | 50.3 <sup>b</sup> ± 4.6  |
|                           | Kusabue        | 3.2 <sup>b</sup> ± 0.5             | 43.8 <sup>abc</sup> ± 5.1 | 60.3 <sup>ab</sup> ± 6.4 |
|                           | Nipponbare     | 3.9 <sup>b</sup> ± 1.5             | 35.9 <sup>abc</sup> ± 6.8 | 56.9 <sup>ab</sup> ± 5.4 |
| Li1497                    | CO 39          | 16.0 <sup>a</sup> ± 2.6            | 51.3 <sup>a</sup> ± 5.5   | 75.9 <sup>a</sup> ± 5.6  |
|                           | IR64           | 1.4 <sup>b</sup> ± 0.4             | 1.8 <sup>de</sup> ± 0.4   | 1.8 <sup>d</sup> ± 0.4   |
|                           | Koshihikari    | 6.5 <sup>b</sup> ± 1.9             | 49.1 <sup>a</sup> ± 5.2   | 72.5 <sup>a</sup> ± 5.1  |
|                           | Kusabue        | 1.0 <sup>b</sup> ± 0               | 1.3 <sup>e</sup> ± 0.3    | 1.3 <sup>d</sup> ± 0.4   |
|                           | Nipponbare     | 4.8 <sup>b</sup> ± 1.4             | 41.9 <sup>abc</sup> ± 6.5 | 67.5 <sup>ab</sup> ± 5.1 |
| TH6772                    | CO 39          | 21.6 <sup>a</sup> ± 2.9            | 23.1 <sup>cd</sup> ± 3.4  | 25.6 <sup>c</sup> ± 2.9  |
|                           | IR64           | 0.9 <sup>b</sup> ± 0.1             | 1.0 <sup>e</sup> ± 0      | 1.0 <sup>d</sup> ± 0     |
|                           | Koshihikari    | 2.0 <sup>b</sup> ± 0.4             | 24.7 <sup>bc</sup> ± 3.8  | 48.8 <sup>b</sup> ± 4.8  |
|                           | Kusabue        | 1.3 <sup>b</sup> ± 0.3             | 45.6 <sup>ab</sup> ± 6.8  | 65.0 <sup>ab</sup> ± 5.0 |
|                           | Nipponbare     | 1.8 <sup>b</sup> ± 0.4             | 32.8 <sup>abc</sup> ± 3.0 | 57.5 <sup>ab</sup> ± 4.0 |

Means followed by the same superscript letter in the same column for each *M. oryzae* isolate are not significantly different (n = 16; P < 0.05; Tukey's HSD test). SEM; Standard error of the mean.

**Table S2.2:** ANOVA analysis for the effect of *M. oryzae* isolates, rice genotypes and *M. oryzae* isolates x rice genotype interaction on leaf blast severity.

|  | Df  | Sum Sq | Mean Sq | F value | Pr(>F)  |
|--|-----|--------|---------|---------|---------|
| <i>M. oryzae</i> isolate                 | 2   | 3107   | 1553    | 5.19    | 0.006   |
| Rice genotype                            | 4   | 118987 | 29747   | 99.39   | < 0.001 |
| <i>M. oryzae</i> isolate x Rice genotype | 8   | 69159  | 8645    | 28.88   | < 0.001 |
| Residuals                                | 225 | 67343  | 299     |         |         |

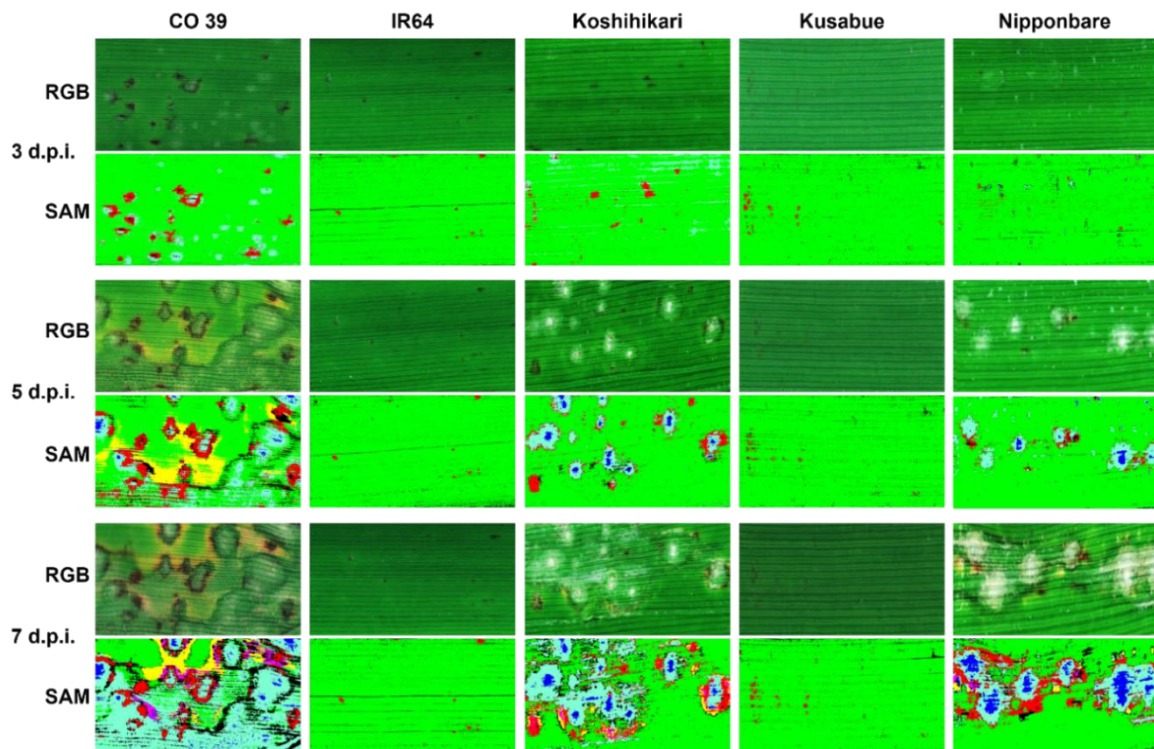


**Fig. S2.1.** Dynamics of blast symptom development and hyperspectral classification of reflectance according to spectral angle mapper (SAM) at different stages of pathogenesis for five rice genotypes inoculated with Li1497. Different subareas of blast symptom types were classified in supervised classification by spectral angle mapper (SAM) algorithm at 3, 5 and 7 days post inoculation (d.p.i.).

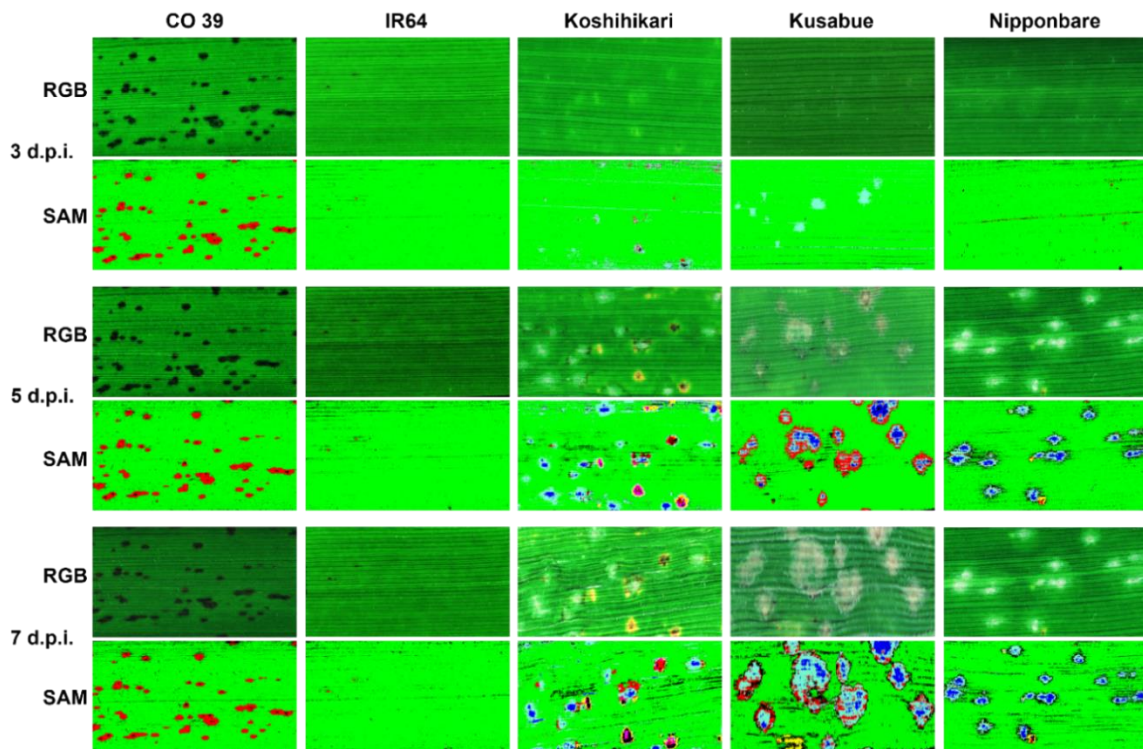


**Fig. S2.2.** Dynamics of blast symptom development and hyperspectral classification of reflectance according to spectral angle mapper (SAM) at different stages of pathogenesis for five rice genotypes inoculated with TH6772. Different subareas of blast symptom types were classified in supervised classification by spectral angle mapper (SAM) algorithm at 3, 5 and 7 days post inoculation (d.p.i.).

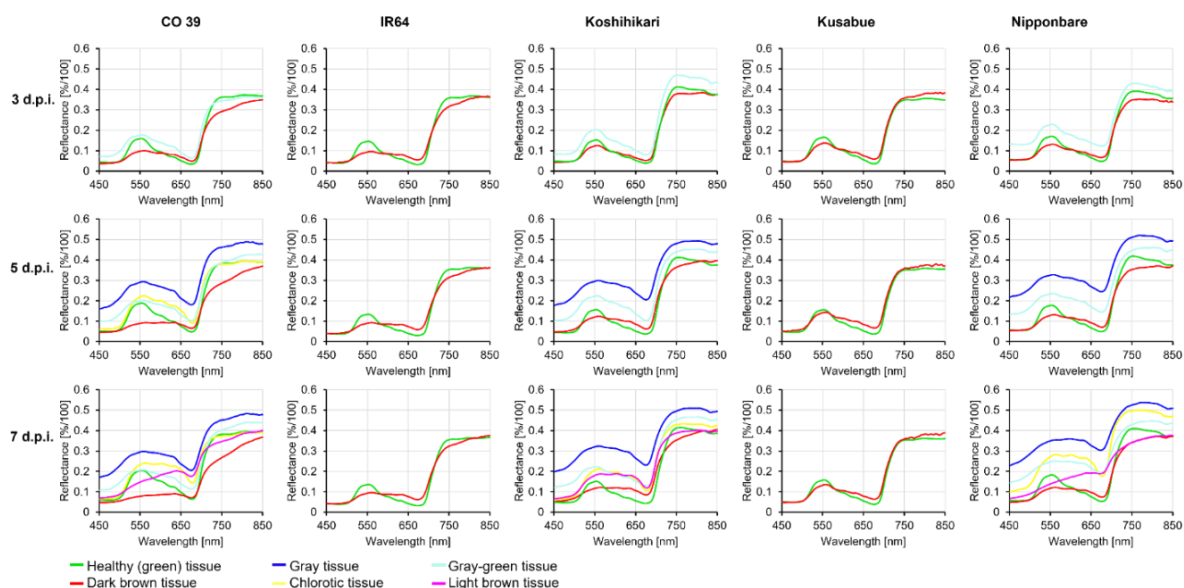


**Fig. S2.3.** Spectral signatures of healthy (green) and infected leaf tissue of five rice genotypes CO 39, IR64, Koshihikari, Kusabue, Nipponbare inoculated with *M. oryzae* isolate Li1497 at 3, 5 and 7 days post inoculation (d.p.i.). For genotype IR64 (resistant) and Kusabue (resistant) two classes were defined at all stages of pathogenesis. For genotypes Koshihikari and Nipponbare, three, four and five classes of blast symptom subareas were defined 3, 5 and 7 days post inoculation (d.p.i.), respectively; For genotype CO 39 (highly susceptible), three, five and six classes of blast symptom subareas were defined 3, 5 and 7 days post inoculation (d.p.i.), respectively.

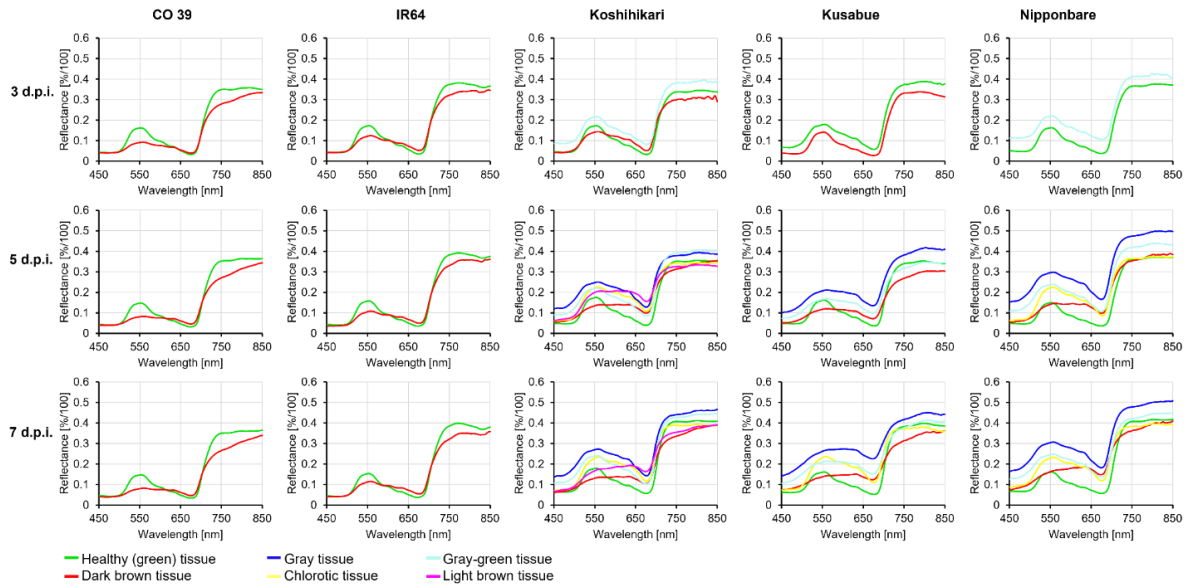


**Fig. S2.4.** Spectral signatures of healthy (green) and infected leaf tissue of five rice genotypes CO 39, IR64, Koshihikari, Kusabue, Nipponbare inoculated with *M. oryzae* isolate TH6772 at 3, 5 and 7 days post inoculation (d.p.i.). For genotype IR64 (resistant) and CO 39 (moderately resistant) two classes of blast symptom subareas were defined at all stages of pathogenesis. For genotypes Koshihikari, three and six classes of blast symptom subareas were defined 3, 5 and 7 days post inoculation (d.p.i.), respectively; Kusabue genotype, three and four classes of blast symptom subareas were defined 3, 5 and 7 days post inoculation (d.p.i.), respectively; For genotype Nipponbare, three and five classes of blast symptom subareas were defined 3, 5 and 7 days post inoculation (d.p.i.), respectively.

### 3 Assessing interactions between nitrogen supply and leaf blast in rice by hyperspectral imaging

Chapter 3 has been published:

**Angeline Wanjiku Maina**<sup>1</sup>, Mathias Becker<sup>2</sup> and Erich-Christian Oerke<sup>1\*</sup>, 2024. Assessing interactions between nitrogen supply and leaf blast in rice by hyperspectral imaging. *Remote Sensing*, 16(6), 939. <https://doi.org/10.3390/rs16060939>

<sup>1</sup>Institute for Crop Science and Resource Conservation (INRES) - Plant Pathology, Rheinische Friedrich-Wilhelms University of Bonn, Germany

<sup>2</sup>Institute for Crop Science and Resource Conservation (INRES) - Plant Nutrition, Rheinische Friedrich-Wilhelms University of Bonn, Germany

#### Author contributions

**A.W.M.**, E.-C.O. and M.B. designed the experiment. **A.W.M.** performed the experiments; she carried out the hyperspectral measurements, analyzed the data, and drafted the manuscript. All authors have read and agreed to the published version of the manuscript.

### 3.1 Abstract

Mineral nitrogen (N) supply reportedly increases rice susceptibility to the fungal pathogen *Magnaporthe oryzae* causing blast disease. These biotic and abiotic factors cause changes in spectral reflectance of leaves; however, the effects of N × pathogen interactions on spectral characteristics of rice have not been studied. In this study, hyperspectral imaging was used to assess the effect of N supply on symptoms of rice leaf blast under greenhouse conditions. Three rice genotypes differing in blast susceptibility grown at low, medium, and high N supply were inoculated at the four-leaf stage with three *M. oryzae* isolates differing in virulence. The reflectance spectra (400 to 1000 nm) of healthy and symptomatic leaves were analyzed using the spectral angle mapper algorithm for supervised classification. Mineral N supply increased the contents of chlorophyll and total N. The number and area of lesions and total blast severity varied depending on rice genotype—*M. oryzae* isolate interactions and the amount of mineral N applied. The reflectance spectra of healthy tissue and of blast symptom subareas differed with N supply; rice genotypes differed in the response to N supply. Infected plants at high mineral N supply could be distinguished from those at low N supply due to higher differences in the spectra of symptom subareas. Results reveal the potential (and limitations) of hyperspectral imaging for quantifying N effects on rice leaves, disease severity, and symptom expression. The impact of these findings on plant phenotyping and remote sensing under field conditions is discussed.

Keywords: *Magnaporthe oryzae*; nitrogen application; *Oryza sativa*; spectral reflectance; symptom type

### 3.2 Introduction

Nitrogen (N) is essential for plant growth, and N deficiency is widely limiting rice production [1]. While N deficiency reduces crop productivity, excessive mineral N application can lead to negative environmental effects [2] and increases the impact of crop diseases caused by foliar pathogens [3]. Optimizing N application according to the crops' specific needs and through precision farming will not only enhance the N use efficiency but may also reduce the risk and the severity of crop diseases.

Mineral N fertilizer is known to affect the level of pathogen infection in plants, with higher N being correlated with increased host tissue susceptibility to diseases in wheat [4] and a number of other crops [5]. In rice, high N is reportedly associated with increased susceptibility to blast caused by the hemibiotrophic ascomycetous fungus *Magnaporthe oryzae* [6]. It is the most important pathogen in rice production worldwide, causing leaf and panicle blast, and resulting in yield losses [7]. Several studies have documented an increase in the severity of rice blast due to high N application rates [8,9]. High doses of N fertilizer accelerate plant growth, increasing the canopy density, thus creating a

favorable microclimate for the development of the blast pathogen [6]. The effect of N on the disease is also mediated via an increased availability of nitrogenous compounds in rice tissues, which are substrates for pathogen growth [5]. While high N supply stimulates the development of the pathogen [10], also a limited N availability to *M. oryzae* on plant surfaces reportedly stimulate the expression of effector genes, e.g., hydrophobin *MPG1*, thus increasing the blast susceptibility of rice [11].

The chemical methods currently used for assessing N in crops are destructive and involve tedious procedures [12]. The non-destructive determination of the leaf greenness (proxy for N content) by chlorophyll meter (SPAD-502) has increasingly replaced destructive sampling and chemical N analysis. However, such photometric measurements disregard leaf chlorosis caused by nutrients other than N (e.g., magnesium, sulfur, iron, zinc) and are limited to spectral bands at 650 and 940 nm, potentially overlooking important information in other regions of the spectrum [13]. SPAD may also fail to distinguish differences in N nutritional status of plants under high N conditions [12]. Likewise, conventional methods of monitoring plant diseases mainly rely upon visual plant inspection, which is time-consuming, labor-intensive, subjective, and unable to monitor the severity of diseases over large areas [14,15].

Optical sensing techniques provide a non-invasive and efficient way for evaluating both abiotic and biotic stresses in plants [14]. Non-imaging reflectance spectroscopy has proven effective in assessing both the crop's N status [16,17] and plant diseases [18,19]. However, this method averages spectral data over a field of view, without providing information on the spatial distribution of the measured parameters [20]. While low spatial resolutions may suffice to assess abiotic stresses that affect all plant parts, pathogen infections are highly restricted to specific plant tissues, at least in the early stages of epidemics, and consequently require high spatial resolutions of the sensing system.

Hyperspectral imaging (HSI) has proven to be an effective way to detect plant diseases as well as to monitor the nutritional status of crops [21,22]. It captures high-resolution spectral and spatial information of crops in the visible (VIS; 400 to 700 nm) and near-infrared (NIR; 700 to 1000 nm) ranges of the spectrum, which is associated with important biochemical and biophysical properties of the plant [23]. This technology detects rapidly and non-destructively changes in important indicators of plant health, such as the status of leaf pigments, the leaf water and nutrient contents, and leaf structure [15,24]. Numerous studies have documented HSI to effectively determine both the crop's nutritional status [25,26], and to diagnose plant diseases, including *Fusarium* in wheat [27], leaf diseases in sugar beet [28], and *Plasmopara viticola* in grapevine [21]. In rice, HSI has been used for assessing blast on panicles [29] and on leaves [30]. Maina and Oerke [31] demonstrated the suitability of HSI for assessing the gene-for-gene-specific interactions between genotypes of *Oryza sativa* and *M. oryzae*. These studies used HSI to assess either the crop nutrient status or plant diseases separately.

HSI provides spectral details for each pixel, enabling the assessment of spatial and spectral patterns of affected leaf tissues. While abiotic and biotic factors affect the same plant tissue at the same time, the mixed effect is displayed within the same pixel(s) of an image. Hyperspectral data have successfully discriminated combined stresses, e.g., symptoms caused by N deficiency and stripe rust infection in wheat [32], and the distribution of chlorophyll and carotenoids in cucumber leaves infected by angular leaf spot [33]. Liu and colleagues [34] successfully monitored wheat powdery mildew under different N levels using a spectrometer. Leaf rust-infected wheat leaves could be distinguished from N-deficient leaves because of the higher spatial variability of the chlorophyll fluorescence ratio at 686 and 740 nm [35]. Despite these promising reports for discriminating biotic and abiotic factors, no study to date has used HSI for simultaneously measuring the effects of different rates of N supply and of blast infection on rice, and generally on potential interactions of combinations of biotic and abiotic factors on spectral reflectance of rice tissues.

The hypothesis was that HSI can visualize and differentiate the effects of both mineral N supply, leaf blast infection, as well as their interactions. Consequently, HSI was applied to investigate the interactive effects of three mineral N application rates and of three *M. oryzae* isolates in three rice genotypes. Selected blast isolates differed in their virulence, while rice genotypes differed in their blast resistance. The study addressed the following specific objectives: (i) determine growth responses, leaf chlorophyll and total N contents, and spectral leaf characteristics of rice genotypes at increasing mineral N supply; (ii) assess effects of mineral N supply on the severity of leaf blast; and (iii) quantify spectral variations of blast symptom subareas of rice genotypes subjected to different mineral N application rates. Ultimately, the study aimed at understanding the potential of HSI as an integrated tool for monitoring disease response in relation to the nutritional status of rice.

### 3.3 Materials and Methods

#### 3.3.1 Origin and cultivation of rice and blast isolates

Three rice (*Oryza sativa* L.) genotypes were used in this study, comprising CO 39 (accession number IRGC 51231, obtained from IRRI, Philippines), IR64, and Nipponbare (provided by Michael Frei, Department for Plant Nutrition, University of Bonn). They represent the prevailing diversity of rice types and reported blast susceptibility, with CO 39 (*indica* type) representing the highly susceptible reference genotype, IR64 being a reportedly blast-resistant *indica* type, and Nipponbare being a susceptible *japonica* type.

Seeds were sown directly into pots (Ø 9 cm, height 6.8 cm) (Kausek, Mittenwalde, Germany), filled with 0.3 kg of loam soil at 5 seeds per pot. Plants were grown in the greenhouse at day/night

temperature of 25/22°C. The supplemental light simulated a 12 h photoperiod (7:00 to 19:00 h). Relative humidity (RH) was maintained at approximately 60% (every 15 min, spells of 1 min misting the air to increase RH). Eighteen days after sowing, the rice plants were divided into three groups receiving different mineral N application rates: low-N fertilizer (no supplementary mineral N fertilizer (0 mg Nmin/kg soil)), medium-N fertilizer (adding 75 mg Nmin/kg soil of ammonium-nitrate-N, corresponding to 125 kg N/ha), and high-N fertilizer (adding 150 mg Nmin/kg soil of ammonium-nitrate-N, corresponding to 250 kg N/ha). All treatments received NPKMg and trace elements in the form of *NovaTec® Classic* (COMPO EXPERT GmbH, Krefeld, Germany) four days before inoculation.

The experiment was carried out twice, with a total of 117 pots for each experiment. The pots were divided into three groups: (1) a set of 45 pots were used (three rice genotypes, three N treatments, and five replications (pots) per treatment) for the SPAD and total nitrogen (N) analysis; (2) 54 pots were used (three rice genotypes, three N treatments, three pathogen isolates, and two replications) for pathogen inoculation; (3) 18 pots were used (three rice genotypes, three N treatments, and two replications) for non-inoculated control plants.

As interactions between rice and *M. oryzae* are gene-for-gene-specific, three isolates were used for inoculating rice leaves, comprising isolate Guy 11 (supplied by Didier Tharreau, CIRAD, Montpellier, France), isolate Li1497 (obtained from BASF, Limburgerhof, Germany), and isolate TH6772 (provided by Ulrich Schaffrath, University of Aachen, Germany). All isolates were cultivated on rice leaf agar medium. Conidia were produced, and the inoculum prepared as described [31]. At the 4-leaf stage (22-day-old seedlings), rice plants were spray-inoculated with a *M. oryzae* conidia suspension ( $10^5 \text{ mL}^{-1}$ ), using a hand sprayer. Inoculated plants were kept in a dark moist incubation chamber at 25°C and >95% of RH for 24 h, before being returned to the greenhouse. During the incubation period, healthy (non-inoculated) control plants were maintained at 25°C and 60% RH. The experiment was performed two times.

### 3.3.2 Measurements of leaf chlorophyll and N content

The relative chlorophyll content (leaf greenness) was estimated as a proxy for the leaf N content using a SPAD-502 m (Konica Minolta, Inc., Osaka, Japan) [36]. The SPAD values were determined from the three uppermost fully expanded leaves of each individual plant four days after mineral N application. Three composite SPAD readings were taken from the base, the middle, and the tip of each leaf. Five plants were measured from every pot and the SPAD readings were averaged to represent the mean value of each pot. Each experiment consisted of 45 pots, whereby the average of 5 composite SPAD values was recorded separately for each genotype and each mineral N treatment (n = 5 replications).

After recording of SPAD values, the aboveground biomass of rice plants was obtained for the analysis of total N content, following oven drying at 70°C for 72 h and subsequently mill-grinding (Wiley Mill, Thomas Scientific, Philadelphia, PA, USA). Total N content was analyzed by Duma's combustion method using a CNS elemental analyzer (Model: EUROEAP, EuroVector, Milan, Italy). The experimental unit for dry matter and N content was the biomass per pot (n = 5).

### **3.3.3 Measurement of leaf reflectance of spectral information**

Hyperspectral images of healthy leaves were recorded 4 and 11 days after mineral N supply, and 7 days post inoculation (dpi) for diseased leaves. Spectral reflectance was obtained under controlled conditions in a dark room using an ImSpector V10E hyperspectral imaging system (Specim, Spectral Imaging Ltd., Oulu, Finland) at a spectral range of 400–1000 nm, and with 2.8 nm spectral resolution (212 wavebands). The line-scanning spectrograph capturing 1600 pixels per line was mounted on a stereo microscope foreoptic (Z6 APO, Leica, Wetzlar, Germany) equipped with an OLE-23 lens (Spectral Imaging Ltd., Oulu, Finland). Plant leaves were positioned on a XY-motorized table (H105/2/0 ProScan Upright Stage, Prior Scientific, Jena, Germany), which was moved below the optical system, resulting in the recording of spectral data cubes for imaging approaches. The working distance between leaf tissue and optical lens was 105 mm; a 3.6x magnification resulted in a spatial resolution of 6.3 µm per pixel. Two linear line lights attached to a 150 W cold light source (Schott, Mainz, Germany) via a non-absorbing fiber (DCR® Light Source EKE, Polytec, Waldbronn, Germany) provided homogenous illumination. The instrument was warmed-up for 60 min before measurements were taken to maintain constant and reproducible illumination and constant sensitivity of the sensor unit.

For image recording, a single leaf attached to the rice plant was placed flat on the stage. Four hyperspectral images were taken for each sample, using the software Lumo Recorder® (Spectral Imaging Ltd., Oulu, Finland): (i) an image of the object area of interest with an optimized exposure time; (ii) a dark current image of the object; (iii) an image of a white reference bar (Zenith Polymer Target, SphereOptics GmbH., Uhldingen-Mühlhofen, Germany); and (iv) a dark current image of the white reference. In each mineral N treatment, spectra from four leaves per genotype were measured. A total of 72 leaf images (2 time steps × 3 genotypes × 3 N levels × 4 replications) were analyzed for non-inoculated plants, and 108 leaves (3 × 3 × 3 × 4 replicates) in inoculated plants.

### **3.3.4 Pre-processing of hyperspectral images**

Hyperspectral images were pre-processed using IDL 8.3/ENVI 5.3 software (ITT Visual Information Solutions, Boulder, CO, USA). The reflectance of hyperspectral images was calculated by normalizing the images relative to the reflection of the white reference and using the dark current

image for signal correction. Because of a low signal-to-noise ratio at the extremes of spectra, only wavelengths between 450 and 850 nm (=140 wavebands) were used for analyses. The resultant spectral signals were smoothed using the Savitzky–Golay filter [37].

### 3.3.5 Analysis of hyperspectral data

For supervised classification of spectral information, the spectral angle mapper (SAM) algorithm was applied [38]. SAM calculates the spectral angle between the spectrum of each pixel and reference spectra from a spectral library by treating them as vectors in a dimensionality that equals the number of bands. The smaller the angle, the higher the similarity. SAM is relatively robust to changes in illumination conditions. As a supervised classification algorithm, SAM has the advantage that classes (=phenotypes/endmembers) to be included in the data analysis are predefined. Image pixels were categorized as belonging to the classes (=endmember) healthy (green) tissue or various blast symptom subareas. A spectral library including reference spectra of the classes was created, using manually marked regions of interest (ROIs) for the different tissue types, i.e., healthy tissue, and dark brown, grey, chlorotic, grey green, and light brown tissues for subareas of blast symptoms at each level of mineral N supply. ROIs included >37,500 pixels for healthy tissue and ranged from 33 to >1000 pixels for blast symptom subareas. The mean spectrum of each ROI was stored as reference spectra in a spectral library and used for pixelwise SAM classification of hyperspectral images.

The SAM algorithm calculated spectral similarities of pixels of interest and all reference spectra selected in an n-dimensional space, depending on the number of spectral bands. The algorithm categorizes pixels by assigning them to the reference components or leaves them unclassified. Classification results are visualized in false-color images. Four leaves for each rice genotype × *M. oryzae* interaction at low, medium, and high mineral N levels were analyzed. To investigate the effect of mineral N supply on the spectra of healthy tissue and blast symptom subareas, differences between spectra were calculated by subtracting the reflectance of leaves at low N supply from the reflectance of those at medium and high N supply for each wavelength. Peaks in difference spectra ( $\Delta$  medium N – low N, and  $\Delta$  high N – low N) indicated to wavelengths at which significant differences between mineral N application rates occurred.

The red edge inflection point (REIP) of spectra was calculated according to the equation:

$$\text{REIP} = 700 + 40 \left( \frac{(R_{670} + R_{780})}{2} - R_{700} \right) / (R_{740} - R_{700}) \quad (1)$$

where  $R_{670}$ ,  $R_{700}$ ,  $R_{740}$ , and  $R_{780}$  represent reflectance values at 670, 700, 740, and 780 nm wavelengths, respectively [39].

### 3.3.6 Assessment of blast symptoms in RGB images

In addition, RGB images of diseased leaves, taken with the HSI system were used for digital image analysis. The images were analyzed using the software Assess 2.0 (American Phytopathological Society, St. Paul, MN, USA) to determine the percentage of diseased leaf area, mean lesion area [mm<sup>2</sup>], and the number of blast lesions per leaf area on the leaves of rice genotypes grown at low, medium, and high mineral N supply. In these experiments, leaf images were the experimental unit (n = 4).

### 3.3.7 Statistical analysis

Standard analysis of variance (ANOVA) was applied to determine the significance of effects of mineral N supply on relative chlorophyll and total N content, disease severity (percentage leaf area diseased), blast lesion area, and on lesion number, using R studio version 4.2.1 statistical software [40]. Mean separation was performed by Tukey's HSD test at ( $P = 0.05$ ). The number of replicates used for statistical analysis (n) is provided in the results. All experiments were performed two times. Despite minor differences in absolute values among experiments, biological repetitions confirmed a significant difference between treatments or the ranking of treatments.

## 3.4 Results

### 3.4.1 Rice plant response to increased mineral N supply

The phenotypic response of the rice genotypes CO 39, IR64, and Nipponbare to low, medium, and high N supply was assessed 4 days after N fertilizer application (Fig. S3.1). At a low N supply, plant height, and leaf size were smallest, and leaves showed symptoms of slight chlorosis. All genotypes responded to increasing N application by significantly ( $P < 0.05$ ) enhancing leaf greenness, leaf size (Fig. S3.1), and dry biomass (Fig. S3.2). Similarly, across genotypes, mineral N supply significantly increased relative leaf chlorophyll content or leaf greenness by 47–56%, and total N contents from 1.8 (low) to over 4.0 (medium) to 4.5 (high) %N in the dry matter (Fig. 3.1). In general, Nipponbare had significantly more leaf chlorophyll and higher total N than CO 39 and IR64, irrespective of the mineral N rate applied.

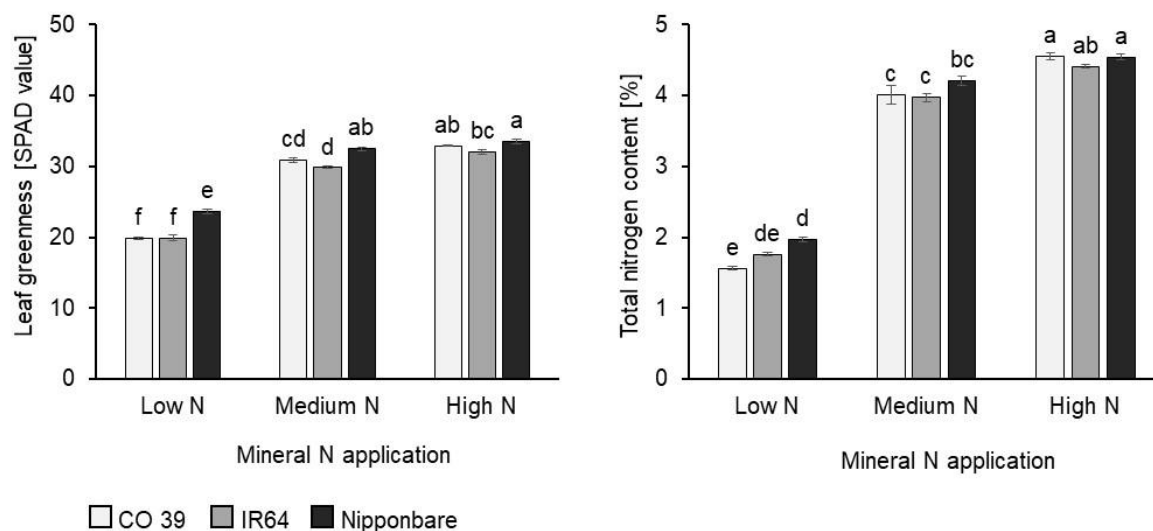


**Fig. 3.1:** Effect of mineral N supply (low, medium, high) on leaf greenness (SPAD) and leaf N content of rice genotypes CO 39, IR64, and Nipponbare 4 days after N fertilizer application. Data represent the mean  $\pm$  standard error ( $n = 4$ ). Letters from Compact Letter Display (CLD) denote statistically significant differences by Tukey's HSD test ( $P = 0.05$ ).

### 3.4.2 Effect of mineral N supply on the spectral signature of healthy leaves

The spectral reflectance of non-inoculated rice leaves in the visible (VIS) and near-infrared (NIR) ranges was recorded at 4 and 11 days after mineral N application. The reflectance patterns were similar in healthy (non-inoculated) plants at all three mineral N supply rates (Fig. 3.2). In the range 400–700 nm, mean reflectance signatures were higher at a low mineral N supply than at a medium and high mineral N supply. Differences between the medium and high N rates were moderate to low, irrespective of rice genotypes or time after mineral N supply (4 and 11 days, Fig. 3.2a and Fig. 3.2b, respectively). Except in IR64 and Nipponbare that showed a reflectance decrease in the VIS at high N supply, reflectance in this spectral region increased with time after N supply (Fig. 3.2), and it was consistently and significantly highest at a low N supply, regardless of the rice genotype. At medium N supply, significant differences between spectral signatures appeared only 11 days after N supply, while minor differences in the spectral reflectance were already apparent 4 days after N application at high N application rates. Genotypes CO 39 and IR64 reacted similarly to mineral N supply and were significantly different from Nipponbare (Fig. S3.3). Similarly, mineral N application differentially affected the REIP and the reflectance in the NIR range (780 – 800 nm) of the spectrum. Increased mineral N supply caused a decrease in the green peak, while increasing the reflectance in the NIR range, and showed a shift in REIP to longer wavelengths (Fig. 3.2).

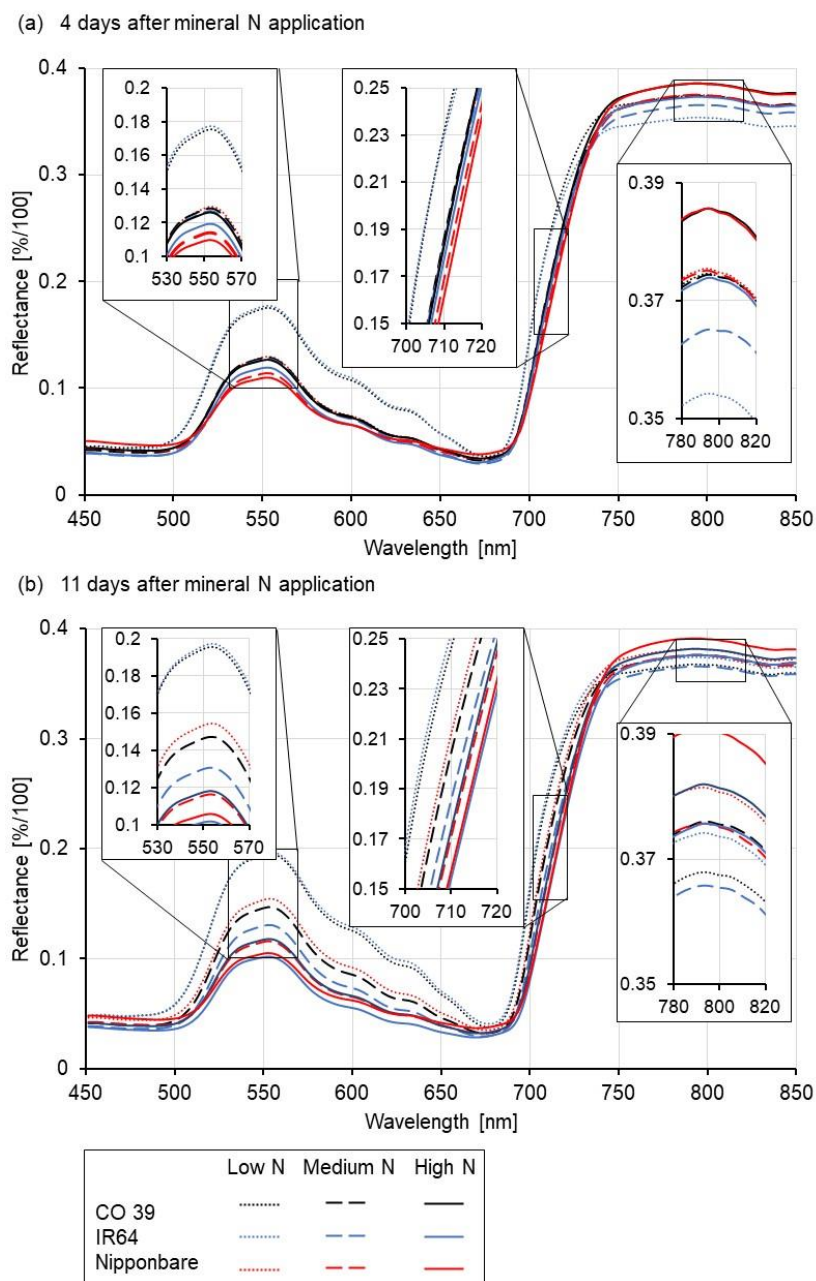


**Fig. 3.2:** Effect of mineral N supply (low, medium, high) on the reflectance of healthy leaves of three rice genotypes. Average reflectance spectra of rice genotypes CO 39, IR64, and Nipponbare at (a) 4 and (b) 11 days after N fertilizer application. Scaled-up inserts highlight the spectral ranges showing the most prominent changes.

Difference spectra also revealed significant differences among leaves of genotypes grown under different N supply (Fig. 3.3). In the range of the green peak and the red edge, spectral differences between high and low mineral N supply were significant for all genotypes. While the spectra of CO 39 did not differ in the visible and the red-edge regions at 4 days, spectral differences between N rates were significant for all genotypes 11 days after N application. However, spectra in the NIR range differed as early as 4 days after mineral N application in all genotypes. While being less pronounced,

the reflectance spectra in the NIR range increased more at high than at moderate N supply. The effect of mineral N on the reflectance of healthy leaf tissue was strongest in IR64 and weakest in Nipponbare, while CO 39 showed an intermediate response (Fig. 3.3). Between 4 and 11 days after N application, leaf reflectance in the VIS range increased with a low N supply and decreased with a high N supply. At medium N supply, IR64 and Nipponbare showed intermediate reflectance patterns, while in CO 39, the genotype with the highest biomass, reflectance consistently increased with the N rate. The strongest time effects (changes from 0 over 4 to 11 days after N application) were observed in IR64, indicating significant interactions between N rates and time (Fig. S3.4).

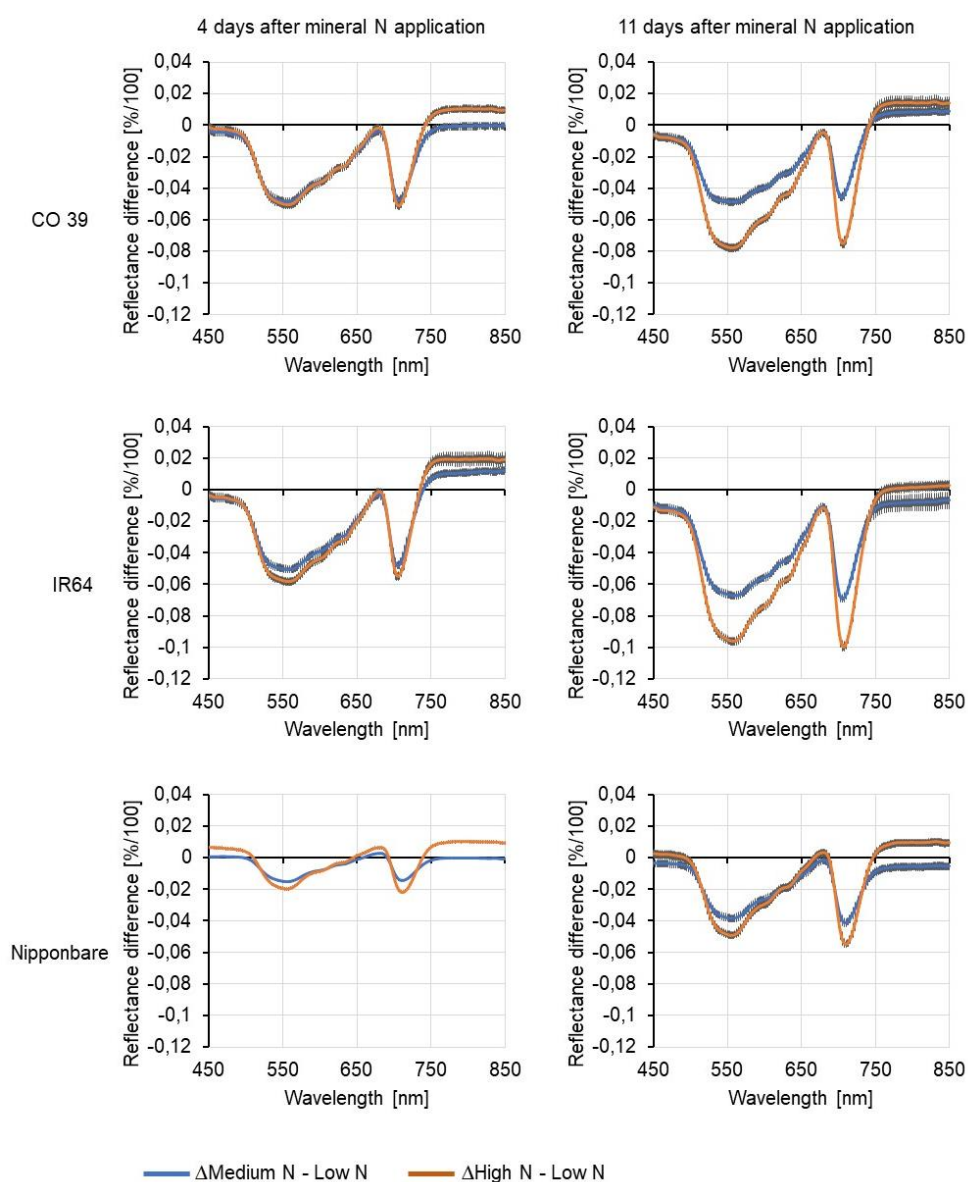


**Fig. 3.3:** Difference spectra of reflectance of healthy leaf tissue of rice genotypes CO 39, IR64, and Nipponbare grown at low, medium, and high N supply 4 and 11 days after N fertilizer application. The zero line displays the reflectance of plants grown at low N supply as a reference. For each waveband, the bars represent the standard error of the mean ( $n = 4$ ).

### 3.4.3 Effects of mineral N supply on the expression of leaf blast symptoms

The reaction of rice genotypes grown at low, medium, and high mineral N supply to infection by *M. oryzae* was assessed 7 days post inoculation (=11 days after mineral N supply; Fig. 3.4). The number, size, and intensity of leaf blast symptoms varied depending on the interaction among rice genotypes, *M. oryzae* isolates, and rates of mineral N supply, indicating gene-for-gene-specific and N × cultivar interactions. Genotype IR64, infected by *M. oryzae* isolates Guy 11, Li1497, and TH6772, retained its blast resistance at all N application rates. On the other hand, rice genotype CO 39, moderately resistant to isolate TH6772, showed less and smaller dark-brown spots at a low N supply than at a medium and high N supply (Fig. 3.4). Characteristic blast lesions in Nipponbare consisted of a grey tissue surrounded by a dark-green border, with chlorotic areas and brown tissue at the margins. The symptoms associated with isolates Guy 11 and Li1497 on the blast-susceptible rice genotype CO 39 ranged from dark brown areas to white or grey centers, surrounded by grey green tissue. The size of these lesions tended to increase with mineral N supply (Fig. 3.4).

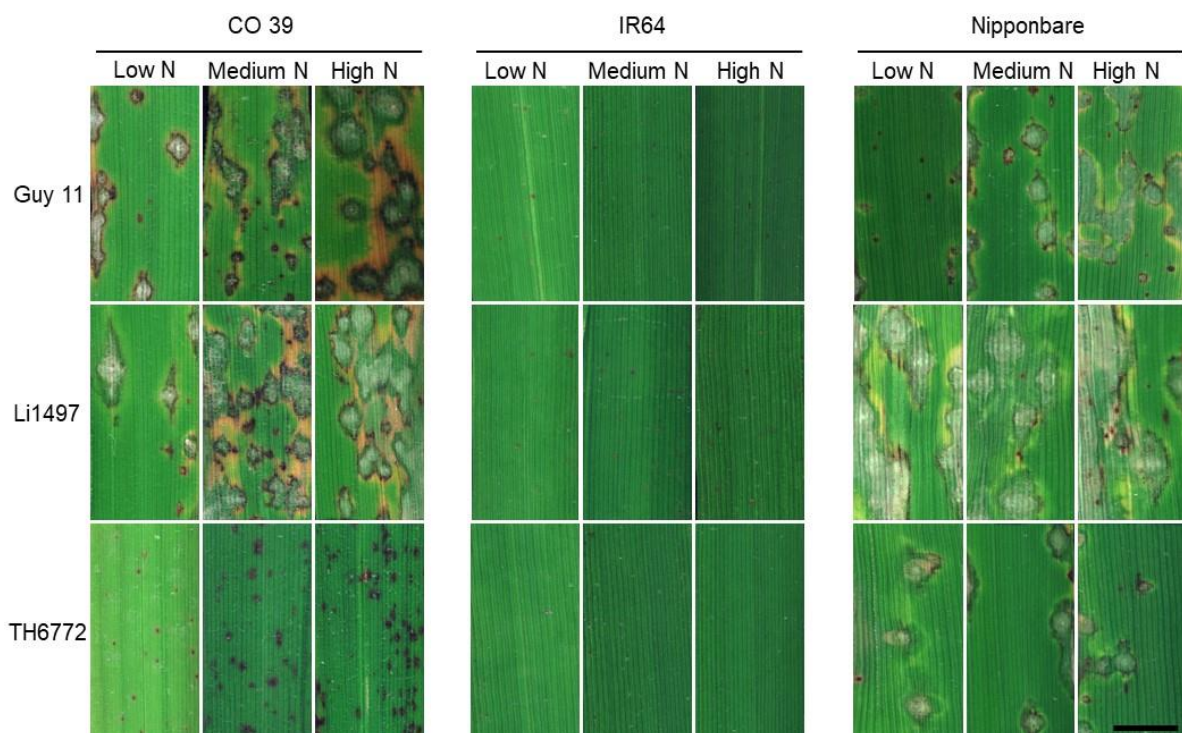


**Fig. 3.4:** Phenotypes of representative leaf blast symptoms on rice genotypes CO 39, IR64, and Nipponbare infected by *M. oryzae* isolates Guy 11, Li1497, and TH6772 at low, medium, and high N supply, respectively. Images were taken 7 days post inoculation corresponding to 11 days after N fertilizer application (bar size = 5 mm).

#### 3.4.4 Effects of mineral N supply on rice blast intensity

The number and the size of blast lesions as well as the percentage of diseased leaf area 7 days post inoculation depended on the mineral N supply. The number of lesions was lowest at low mineral N supply, irrespective of the host–pathogen genotypes involved (Fig. 3.5, top row). However, with increasing N supply, the number of blast lesions increased significantly ( $P < 0.05$ ) in rice genotypes CO 39 and Nipponbare, inoculated with isolate TH6772. Lesion numbers in resistant interactions were often higher than in highly susceptible interactions. Apart from the number of lesions, lesion sizes also differed among rice genotypes, *M. oryzae* isolates, and mineral N application rates. The mean size of blast lesions was very small in resistant interactions and was not significantly affected by N supply. The lesion size in susceptible interactions tended to increase with mineral N supply (Fig. 3.5, middle row). In the Nipponbare × Li1497 combination, lesion size in low and high N was higher than in medium N; however, the differences were not significant ( $P < 0.05$ ). In the Nipponbare × TH6772 interaction, lesion sizes in low N tended to be higher than in medium and high N. Depending on the specific combination of host, pathogen, and mineral N level, rice leaves at low N supply exhibited N depletion earlier at the site of pathogen infection and consequently disease lesions developed faster than in plants under medium and high N supply.

The percentage of diseased leaf area was the parameter most suitable to measure the effect of mineral N on leaf blast intensity. In genotype Nipponbare, infected with isolates Li1497 and TH6772, respectively, disease severity at low and high N was higher than at medium N; however, differences in blast severity were not significant ( $P < 0.05$ ) as plants were susceptible at all N levels. Similarly, the higher blast severity at low and high N in genotype IR64 infected with Guy 11 was not significantly ( $P < 0.05$ ) different from the severity at medium N level. In all other combinations of host genotypes and pathogen isolates, the leaf blast intensity was lowest at low N supply, and it increased with N application rates (Fig. 3.5, bottom row). Differences between high and low N supplies were significant ( $P < 0.05$ ) in susceptible interactions, with no significant effects on blast intensity in the case of incompatible interactions (i.e., IR64 × all isolates). In the moderately resistant interaction CO 39 × TH6772, leaf blast increased with N supply, albeit at an overall low disease level.

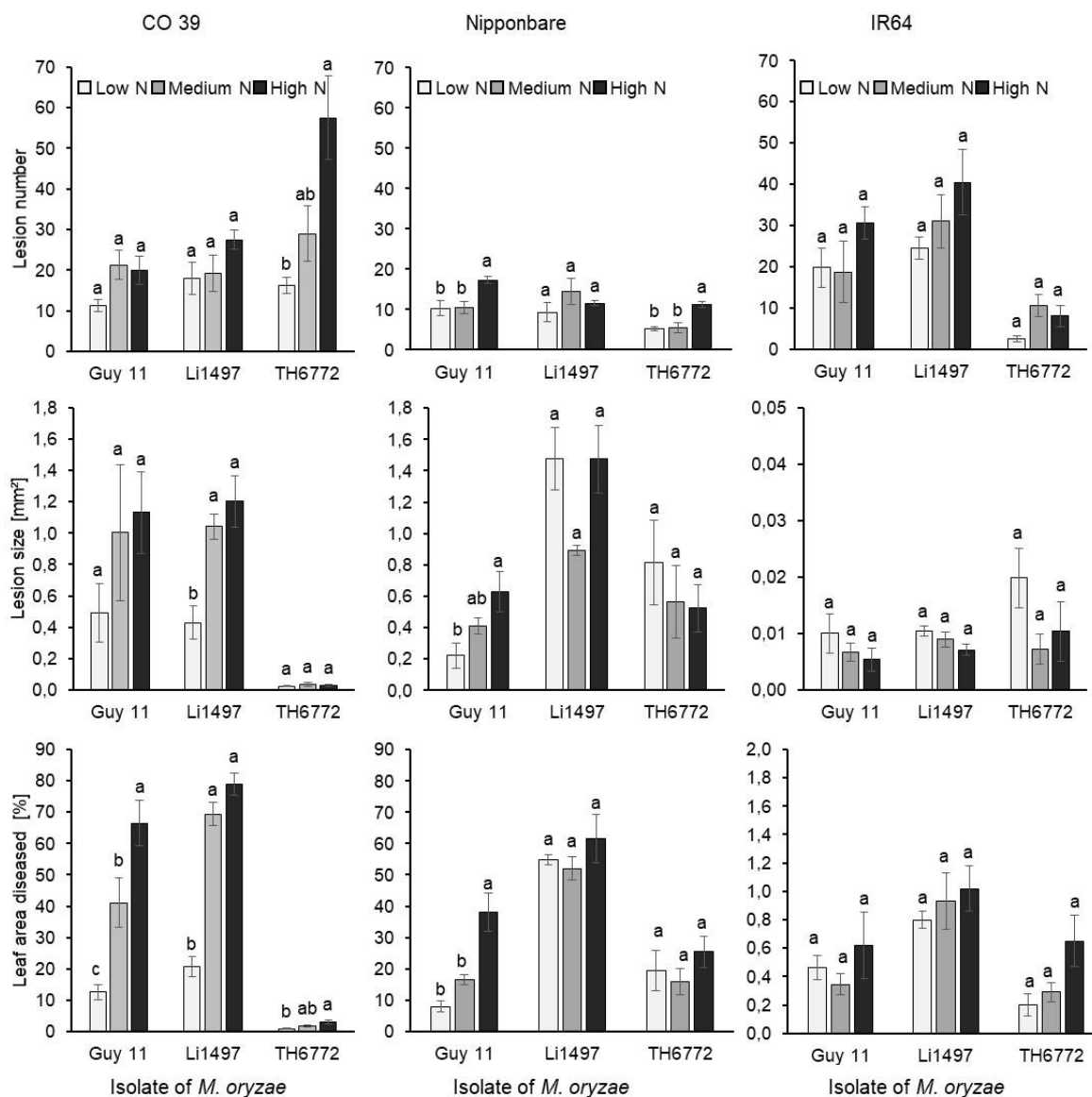


**Fig. 3.5:** Effect of low, medium, and high mineral N supply on the number of blast lesions, mean lesion area, and disease severity due to infection of three rice genotypes CO 39, IR64, and Nipponbare by three isolates of *M. oryzae* Guy 11, Li1497, and TH6772. Number of blast lesions/leaf area [mm<sup>2</sup>], mean area of blast lesions [mm<sup>2</sup>], and leaf area covered by blast symptoms [%] were measured 7 days post inoculation. Data represent the mean  $\pm$  standard error (n = 4). Bars annotated by the same letter from Compact Letter Display (CLD) do not differ significantly according to Tukey's HSD test ( $P = 0.05$ ).

### 3.4.5 Effect of mineral N supply on leaf blast symptom types of rice genotypes

The SAM algorithm was used for the supervised classification of blast symptom types on leaves of the three rice genotypes grown at low, medium, and high N supply (Fig. 3.6). Irrespective of N rates, the susceptible genotypes CO 39 and Nipponbare were characterized by more complex blast symptoms, resulting in five symptom subareas: (1) dark brown tissue, (2) grey tissue, (3) chlorotic

tissue, (4) grey green tissue, and (5) light brown tissue. In the resistant genotype IR64, only small dark brown leaf spots were observed, irrespective of the mineral N rates applied. The number of tissue types varied with the compatibility of the host–pathogen interaction and mineral N supply rate.

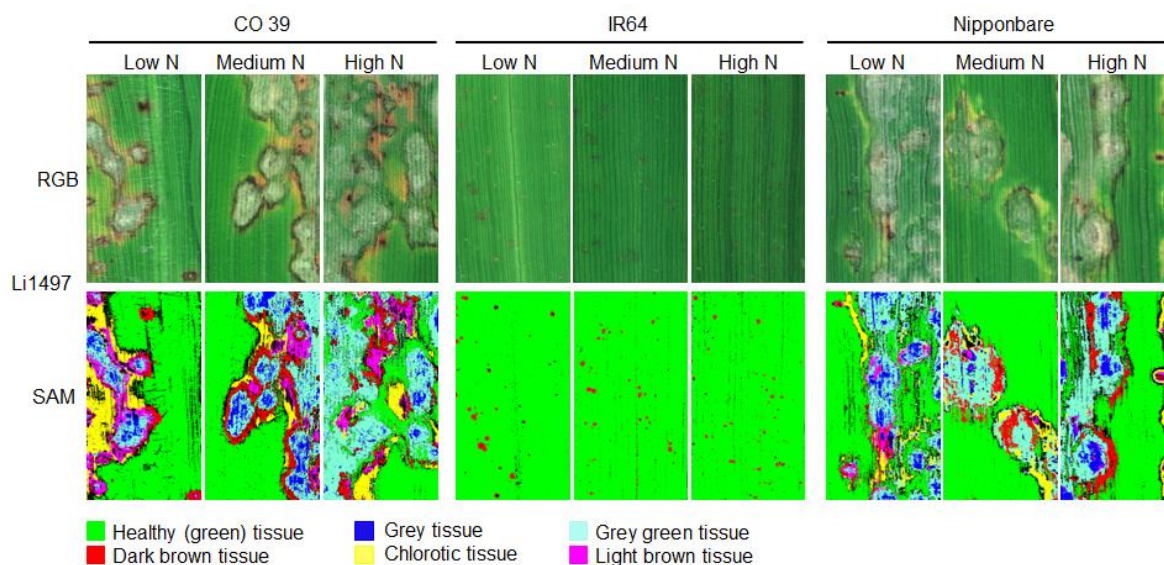


**Fig. 3.6:** Classification of blast symptom subareas on leaves of three rice genotypes CO 39, IR64, and Nipponbare inoculated with *M. oryzae* isolate Li1497 at low, medium, and high mineral N supply. Images were recorded 7 days post inoculation. RGB images of the different tissue reactions were used as ground truth. Healthy green tissue and different subareas of blast symptom types were classified in supervised classification by spectral angle mapper (SAM) algorithm. For genotype IR64 (resistant), small dark brown leaf spots were classified, while for genotypes CO 39 (highly susceptible) and Nipponbare (susceptible), blast symptom subareas included dark brown tissue, grey tissue, chlorotic tissue, grey green tissue, and light brown tissue.

### 3.4.6 Variability of spectral signatures of blast symptom types as affected by mineral N supply

From the interactions between rice genotypes CO 39, IR64, Nipponbare, and *M. oryzae* isolates Guy 11, Li1497, and TH6772, respectively, representative spectra of healthy green tissue and subareas of blast symptom were analyzed 7 days post inoculation. The reflectance of leaf tissue was affected by both mineral N supply and blast symptom subareas as shown for the interaction between rice genotypes and *M. oryzae* isolate Li1497 (Fig. 3.7). For healthy tissues, the spectral reflectance of the green peak decreased with increasing N supply in genotype IR64 and was unaffected in the other genotypes. In the compatible interaction between genotypes CO 39 and Nipponbare the spectral reflectance of grey blast symptom subareas were consistently higher than that of healthy tissues. While the spectral reflectance of grey green and chlorotic tissues (exclusively occurring in compatible rice—*M. oryzae* interactions) increased in the VIS region, the reflectance of dark brown tissues

(representative for resistance reactions to pathogen infection) decreased in the VIS and NIR regions of the spectrum compared to healthy tissues (Fig. 3.7).

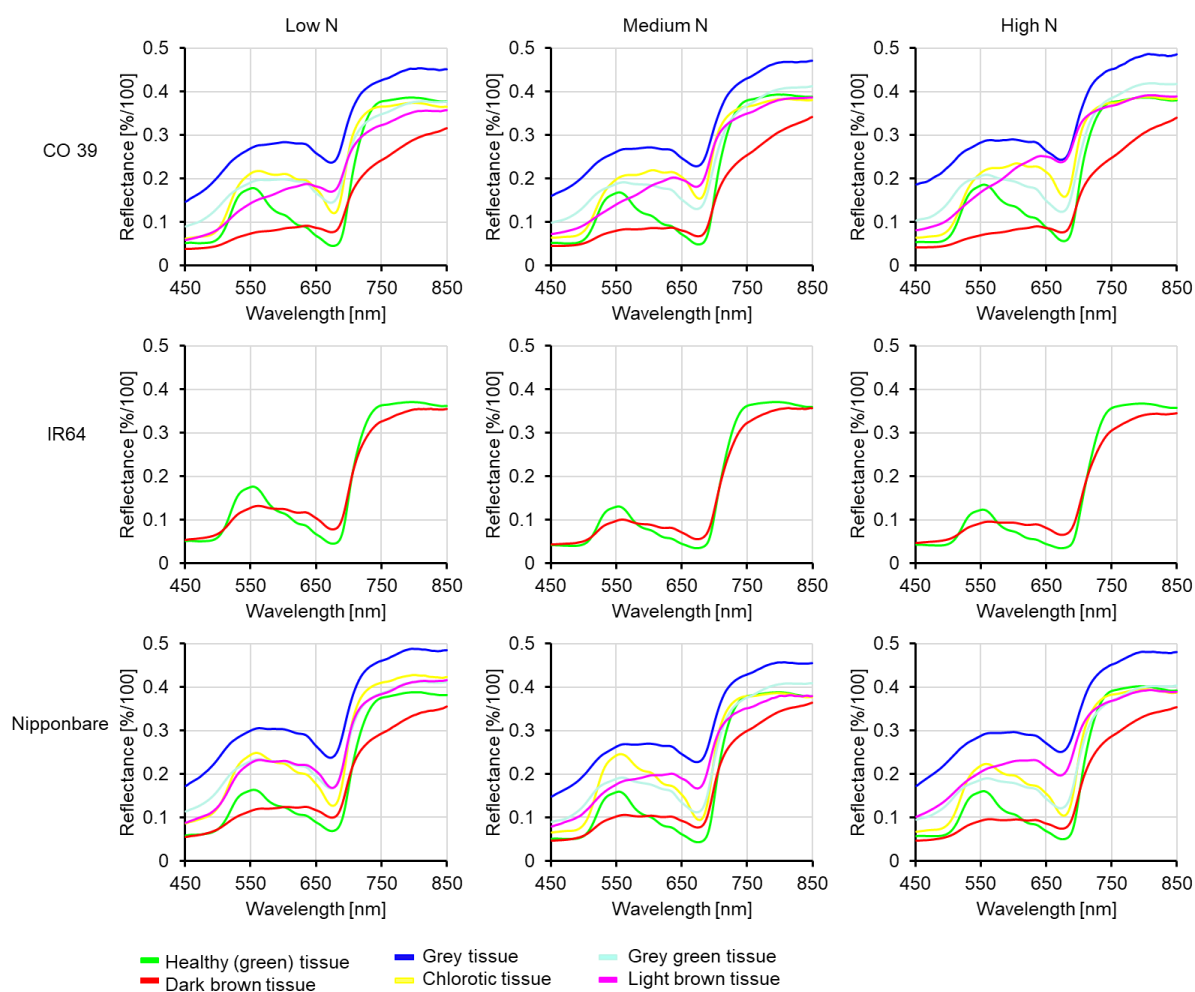


**Fig. 3.7:** Mean spectral signatures of healthy green tissue and various blast symptom subareas of the three rice genotypes CO 39, IR64, and Nipponbare inoculated with *M. oryzae* isolate Li1497 at low, medium, and high mineral N supply, respectively, 7 days post inoculation.

The effects of N supply on reflectance signatures were further investigated by calculating reflectance differences between medium and low N supplies, and between high and low N supplies. In the susceptible interaction CO 39  $\times$  Li1497, mineral N supply affected the spectrum of dark brown tissues. In Nipponbare and the resistant genotype IR64, increasing the N supply reduced the reflectance of dark brown tissues in the green and red range of the spectrum. The grey tissue type, representing leaf tissue with highest reflectance values, reacted differently to mineral N supply. Thus, high mineral N significantly affected reflectance in the blue range of susceptible genotype CO 39, and in the blue and green ranges of moderately susceptible genotype Nipponbare. The effect of mineral N supply on spectral characteristics of grey green tissues differed between genotypes CO 39 and Nipponbare. Thus, CO 39 showed a significant effect in the green, red edge, and NIR ranges, while in

Nipponbare, the reflectance was significantly reduced in the VIS range (Fig. 3.8). In general, each rice genotype reacted differently to increasing N supply, revealing genotype-specific response patterns (Fig. 3.9a–f). Consequently, genotype-specific responses to blast infection and mineral N supply can be differentiated by their distinct spectral signatures, permitting tissue-type-specific differentiations of susceptible and resistance blast response patterns.

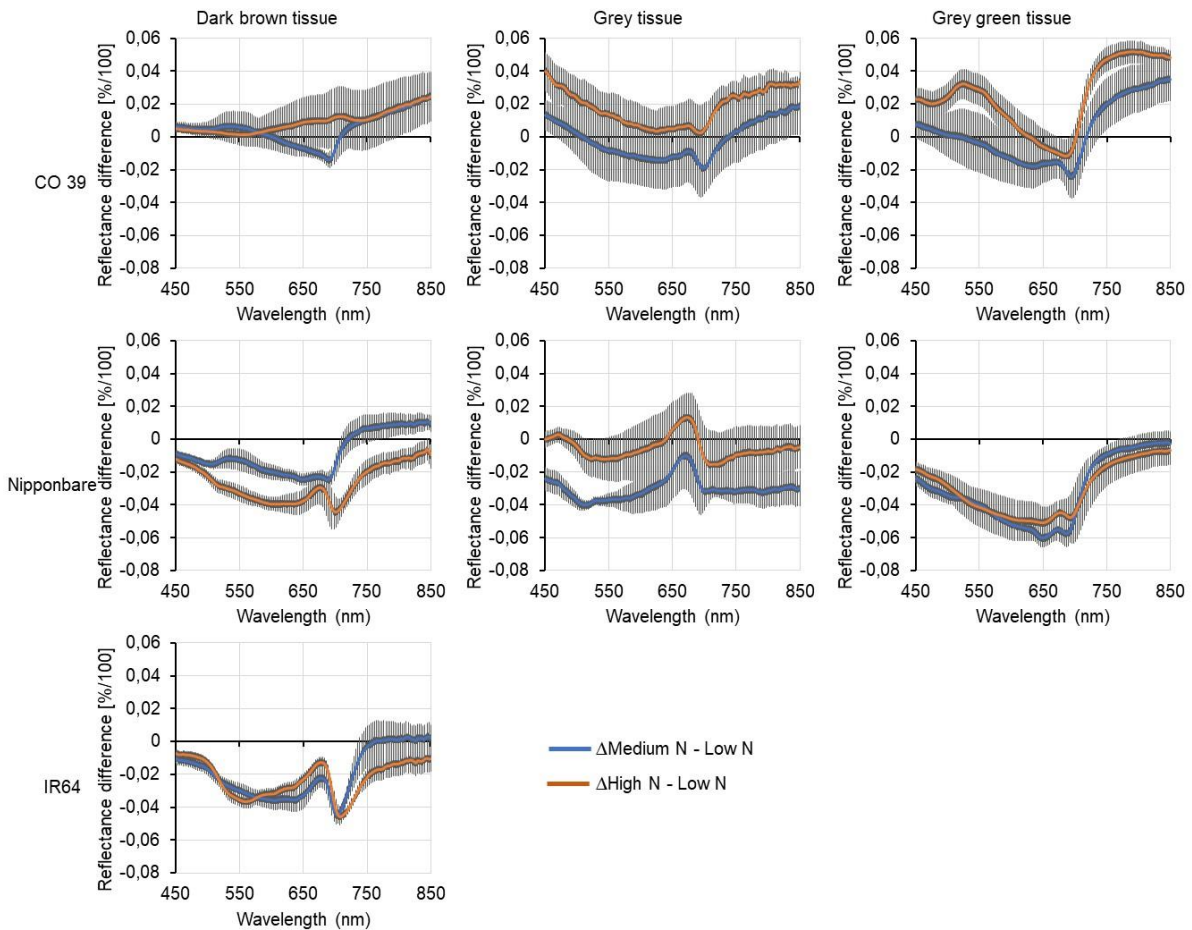


**Fig. 3.8:** Difference spectra of blast symptom subareas of rice genotypes CO 39, IR64, and Nipponbare infected by *M. oryzae* isolate Li1497 at low, medium, and high mineral N supply, respectively. Differences were computed by subtracting the reflectance of blast symptom subareas from diseased leaves at low N supply from corresponding subareas from leaves at medium and high N supply, respectively. The baseline reflects the average reflectance of symptom subareas from leaves at low N supply. Bars represent the standard error of the mean for each waveband (n = 4).

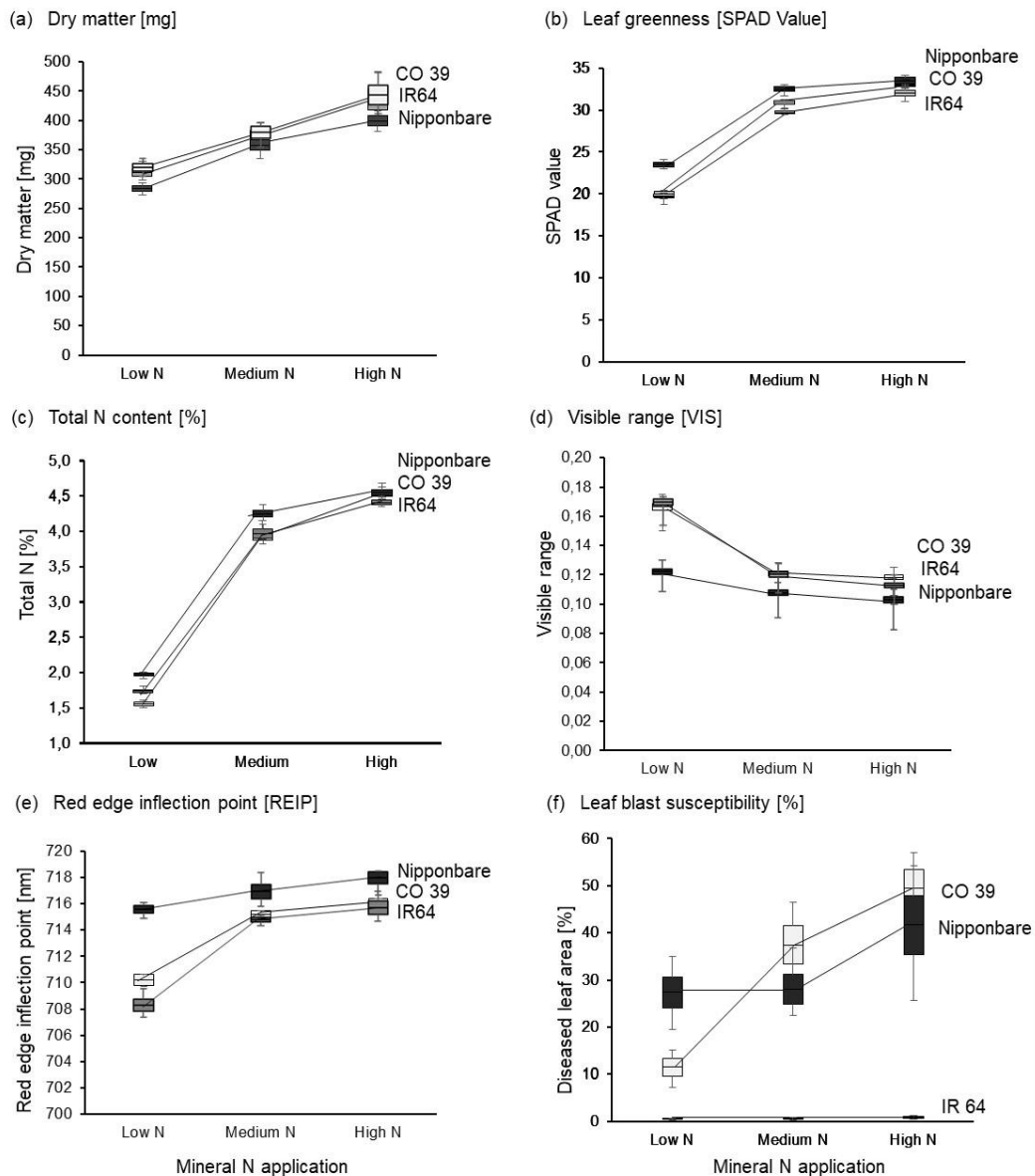


**Fig.3. 9:** Genotype-specific differences among rice genotypes CO 39, IR64, and Nipponbare for (a) dry matter content [mg], (b) leaf greenness, (c) total N content [%], (d) visible range, (e) the red edge inflection point, and (f) disease severity [%], at low, medium, and high mineral N supply. The boxes denote the mean as well as the standard error of the mean; whiskers represent the minimum and maximum values (n = 4).

### 3.5 Discussion

The present study confirms the reported literature data, showing that mineral N supply to rice is associated with increased plant growth and leaf greenness [41,42], and a near-doubling of the leaf N content [43,44], albeit while increasing rice plants' susceptibility to leaf blast. Both rice performance attributes and the type and severity of blast symptoms related to mineral N supply were differentiated by their spectral signatures.

Mineral N supply increases the leaf chlorophyll content, and a photometer-based sensing of the leaf greenness is used as a proxy for determining leaf N concentrations. The N-induced decrease in leaf reflectance in the VIS and red-edge ranges is the result of absorption of irradiance by chlorophyll [25]. These relationships are used for guiding site-specific N management in maize [45], wheat [4], and rice [46]. In the present study, mineral N supply affected the spectral characteristics of rice leaves only 4 days after N application. However, the extent of the spectral responses differed by rice genotype. For two out of three rice genotypes, the effect of mineral N supply on spectral characteristics and total N content of leaves was stronger for the increase from low to medium N than for the increase from medium to high N supply. Such differences are related to anatomical and to physiological attributes of rice. Consequently, the leaf thickness (or specific leaf weight), is recommended to be used as a correction factor for guiding site-specific (photometer-based) N management in rice [46]. Additionally, attributes in N use efficiency traits may reportedly account for genotype-specific differences in spectral responses of upland rice [41]. Such interactions between genotypes and mineral N supply rates, and their effects on the leaf greenness, require genotype-specific adjustments of photometer readings. This complicates the interpretation of reflectance data and may hamper the extrapolation of findings to very diverse sets of rice genotypes.

The observed shift in REIP appears to be the most robust indicator of mineral N supply. Being sensitive to small differences in the plant's N status, this parameter appears most suitable for optimizing the N supply to rice plants. Changes in NIR reflectance were less consistent, which is reportedly associated with scattering of NIR wavelengths [23]. This result is also consistent with other recent studies, using non-imaging hyperspectral systems [47,48].

While increased N availability improves plant performance attributes, it may also increase the rice plants' susceptibility to fungal pathogens. Thus, high mineral N supply reportedly increases the severity of rice blast [9], wheat blast [49], and wheat stripe rust [4]. In the present study, high N supply generally increased the intensity of the rice blast disease similarly to earlier reports [9,50,51]. High mineral N supply thus increases the content of amino acids in rice leaf tissues and can serve as a substrate for the growth of pathogen [6]. In addition, elevated concentrations of nitrate in the vacuoles have been suggested to act as an N source for *M. oryzae*, increasing the susceptibility of tissues to the blast disease [52]. On the other hand, in some instances N-limited conditions can also trigger *M. oryzae* to induce its pathogenicity genes [53], and the *MPG1* gene has been highly expressed during appressorium formation and blast infection under N starvation in vitro [11].

However, such trade-offs of increased N fertilizer use on the occurrence of blast disease symptoms depend on rice genotypes and their interactions with different *M. oryzae* isolates [9,51]. In our study, the effect of mineral N supply on the development of leaf blast symptoms varied among

rice—*M. oryzae* interactions, revealing gene-for-gene-specific interactions. While mineral N supply increased blast severity in the highly susceptible genotype CO 39 infected by *M. oryzae* isolate Li1497, it had no effect in the resistant genotype IR64, irrespective of the blast isolate. In rice genotype CO 39, infected by isolate Guy 11, mineral N supply increased blast severity by 25%, while the susceptibility of genotype Nipponbare to the same isolate increased only at the highest N rates. On the other hand, a high blast severity was observed in N-starved genotype Nipponbare when infected by *M. oryzae* isolate Li1497. Limited N availability in planta may thus stimulate pathogen growth and infection in blast-susceptible genotypes or genotypes × isolate combinations, while high N availability does not affect the compatibility of host–pathogen interactions with the blast-resistant rice genotype.

The effects of a fungal disease on spectral signatures of leaf tissues depend on the type and intensity of biochemical and physiological changes in processes associated with infection and on the composition of disease symptoms [28,54]. The present study demonstrates that beyond fungal infection, the N status of plants affects reflectance patterns of diseased leaves and of different subareas of disease symptoms.

Leaf lesions are associated with the degradation of chlorophyll, which absorbs irradiance in the VIS range [29]. Similarly, cucumber leaves infected with angular spot disease increased the reflectance in the VIS region due to reduced leaf chlorophyll contents [33]. On the other hand, decreased VIS reflectance of dark brown spots results from light absorption by non-photosynthetic brown pigments [23]. The present study additionally showed that grey blast subareas were characterized by increased reflectance in the VIS and NIR regions, while grey green subareas and chlorotic tissues were characterized by either an increase or decrease in reflectance spectra in the NIR range, depending on the rice genotype and the N status of the leaf. A decrease in the reflectance spectra of dark brown tissues in the NIR range has been previously linked to the structural damage of rice tissue caused by the growth of *M. oryzae* within the leaf [29].

The spectral signature of blast symptom subareas demonstrated strong interactions with the N status of leaves; the largest spectral differences were observed in the VIS and red-edge ranges. The leaf N status increased or decreased spectral characteristics of symptom subareas, which significantly differed among rice genotype × *M. oryzae* × N supply rate interactions. As small spectral differences in reflectance of dark brown, grey, and grey green subareas of blast lesions could not be detected visually, HSI allowed for a more detailed analysis of the optical properties of diseased rice leaves.

Hyperspectral imaging at the microscopic level revealed high spatial and spectral variabilities in plant × pathogen × mineral N interactions at the leaf scale. Basic laboratory research benefits from the high spatial resolution and provides valuable insights into biophysical and biochemical changes

caused by combined effects of both biotic and abiotic stressors. However, high labor requirements and a low throughput/small field of view limit the applicability of this approach in phenotyping and for field applications. In addition, the rice genotype  $\times$  *M. oryzae*  $\times$  N supply interactions resulted in a large diversity of blast subareas, hampering the establishment of a general library of reference spectra required in phenotyping platforms for quantitative blast resistance screening.

Proximal hyperspectral technologies at canopy scales may enable the establishment of a connection between leaf-level observations and large-scale measurements [55] and to upscale methods of canopy reflectance that were developed under controlled environments to field-scale studies [56]. Nevertheless, an increase in the HSI platform level is critical for the detection and characterization of small disease symptoms and low disease severities in contrast to the assessment of abiotic effects on crops. Spectral differences at larger scales may be used for disease detection and for characterizing the crop's N status, provided the user accepts a coarse resolution of detecting the disease level. More detailed resolution data will require combining remote sensing, ground-truthing, and additional monitoring of environmental conditions. The more data available, the more reliable and detailed will be the information extracted from reflectance data.

### 3.6 Conclusions

Hyperspectral imaging at the microscopic level proved to be an effective tool for evaluating the effects of N supply on the spectral characteristics of healthy rice leaves, as well as on the variability of leaf blast symptoms, depending on gene-for-gene-specific host– pathogen interactions. Combining HSI with supervised classification by SAM could be adapted to a pixel-wise characterization of blast symptoms that differ in size and subarea attributes. Multiple interactions between plant genotypes, the level of N supply, and pathogen isolates result in large spectral variations, which complicate the interpretation of spectral data. In phenotyping for breeding under (semi-)controlled conditions, spectral information may be used for identifying sources for disease resistance. However, the sensitivity and reliability of the sensor system will depend on its spatial resolution and on the variability of disease symptoms. A desired future application in remote sensing at the field level requires more data on factors affecting crop reflectance.

### 3.7 References

1. Makino, A. Photosynthesis, grain yield, and nitrogen utilization in rice and wheat. *Plant Physiol.* 2011, 155, 125–129. [CrossRef] [PubMed]
2. Dordas, C. Role of nutrients in controlling plant diseases in sustainable agriculture. A review. *Agron. Sustain. Dev.* 2008, 28, 33–46. [CrossRef]

3. Veresoglou, S.D.; Barto, E.K.; Menexes, G.; Rillig, M.C. Fertilization affects severity of disease caused by fungal plant pathogens. *Plant Pathol.* 2013, 62, 961–969. [CrossRef]
4. Devadas, R.; Simpfendorfer, S.; Backhouse, D.; Lamb, D.W. Effect of stripe rust on the yield response of wheat to nitrogen. *Crop J.* 2014, 2, 201–206. [CrossRef]
5. Walters, D.R.; Bingham, I.J. Influence of nutrition on disease development caused by fungal pathogens: Implications for plant disease control. *Ann. Appl. Biol.* 2007, 151, 307–324. [CrossRef]
6. Long, D.H.; Lee, F.N.; TeBeest, D.O. Effect of nitrogen fertilization on disease progress of rice blast on susceptible and resistant cultivars. *Plant Dis.* 2000, 84, 403–409. [CrossRef]
7. Wilson, R.A.; Talbot, N.J. Under pressure: Investigating the biology of plant infection by *Magnaporthe oryzae*. *Nat. Rev. Microbiol.* 2009, 7, 185–195. [CrossRef]
8. Mukherjee, A.K.; Mohapatra, N.K.; Suriya Rao, A.V.; Nayak, P. Effect of nitrogen fertilization on the expression of slow-blasting resistance in rice. *J. Agric. Sci.* 2005, 143, 385–393. [CrossRef]
9. Huang, H.; Nguyen Thi Thu, T.; He, X.; Gravot, A.; Bernillon, S.; Ballini, E.; Morel, J.-B. Increase of fungal pathogenicity and role of plant glutamine in nitrogen-induced susceptibility (NIS) to rice blast. *Front. Plant Sci.* 2017, 8, 265. [CrossRef] [PubMed]
10. Sun, Y.; Wang, M.; Mur, L.A.J.; Shen, Q.; Guo, S. Unravelling the roles of nitrogen nutrition in plant disease defences. *Int. J. Mol. Sci.* 2020, 21, 572. [CrossRef] [PubMed]
11. Talbot, N.J.; Ebbole, D.J.; Hamer, J.E. Identification and characterization of *MPG1*, a gene involved in pathogenicity from the rice blast fungus *Magnaporthe grisea*. *Plant Cell* 1993, 5, 1575–1590.
12. Muñoz-Huerta, R.; Guevara-Gonzalez, R.; Contreras-Medina, L.; Torres-Pacheco, I.; Prado-Olivarez, J.; Ocampo-Velazquez, R. A review of methods for sensing the nitrogen status in plants: Advantages, disadvantages and recent advances. *Sensors* 2013, 13, 10823–10843. [CrossRef]
13. Dordas, C. Nitrogen nutrition index and leaf chlorophyll concentration and its relationship with nitrogen use efficiency in barley (*Hordeum vulgare* L.). *J. Plant Nutr.* 2017, 40, 1190–1203. [CrossRef]
14. Bock, C.H.; Barbedo, J.G.A.; Del Ponte, E.M.; Bohnenkamp, D.; Mahlein, A.-K. From visual estimates to fully automated sensor-based measurements of plant disease severity: Status and challenges for improving accuracy. *Phytopathol. Res.* 2020, 2, 9. [CrossRef]
15. Lowe, A.; Harrison, N.; French, A.P. Hyperspectral image analysis techniques for the detection and classification of the early onset of plant disease and stress. *Plant Methods* 2017, 13, 80. [CrossRef] [PubMed]
16. Gnyp, M.L.; Miao, Y.; Yuan, F.; Ustin, S.L.; Yu, K.; Yao, Y.; Huang, S.; Bareth, G. Hyperspectral canopy sensing of paddy rice aboveground biomass at different growth stages. *Field Crops Res.* 2014, 155, 42–55. [CrossRef]

17. Stellacci, A.M.; Castrignanò, A.; Troccoli, A.; Basso, B.; Buttafuoco, G. Selecting optimal hyperspectral bands to discriminate nitrogen status in durum wheat: A comparison of statistical approaches. *Environ. Monit. Assess.* 2016, 188, 199. [CrossRef]
18. Zhou, C.; Bucklew, V.G.; Edwards, P.S.; Zhang, C.; Yang, J.; Ryan, P.J.; Hughes, D.P.; Qu, X.; Liu, Z. Portable diffuse reflectance spectroscopy of potato leaves for pre-symptomatic detection of late blight disease. *Appl. Spectrosc.* 2023, 77, 491–499. [CrossRef] [PubMed]
19. Tian, L.; Wang, Z.; Xue, B.; Li, D.; Zheng, H.; Yao, X.; Zhu, Y.; Cao, W.; Cheng, T. A disease-specific spectral index tracks *Magnaporthe oryzae* infection in paddy rice from ground to space. *Remote Sens. Environ.* 2023, 285, 113384. [CrossRef]
20. West, J.S.; Bravo, C.; Oberti, R.; Moshou, D.; Ramon, H.; McCartney, H.A. Detection of fungal diseases optically and pathogen inoculum by air sampling. In *Precision Crop Protection—The Challenge and Use of Heterogeneity*; Oerke, E.-C., Gerhards, R., Menz, G., Sikora, R.A., Eds.; Springer: Dordrecht, The Netherlands, 2010; pp. 135–149.
21. Oerke, E.-C.; Herzog, K.; Toepfer, R. Hyperspectral phenotyping of the reaction of grapevine genotypes to *Plasmopara viticola*. *J. Exp. Bot.* 2016, 67, 5529–5543. [CrossRef]
22. Berger, K.; Verrelst, J.; Féret, J.-B.; Wang, Z.; Woche, M.; Strathmann, M.; Danner, M.; Mauser, W.; Hank, T. Crop nitrogen monitoring: Recent progress and principal developments in the context of imaging spectroscopy missions. *Remote Sens. Environ.* 2020, 242, 111758. [CrossRef]
23. Ustin, S.L.; Jacquemoud, S. How the optical properties of leaves modify the absorption and scattering of energy and enhance leaf functionality. In *Remote Sensing of Plant Biodiversity*; Cavender-Bares, J., Gamon, J.A., Townsend, P.A., Eds.; Springer International Publishing: Cham, Switzerland, 2020; pp. 349–384.
24. Mahlein, A.-K. Plant disease detection by imaging sensors—Parallels and specific demands for precision agriculture and plant phenotyping. *Plant Dis.* 2016, 100, 241–251. [CrossRef]
25. Feng, W.; Yao, X.; Zhu, Y.; Tian, Y.C.; Cao, W.X. Monitoring leaf nitrogen status with hyperspectral reflectance in wheat. *Eur. J. Agron.* 2008, 28, 394–404. [CrossRef]
26. Zheng, J.; Song, X.; Yang, G.; Du, X.; Mei, X.; Yang, X. Remote sensing monitoring of rice and wheat canopy nitrogen: A review. *Remote Sens.* 2022, 14, 5712. [CrossRef]
27. Bauriegel, E.; Giebel, A.; Geyer, M.; Schmidt, U.; Herppich, W.B. Early detection of *Fusarium* infection in wheat using hyper- spectral imaging. *Comput. Electron. Agric.* 2011, 75, 304–312. [CrossRef]
28. Mahlein, A.-K.; Steiner, U.; Hillnhütter, C.; Dehne, H.-W.; Oerke, E.-C. Hyperspectral imaging for small-scale analysis of symptoms caused by different sugar beet diseases. *Plant Methods* 2012, 8, 3. [CrossRef] [PubMed]

29. Kobayashi, T.; Sasahara, M.; Kanda, E.; Ishiguro, K.; Hase, S.; Torigoe, Y. Assessment of rice panicle blast disease using airborne hyperspectral imagery. *Open Agric. J.* 2016, 10, 28–34. [CrossRef]
30. Zhang, G.; Xu, T.; Tian, Y.; Feng, S.; Zhao, D.; Guo, Z. Classification of rice leaf blast severity using hyperspectral imaging. *Sci. Rep.* 2022, 12, 19757. [CrossRef] [PubMed]
31. Maina, A.W.; Oerke, E.-C. Characterization of rice– *Magnaporthe oryzae* interactions by hyperspectral imaging. *Plant Dis.* 2023, 107, 3139–3147. [CrossRef] [PubMed]
32. Devadas, R.; Lamb, D.W.; Simpfendorfer, S.; Backhouse, D. Evaluating ten spectral vegetation indices for identifying rust infection in individual wheat leaves. *Precis. Agric.* 2009, 10, 459–470. [CrossRef]
33. Zhao, Y.-R.; Li, X.; Yu, K.-Q.; Cheng, F.; He, Y. Hyperspectral imaging for determining pigment contents in cucumber leaves in response to angular leaf spot disease. *Sci. Rep.* 2016, 6, 27790. [CrossRef] [PubMed]
34. Liu, W.; Sun, C.; Zhao, Y.; Xu, F.; Song, Y.; Fan, J.; Zhou, Y.; Xu, X. Monitoring of wheat powdery mildew under different nitrogen input levels using hyperspectral remote sensing. *Remote Sens.* 2021, 13, 3753. [CrossRef]
35. Tartachnyk, I.I.; Rademacher, I.; Kühbauch, W. Distinguishing nitrogen deficiency and fungal infection of winter wheat by laser-induced fluorescence. *Precis. Agric.* 2006, 7, 281–293. [CrossRef]
36. Markwell, J.; Osterman, J.C.; Mitchell, J.L. Calibration of the Minolta SPAD-502 leaf chlorophyll meter. *Photosynth. Res.* 1995, 46, 467–472. [CrossRef]
37. Savitzky, A.; Golay, M.J.E. Smoothing and differentiation of data by simplified least squares procedures. *Anal. Chem.* 1964, 36, 1627–1639. [CrossRef]
38. Kruse, F.A.; Heidebrecht, K.B.; Shapiro, A.T.; Barloon, P.J.; Goetz, A.F.H. The spectral image processing system (SIPS) interactive visualization and analysis of imaging spectrometer data. *Remote Sens. Environ.* 1993, 44, 145–163. [CrossRef]
39. Guyot, G.; Baret, F.; Major, D.J. High spectral resolution: Determination of spectral shifts between the red and the near infrared. *Int. Arch. Photogram. Remote Sens.* 1988, 11, 750–760.
40. Gelfond, J.; Goros, M.; Hernandez, B.; Bokov, A. A System for an accountable data analysis process in R. *R J.* 2018, 10, 6. [CrossRef]
41. Fageria, N.K.; De Morais, O.P.; Dos Santos, A.B. Nitrogen use efficiency in upland rice genotypes. *J. Plant Nutr.* 2010, 33, 1696–1711. [CrossRef]
42. Gholizadeh, A.; Saberioon, M.; Boru<sup>o</sup> vka, L.; Wayayok, A.; Mohd Soom, M.A. Leaf chlorophyll and nitrogen dynamics and their relationship to lowland rice yield for site-specific paddy management. *Inf. Process. Agric.* 2017, 4, 259–268. [CrossRef]

43. Huang, J.; He, F.; Cui, K.; Buresh, R.J.; Xu, B.; Gong, W.; Peng, S. Determination of optimal nitrogen rate for rice varieties using a chlorophyll meter. *Field Crops Res.* 2008, 105, 70–80. [CrossRef]
44. Ata-Ul-Karim, S.T.; Cao, Q.; Zhu, Y.; Tang, L.; Rehmani, M.I.A.; Cao, W. Non-destructive assessment of plant nitrogen parameters using leaf chlorophyll measurements in rice. *Front. Plant Sci.* 2016, 7, 1829. [CrossRef]
45. Schlemmer, M.; Gitelson, A.; Schepers, J.; Ferguson, R.; Peng, Y.; Shanahan, J.; Rundquist, D. Remote estimation of nitrogen and chlorophyll contents in maize at leaf and canopy levels. *Int. J. Appl. Earth Obs. Geoinf.* 2013, 25, 47–54. [CrossRef]
46. Peng, S.; Garcia, F.V.; Laza, R.C.; Sanico, A.L.; Visperas, R.M.; Cassman, K.G. Increased N-use efficiency using a chlorophyll meter on high-yielding irrigated rice. *Field Crops Res.* 1996, 47, 243–252. [CrossRef]
47. Friedel, M.; Hendgen, M.; Stoll, M.; Löhnertz, O. Performance of reflectance indices and of a hand held device for estimating in-field the nitrogen status of grapevine leaves. *Aust. J. Grape Wine Res.* 2020, 26, 110–120. [CrossRef]
48. Rubo, S.; Zinkernagel, J. Exploring hyperspectral reflectance indices for the estimation of water and nitrogen status of spinach. *Biosyst. Eng.* 2022, 214, 58–71. [CrossRef]
49. Ballini, E.; Nguyen, T.T.; Morel, J.-B. Diversity and genetics of nitrogen-induced susceptibility to the blast fungus in rice and wheat. *Rice* 2013, 6, 32. [CrossRef] [PubMed]
50. Talukder, Z.I.; McDonald, A.J.S.; Price, A.H. Loci controlling partial resistance to rice blast do not show marked QTL environment interaction when plant nitrogen status alters disease severity. *New Phytol.* 2005, 168, 455–464. [CrossRef]
51. Frontini, M.; Boissard, A.; Frouin, J.; Ouikene, M.; Morel, J.B.; Ballini, E. Genome-wide association of rice response to blast fungus identifies loci for robust resistance under high nitrogen. *BMC Plant Biol.* 2021, 21, 99. [CrossRef]
52. Osuna-Canizalez, F.J.; De Datta, S.K.; Bonman, J.M. Nitrogen form and silicon nutrition effects on resistance to blast disease of rice. *Plant Soil* 1991, 135, 223–231. [CrossRef]
53. Snoeijers, S.S.; Perez-Garcia, A. The effect of nitrogen on disease development and gene expression in bacterial and fungal plant pathogens. *Eur. J. Plant Pathol.* 2000, 106, 493–506. [CrossRef]
54. Leucker, M.; Mahlein, A.-K.; Steiner, U.; Oerke, E.-C. Improvement of lesion phenotyping in *Cercospora beticola*–sugar beet interaction by hyperspectral imaging. *Phytopathology* 2016, 106, 177–184. [CrossRef] [PubMed]
55. Sanaeifar, A.; Yang, C.; De La Guardia, M.; Zhang, W.; Li, X.; He, Y. Proximal hyperspectral sensing of abiotic stresses in plants. *Sci. Total Environ.* 2023, 861, 160652. [CrossRef] [PubMed]

56. Laroche-Pinel, E.; Albughdadi, M.; Duthoit, S.; Chéret, V.; Rousseau, J.; Clenet, H. Understanding vine hyperspectral signature through different irrigation plans: A first step to monitor vineyard water status. *Remote Sens.* 2021, 13, 536. [CrossRef]

### 3.8 Supplementary Materials

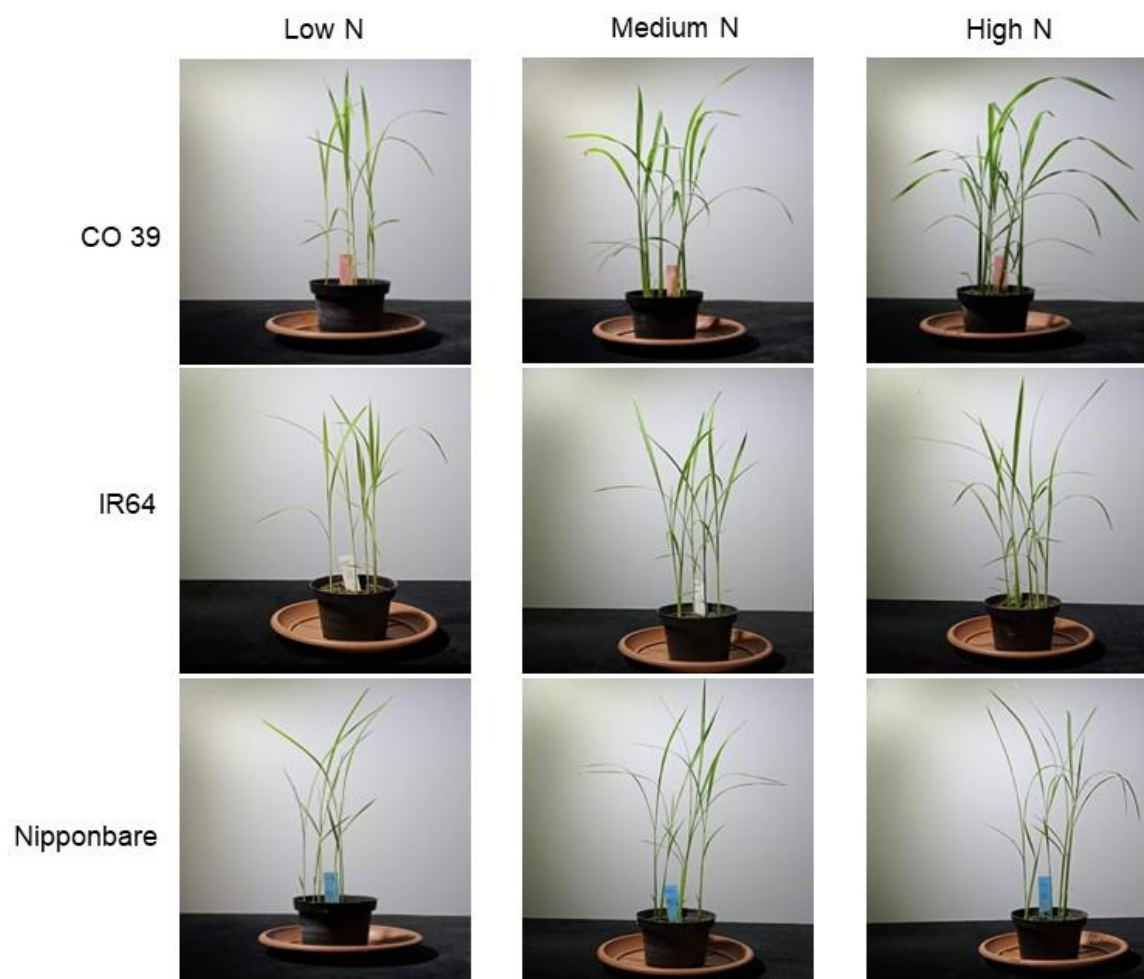


**Fig. S3.1:** Characteristics of rice plants – genotypes CO 39, IR64, and Nipponbare - in response to increasing N levels 4 days after mineral N application. Different N inputs are indicated by low, medium, and high N levels.

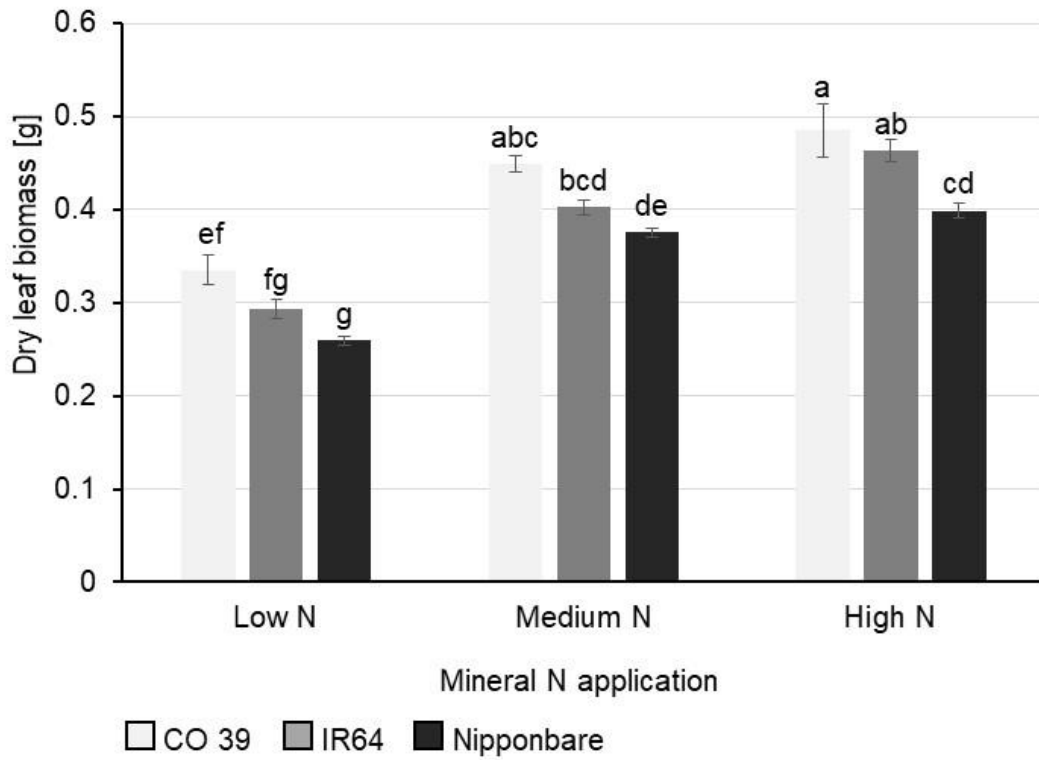


**Fig. S3.2:** Effect of mineral N supply on total dry biomass of the rice genotypes CO 39, IR64, and Nipponbare 4 days N application. The mean  $\pm$  standard error ( $n = 4$ ) is shown. Letters denote statistically significant differences according to Tukey's HSD test ( $P = 0.05$ ).

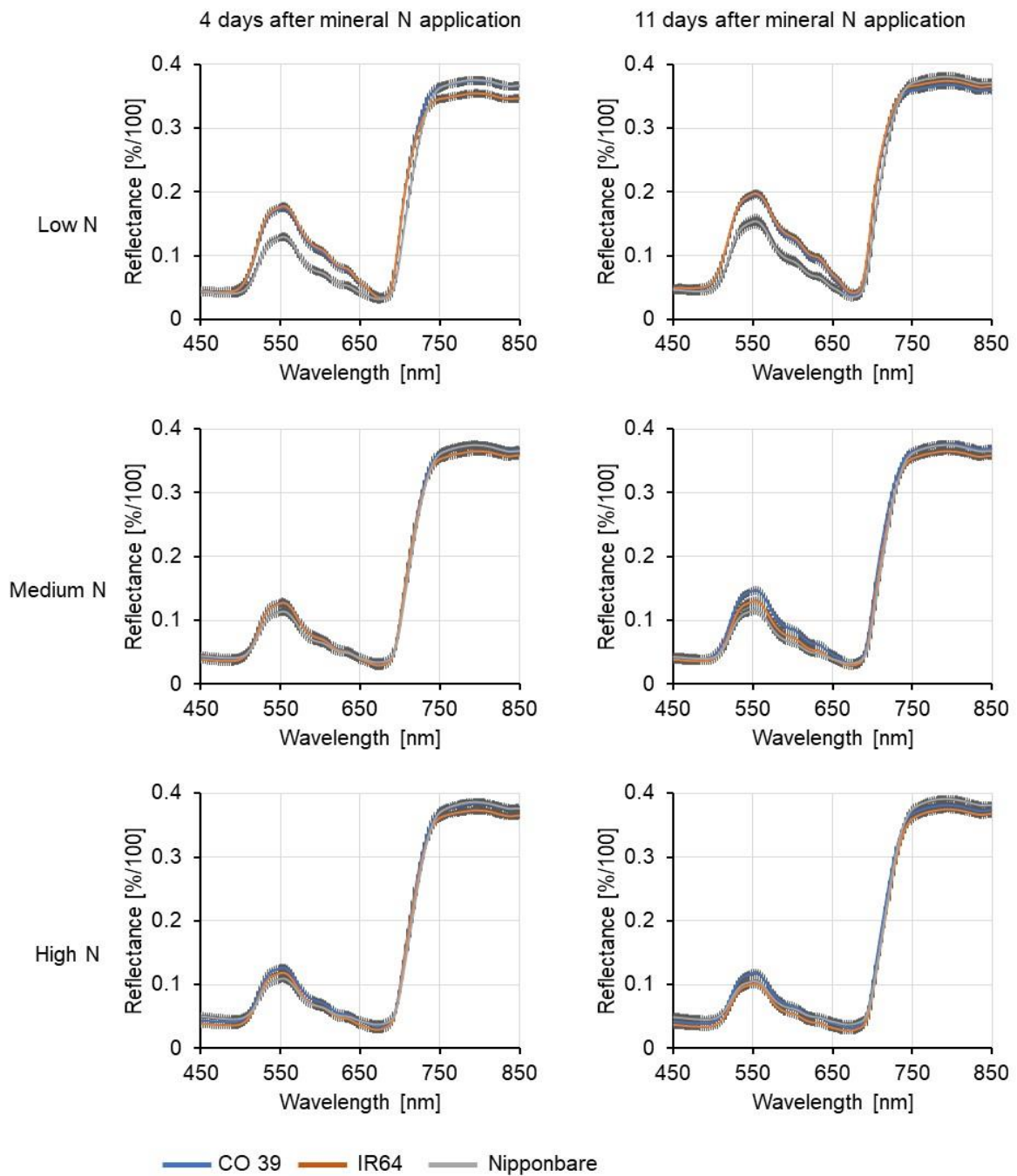


**Fig. S3.3:** Effect of rice genotypes on the reflectance of healthy rice leaves. Average reflectance spectra of rice genotypes CO 39, IR64, and Nipponbare at low, medium, and high N supply at 4 and 11 days after mineral N application. For each waveband, bars represent the standard error of the mean ( $n = 4$ ).

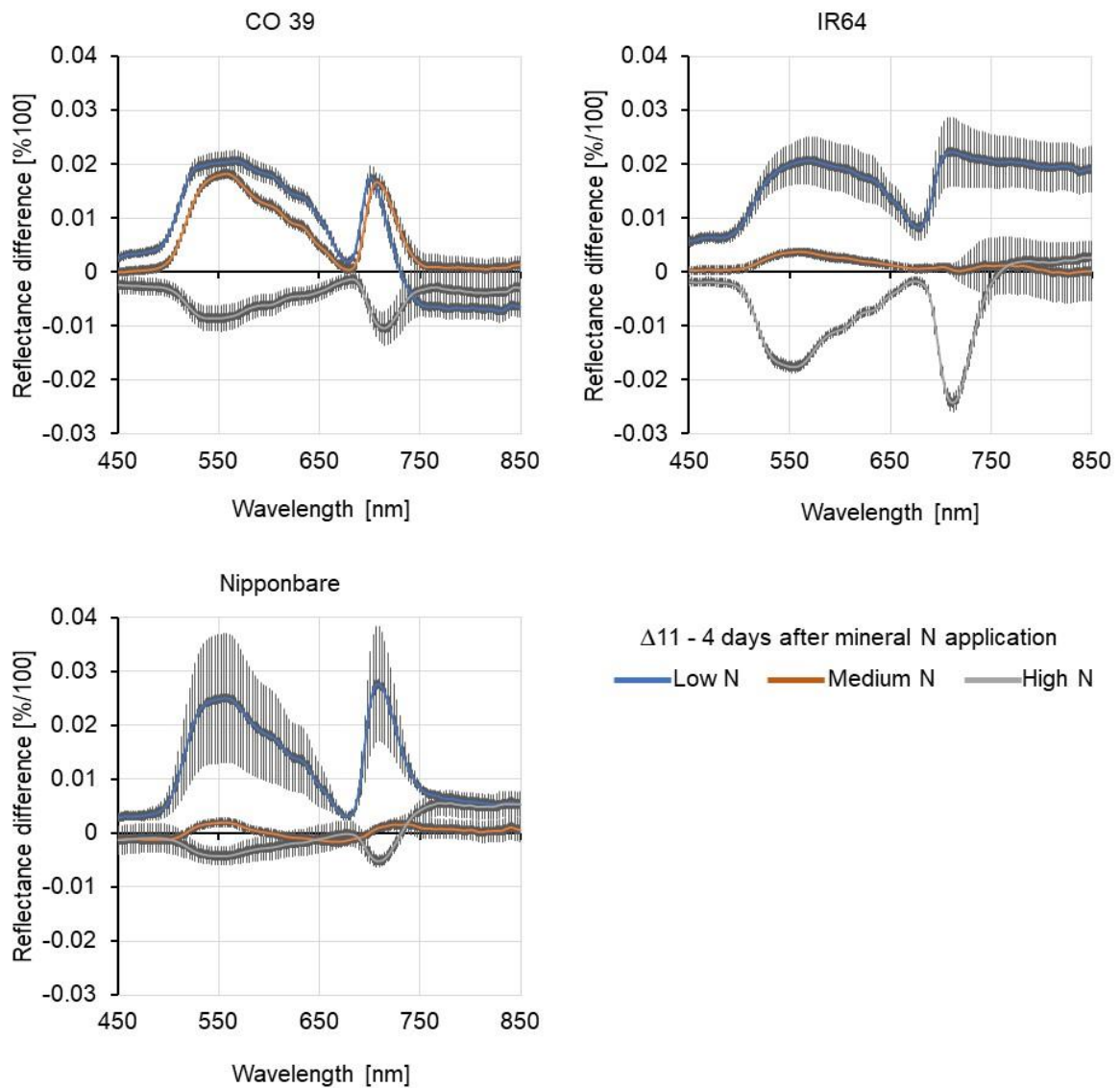


**Fig. S3.4:** Difference spectra of reflectance of healthy leaf tissue of rice genotypes CO 39, IR64, and Nipponbare grown at low, medium, and high mineral N supply, respectively. Differences were calculated by subtracting the spectra at 4 days after fertilizer application from 11 days after fertilizer application to determine the effect of time on mineral N application. For each waveband, bars represent the standard error of the mean (n = 4).

#### 4 Hyperspectral imaging for quantifying *Magnaporthe oryzae* sporulation on rice genotypes

Chapter 4 has been published:

**Angeline Wanjiku Maina\*** and Erich-Christian Oerke, 2024. Hyperspectral imaging for quantifying *Magnaporthe oryzae* sporulation on rice genotypes. *Plant Methods*, 20(1), 87. <https://doi.org/10.1186/s13007-024-01215-1>

Institute for Crop Science and Resource Conservation (INRES) - Plant Pathology, Rheinische Friedrich-Wilhelms University of Bonn, Germany

##### **Author contributions**

The experiment was designed by **A.W.M.** and E.-C.O. **A.W.M.** conducted the experiments, performed hyperspectral measurements, analyzed the data, and drafted the manuscript. All authors reviewed, revised, and approved the final manuscript.

#### 4.1 Abstract

**Background** Precise evaluation of fungal conidia production may facilitate studies on resistance mechanisms and plant breeding for disease resistance. In this study, hyperspectral imaging (HSI) was used to quantify the sporulation of *Magnaporthe oryzae* on the leaves of rice cultivars grown under controlled conditions. Three rice genotypes (CO 39, Nipponbare, IR64) differing in susceptibility to blast were inoculated with *M. oryzae* isolates Guy 11 and Li1497. Spectral information (450–850 nm, 140 wavebands) of typical leaf blast symptoms was recorded before and after induction of sporulation of the pathogen.

**Results** *M. oryzae* produced more conidia on the highly susceptible genotype than on the moderately susceptible genotype, whereas the resistant genotype resulted in no sporulation. Changes in reflectance spectra recorded before and after induction of sporulation were significantly higher in genotype CO 39 than in Nipponbare. The spectral angle mapper algorithm for supervised classification allowed for the classification of blast symptom subareas and the quantification of lesion areas with *M. oryzae* sporulation. The correlation between the area under the difference spectrum (viz. spectral difference without and with sporulation) and the number of conidia per lesion and the number of conidia per lesion area was positive and count-based differences in rice—*M. oryzae* interaction could be reproduced in the spectral data.

**Conclusions** HSI provided a precise and objective method of assessing *M. oryzae* conidia production on infected rice plants, revealing differences that could not be detected visually.

**Keywords:** Blast, conidia production, *Oryza sativa*, partial disease resistance, spectral reflectance

#### 4.2 Background

The filamentous ascomycete fungus *Magnaporthe oryzae* B.C. Couch, causal agent of blast disease is of importance to both worldwide rice cultivation and the understanding of host-pathogen interactions [1]. Blast is directly responsible for annual yield losses of up to 10–30%, and complete loss (100%) may occur during an epidemic [2, 3]. Spatial dissemination of the pathogen relies on the production of conidia by multiple cycles of asexual reproduction [4, 5]. As a polycyclic pathogen, multiple disease cycles (8 to 11) from the germination to the production of conidia occur in a growing season [4, 6]. The fungus sporulates continually for about 20 days and a single leaf blast lesion can produce up to 20,000 conidia [1, 7]. Maximum sporulation occurs at an optimum temperature between 25 and 28 °C, relative humidity (RH) above 90%, and extended periods of leaf wetness [8, 9]. The production of *M. oryzae* conidia is a regulated process that requires a period of darkness [1]. The importance of sporulation lies in its contribution to the spread and survival of *M. oryzae*, as the

production of conidia is a key step in the development of rice blast epidemics [5, 10]. The cultivation of resistant varieties can decrease the inoculum potential within the field and delays disease epidemics.

Due to the short-lived nature of complete resistance to blast, the development of rice varieties with quantitative resistance (also called partial, rate-reducing, or slow-blasting) is vital for disease resistance breeding [11, 12]. Partial resistance in rice is a form of incomplete resistance characterized by reduced pathogen growth and reproduction [13, 14]. This type of resistance is attributed to different components e.g., reduced infection frequency, longer latent period, lesion size, and reduced sporulation [13–15]. The result is a diminished potential for inoculum production and a decreased likelihood of a blast epidemic. Partial resistance is race non-specific and is controlled by multiple genes, each of which makes a relatively small contribution to the overall resistance, and hence remains effective for a longer time [16, 17]. The small differential interactions between genotypes of rice and *M. oryzae* indicate that partial resistance genes in the host interact on a gene-for-gene basis with genes in the pathogen [18, 19].

Assessing a large number of rice genotypes based on their reaction to all components of partial resistance is difficult because they interact among themselves, and their effects are cumulative during the course of disease development [15]. Moreover, the severity of blast is often measured in the field by the end of the rice growth period and represents the cumulative result of all components of partial resistance [14]. While visual assessment of disease severity is a common method for selecting blast-resistant rice varieties in the field, it may not provide detailed information about the underlying mechanisms of partial blast resistance [14]. It is essential to estimate the contribution of each component of partial resistance to disease development followed by selection for a single component [15, 20]. In the case of partial resistance to leaf blast in rice, the sporulating of *M. oryzae* is an important parameter. Measurement of sporulation in the field is difficult due to the presence of inoculum from adjacent plants. Hence, assessment of sporulation in the greenhouse setting offers the advantage of eliminating any interplot interference, a common phenomenon that often occurs in the field [21].

The traditional microscopic method for counting *M. oryzae* conidia and the use of spore trapping methods in combination with quantitative real-time polymerase chain reaction (qPCR) are labor-intensive, time-consuming, and involve the destruction of leaves [22]. Given the time-dependent nature of conidia production, it is recommended to use an automated method for quantifying fungal sporulation. Various image-based approaches have been proposed for quantifying fungal spores. Qi et al. [23] used micro-images to detect and count the spores of rice blast automatically. Xiaolong et al. [24] automatically counted the urediospores of *Puccinia striiformis* f. sp.

*tritici*, the causal agent of wheat stripe rust. Rapid detection of fungal spores in greenhouse crops was accomplished using the complementary metal oxide semiconductor (CMOS) image sensors technique and diffraction finger- print feature processing [25]. These approaches not only automate the spore detection and counting process but also emphasize the crucial role of precise phenotyping methods in plant disease epidemiology.

Hyperspectral imaging (HSI) has the advantage of rapid and non-destructive detection of plant diseases at the tissue level. It has been used in phenotyping leaf blast of rice [26, 27], the reaction of grapevines to *Plasmopara viticola* [28], *Fusarium* head blight (FHB) of wheat [29], and other plant diseases [30, 31]. Using HSI, Maina and Oerke [27] differentiated blast symptoms into subareas differing in coloration, size, and composition depending on the rice  $\times$  *M. oryzae* interaction. They observed rapidly enlarging grey tissue localized at the center of the blast symptom in compatible rice  $\times$  *M. oryzae* interactions. The size of the grey tissue is vital for the assessment of the sporulation rate since sporulation of *M. oryzae* is confined to the central area of blast lesions [32, 33].

HSI captures spectral information in the visible (VIS, 400–700 nm), and near-infrared (NIR, 700–1000 nm) ranges of the spectrum with a high spectral and spatial resolution [34], allowing for the differentiation of subtle changes associated with disease e.g., pathogen sporulation. Both imaging and non-imaging hyperspectral sensors have been used for quantitative analysis of fungal sporulation. Using a non-imaging spectrometer, Ren et. [35] created a robust yellow rust spore index (YRSI) to detect and quantify wheat yellow rust by closely analyzing how fungal spores influenced the overall leaf spectral response. HSI has been used to detect and diagnose wheat rust disease using reference spectra from spore scale observations [36]. Oerke et al. [37] successfully used HSI at the microscope scale to quantify the sporulation of *Cercospora beticola* on sugar beet leaves of varying susceptibility. The combination of hyperspectral imaging and computer vision effectively assessed and quantified the sporulation of downy mildew on grapevine leaves [38]. Segmentation of leaf disc images enabled the differentiation of pixels representing downy mildew sporulation from other parts of the leaf. Zhang et al. [39] used a microfluidic chip-based method combined with microscopic HSI to rapidly detect and quantify fungal spores on rice leaves. These studies suggest that HSI is an effective and objective method for assessing fungal sporulation and studying the dynamics of host-pathogen interactions. Nevertheless, most of these investigations relied on the average reflectance spectra from diseased tissues or focused only on a limited number of wavebands to evaluate the sporulation potential of fungal pathogens and the impact of fungal spores on the spectral characteristics of leaves.

In breeding for disease resistance, the identification of smaller cultivar differences requires a more precise and reliable method [40]. Incorporating a detailed examination of *M. oryzae* sporulation into the selection process under controlled conditions may help to identify small positive effects

related to blast resistance [11, 14, 41]. Accurate estimation of the quantity of inoculum during epidemics demands high precision in data collection and analysis [39, 40]. The characterization and quantification of sporulation using the entire spectrum in the VIS and NIR range may offer insights into the spatial dynamics of pathogen reproduction and disease spread as well as the mechanisms of disease resistance in host plants [37].

In this study, the potential of HSI to measure the sporulation of *M. oryzae*, as a crucial component of the partial resistance of rice to blast was investigated. In greenhouse experiments, the three rice genotypes CO 39, Nipponbare and IR64, varying in the level of susceptibility/resistance to leaf blast, were inoculated with the *M. oryzae* isolates Guy 11 and Li1497. The specific objectives were (a) to determine how host genotypes with different resistance levels affect conidia production of the pathogen; (b) to quantify the sporulation of *M. oryzae* on different rice genotypes by calculating the spectral difference between blast symptoms without and with conidia production, measured as the area under the difference spectrum (AUDS) of the grey tissue; and (c) to establish the relationship between AUDS and the rate of conidia production per lesion and per lesion area, respectively. Eventually, evaluating *M. oryzae* sporulation using HSI would shed light on the complex interactions between rice genotypes and *M. oryzae* isolates. This information can be invaluable in breeding programs to develop rice varieties with durable resistance to blast.

### 4.3 Materials and Methods

#### 4.3.1 Plant material

Three rice (*Oryza sativa* L.) genotypes differing in susceptibility to *M. oryzae* were used in these experiments; genotype CO 39 (*indica* type), which is highly susceptible to blast was obtained from IRRI, Philippines. Nipponbare (susceptible *japonica* type) and IR64 (resistant *indica* type) were generously provided by Michael Frei, Department of Plant Nutrition, University of Bonn. Seeds of each rice genotype were sown directly in plastic pots ( $\varnothing = 9$  cm; Kausek, Mittenwalde, Germany) filled with loam soil at 5 seeds per pot. Plants were cultivated under controlled conditions in the greenhouse as described by Maina and Oerke [27].

#### 4.3.2 Pathogen and inoculation

Two isolates of *M. oryzae* were used separately to inoculate rice leaves in order to take into account the gene- for-gene interactions. Isolate Guy 11 was kindly provided by Didier Tharreau (CIRAD, Montpellier, France), and isolate Li1497 was obtained from BASF SE (Limburgerhof, Germany). The cultivation of *M. oryzae* on rice leaf agar, the production of conidia, and the preparation of inoculum were performed as described earlier [27]. Eighteen days after seeding, rice plants at growth stage (GS)

13 [42] were spray-inoculated with a spore suspension ( $10^5$  conidia/ml) of *M. oryzae* using a hand sprayer. The inoculated plants were incubated in a dark moist incubation chamber at 25 °C and > 95% RH for 24 h, and subsequently returned to the greenhouse at 60% RH until visible blast symptoms developed. At least two independent experiments were conducted, each with 25 plants per genotype.

#### 4.3.3 Measurement of conidia production

Seven days post inoculation (d.p.i.), fungal sporulation was induced on mature blast symptoms by incubating diseased rice plants at 100% RH under alternating dark and light conditions (12 h / 12 h) for 2 days. Conidia production was measured at 9 d.p.i. (= 2 days after induction of sporulation). Leaf disks with a single lesion were separately placed into Eppendorf tubes containing tap water (0.5 ml water with 0.01% Tween 20). The tubes were shaken vigorously using a vortex shaker (Vortex-Genie 2, Bohemia, New York, USA) for 10 s to dislodge the conidia from the conidiophores. The number of conidia detached from the lesions was counted under a microscope (magnification 100x) using a Fuchs-Rosenthal chamber (Brand, Wertheim, Germany). Subsequently, the length and width of each lesion were measured to determine its area. Eight lesions per rice genotype × *M. oryzae* interaction were analyzed, and the results were expressed as the number of conidia per lesion and the number of conidia per lesion area [ $\text{mm}^2$ ].

#### 4.3.4 Microscopy

To study the characteristics of *M. oryzae*, a Leica Leitz DMR stereomicroscope (Leica Microsystems, Wetzlar, Germany) was used for light microscopy. Leaf sections with a single blast lesion were used to visualize the conidiophores and conidia on the surface of the sporulating lesions. Images were recorded using the software Discus (Technisches Büro Hilgers, Königswinter, Germany). For staining for fluorescence microscopy, leaf sections with a single blast lesion were cut and placed in 2 ml Eppendorf tubes containing 1 ml 10% KOH. About 50  $\mu\text{L}$  of Silwet® L-77 was added and the Eppendorf tubes were wrapped in aluminum foil for approximately 90 min. The leaf samples were placed onto clean glass slides, then a drop of calcofluor white was added, covered with a coverslip, and left to absorb the stain for 1 min. Samples were observed under a Leica SP8 confocal laser scanning microscope (Leica Microsystems, Wetzlar, Germany).

#### 4.3.5 Hyperspectral measurements and image analysis

To measure spectral differences between blast lesions without and with conidia, hyperspectral images were recorded using a spectral line scanner (spectral camera PFD V10E, Spectral Imaging Ltd., Oulu, Finland) as previously described [27]. Images of fully developed blast lesions on leaves of rice genotypes were recorded 7 days post inoculation (d.p.i.) as well as 2 days after the induction of

sporulation (= 9 d.p.i.). Eight lesions per rice genotype × *M. oryzae* interaction were analyzed for each time of image recording (before and after sporulation). The reflectance of hyperspectral images was calculated by normalizing the images relative to the reflection of a 100% white reference standard (Zenith Polymer Target, SphereOptics GmbH, Uhldingen, Germany) and to a dark current measurement using ENVI 5.3 + IDL 8.3 (ITT Visual Information Solutions, Boulder, CO). Because of noise at the extremes of the spectra, only wavelengths between 450 and 850 nm (140 wavebands) were used for spectral analysis and the resultant spectral signals were smoothed using a Savitzky-Golay filter [43].

All tissue types (= endmember classes) of the infected rice leaves - healthy (green) tissue, dark brown tissue, grey tissue, chlorotic tissue, grey green tissue, and light brown tissue - were characterized spectrally for images recorded before (7 d.p.i.) and 2 days after sporulation (= 9 d.p.i.). For each tissue type of the rice × *M. oryzae* interactions, at least 4 different areas were used per image to extract the mean (= typical) spectrum, which was stored in a spectral library, the collection of reference spectra (= endmember collection for the spectral angle mapper (SAM) algorithm). The number of pixels per region of interest (ROI) ranged from 2,600 to > 100,000 for healthy (green) tissue and from 50 to > 5,000 pixels for blast symptom subareas. Spectral signatures of different blast symptom subareas (= endmember classes) from eight representative lesions per rice genotype × *M. oryzae* interaction were extracted separately for each time of image recording. The spectral endmembers of the spectral libraries were used for the supervised classification of pixels by using the SAM algorithm [44].

#### 4.3.6 Spectral quantification of *M. oryzae* sporulation

For the spectral quantification of sporulation, reflectance spectra of grey tissue without (7 d.p.i.) and with sporulation (9 d.p.i.) were extracted from the same eight representative lesions from rice genotypes CO 39 and Nipponbare (workflow see Fig. 4.1). The spectral difference between grey tissue without and with sporulation, respectively, was quantified as the area under the difference spectrum (AUDS) (= area between the spectra of grey tissue recorded 7 and 9 d.p.i., respectively). The resulting AUDS [%/100.nm], characterizes the spectral modification caused by *M. oryzae* sporulation across the visible (VIS) and near-infrared (NIR) ranges of the spectrum.

#### 4.3.7 Statistical analysis

Statistical analyses were conducted using the R software [45]. A standard analysis of variance (ANOVA) was performed to determine the significance of differences in the number of conidia per lesion, number of conidia per lesion area, number of pixels of grey tissue, and in the area under the

difference spectrum. Mean separation was performed using Tukey's honest significant difference test ( $P = 0.05$ ). Correlations between AUDS and the number of conidia per lesion and number of conidia per lesion area were calculated using Pearson's correlation coefficient with the significance threshold set at  $P \leq 0.05$ . The number of replicates ( $n$ ) used for statistical analysis is given in the results section.

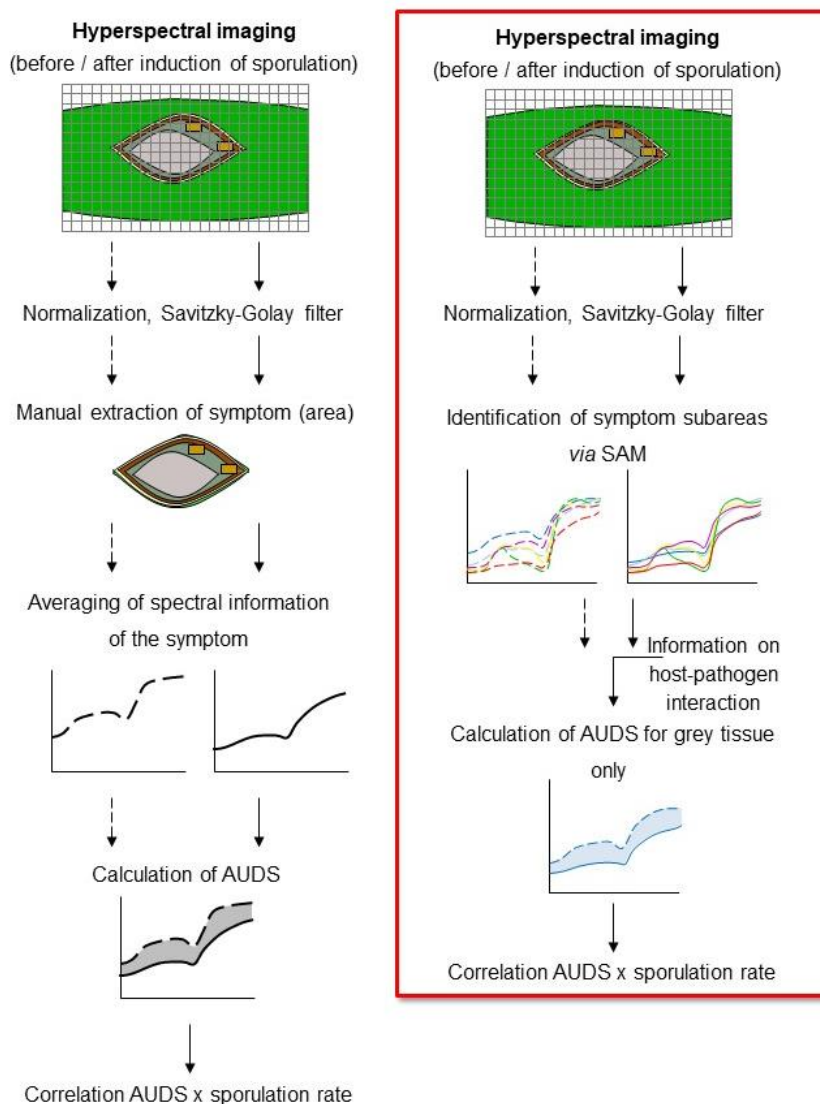


**Fig. 4.1:** Workflow for the quantification of *M. oryzae* sporulation using hyperspectral imaging data. In contrast to the workflow for assessing fungal sporulation by characterizing changes in the mean spectrum per disease symptom defined manually (left), the spectral angle mapper (SAM) was applied onto images after normalization and spectral smoothing by the Savitzky-Golay filter (right). Based on information from literature, the spectral difference (AUDS) between images recorded before and after the induction of *M. oryzae* conidia production was calculated only for the central grey tissue of blast symptoms.

## 4.4 Results

### 4.4.1 Effect of rice genotypes on the intensity of *M. oryzae* sporulation

The production of conidia of *M. oryzae* isolates Guy 11 and Li1497 on rice genotypes CO 39, Nipponbare, and IR64 was quantified microscopically (Fig. 4.2). The number of conidia produced per lesion was counted 2 days after diseased rice plants had been incubated at 100% RH (= 9 d.p.i.). On rice genotypes CO 39 and Nipponbare, more than 2,000 conidia per lesion were produced within 2 days. The number of conidia per lesion differed among rice genotype  $\times$  *M. oryzae* interactions. It was significantly ( $P < 0.05$ ) higher in highly susceptible genotype CO 39 infected by isolates Guy 11 and Li1497 and genotype Nipponbare susceptible to isolate Li1497 compared to genotype Nipponbare which was only moderately susceptible to *M. oryzae* isolate Guy 11. When sporulation was expressed as conidia per lesion area, *M. oryzae* produced more conidia on genotype CO 39 than on Nipponbare for all interactions. Statistically significant ( $P < 0.05$ ) differences were observed between CO 39 infected with Li1497 and Nipponbare infected with Guy 11. Both *M. oryzae* isolates did not produce conidia on the resistant genotype IR64 (Fig. 4.2).

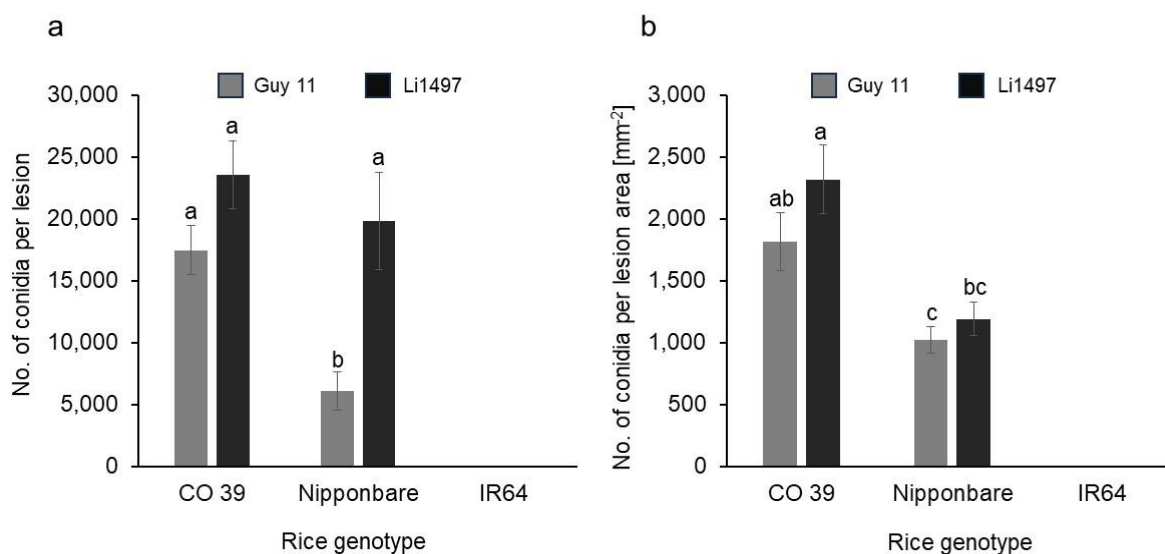


**Fig. 4.2:** Conidia production of *M. oryzae* isolates Guy 11 and Li1497 on the three rice genotypes CO 39, Nipponbare, and IR64 differing in susceptibility to leaf blast; (a) number of conidia produced per lesion; (b) number of conidia produced per lesion area. Sporulation was assessed 9 days post inoculation (= after 2 days of induction of conidia production). Columns with the same letter were not significantly different ( $P = 0.05$ , Tukey's honestly significant difference test). Bars represent standard error of the mean ( $n = 8$ ).

#### 4.4.2 Morphological characteristics of sporulating lesions, conidiophores, and conidia

The characteristics of typical sporulating blast lesions on susceptible rice genotypes were assessed 9 d.p.i. (Fig. 4.3). Incubation of rice plants for two days under high RH led to the formation of aerial mycelia of *M. oryzae* that spread on the surface of the lesion (Fig. 4.3a). Microscopic examination revealed the presence of the conidiophores (bearing conidia) protruding from the lesion surface. The conidiophores were elongated, slender, and septate (Fig. 4.3b). The conidia of *M. oryzae* were hyaline (translucent), pyriform or pear-shaped with a distinct narrow apex (pointed end) and a rounded base, and had two septa, three cells (Fig. 4.3c, Fig. 4.3d).

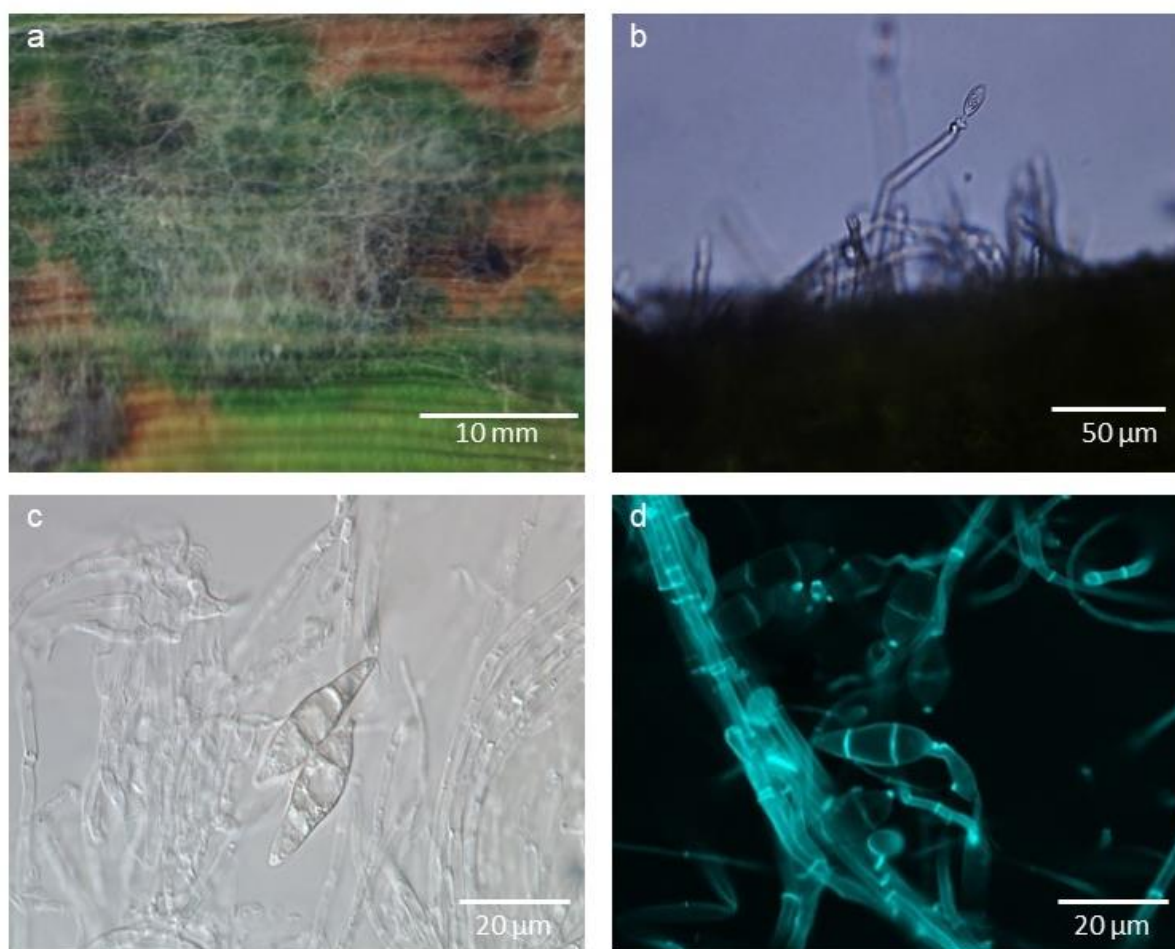


**Fig. 4.3:** Characteristics of *M. oryzae* on the highly susceptible rice genotype CO 39, 9 days post inoculation; (a) typical blast lesion with grey aerial mycelium; (b) hyaline conidiophore with conidia protruding from the surface of blast lesion, (c) morphology of *M. oryzae* conidia in bright field microscopy, (d) image of conidiophores and conidia from confocal laser scanning microscopy (staining with calcofluor).

#### 4.4.3 Phenotypes of typical blast symptom types during conidia production

During conidia production, the typical blast symptoms exhibited variation depending on the specific interaction between the genotypes of host and pathogen and the size, shape, and color of blast symptom subareas varied within leaves (Fig. 4.4). The type of blast symptom and the lesion area had an influence on the production of conidia by *M. oryzae*. In case of the resistant rice genotype IR64, the blast lesions on the leaf surface were small dark brown spots. There was no formation of a sporulating lesion center on resistant genotype IR64, and consequently, no subsequent production of conidia.

In contrast, leaves of CO 39 - highly susceptible to isolates Guy 11 and Li1497 - and Nipponbare - susceptible to Li1497, but only moderately susceptible to Guy 11 - displayed different patterns of blast symptoms. In highly compatible interactions, the characteristic blast lesions were larger, elliptical, or spindle-shaped and rapidly expanded due to vigorous *M. oryzae* growth during the two days of incubation for sporulation. The blast symptoms on the moderately resistant genotype were relatively smaller than in the compatible and highly compatible interactions. The center of blast lesions was characterized by distinct greyish tissue, surrounded by grey green tissue with a brown margin and chlorotic tissues and by light brown tissue. The grey tissue in the center of lesions could be attributed to the growth of superficial mycelia, the formation of conidiophores, and the production of conidia (Fig. 4.4).

#### 4.4.4 Spectral assessment of blast symptom subareas

The average reflectance spectra in the VIS and NIR spectral range of healthy (green) tissue and specific subareas of the blast symptoms were manually extracted before sporulation (7 d.p.i.) and 2 days after induction of sporulation (= 9 d.p.i.) (Fig. 4.5, Additional file 1: Fig. A4.1). The differences in the spectral signatures were used for the classification of lesion pixels. Although similar, the spectra of healthy (green) tissue significantly differed between rice genotypes in the VIS and NIR ranges (Additional file 2: Fig. A4.2). The spectral signatures of different blast symptom subareas considerably differed from healthy (green) tissue as well as from each other. The generation of reference spectra, therefore, required the definition of regions of interest (ROIs) for each blast symptom subarea for the individual rice genotypes (Fig. 4.5).

Using the specific spectra of green tissue and blast symptom subareas as reference spectra (endmembers), the supervised classification of images taken before and after induction of *M. oryzae* sporulation was done using the SAM algorithm (Fig. 4.6, Fig. 4.7). As visualized by the pseudo-color images, SAM was able to differentiate blast symptoms into different subareas based on the color (and structure) of the tissue and depending on the rice  $\times$  *M. oryzae* interaction. In genotype IR64 resistant

to both *M. oryzae* isolates used in this study, only small dark brown spots were classified without differentiation into subareas. For the interaction between CO 39 × Guy 11 or Li1497, Nipponbare × Li1497, and Nipponbare × Guy 11, blast symptoms had a typical zonation into different subareas that included dark brown tissue, grey tissue, grey green tissue, chlorotic tissue, and light brown tissue, indicating the complex nature of the interaction between host and pathogen. Each blast symptom subarea had specific spectral signatures as shown in Fig. 4.5 Additional file 1: Fig. A4.1.



**Fig. 4.4:** Phenotypes of leaf blast symptoms on rice genotypes CO 39, Nipponbare, and IR64 infected with *M. oryzae* isolates Guy 11, and Li1497, respectively. Images were recorded after incubation of rice plants under 100% RH for 2 days to induce sporulation, corresponding to 9 days post inoculation (bar size = 10 mm).

Spectral reflectance of the grey tissue was significantly reduced within the two-day incubation period. In contrast, no significant differences were observed in the spectra of the other blast symptom subareas (dark brown, chlorotic, grey green, and light brown tissues) and healthy tissue during the incubation period, suggesting a specific response in the grey tissue. Grey tissue was confined to the central area of blast lesions for both CO 39 and Nipponbare genotypes, irrespective of the infecting *M. oryzae* isolate. The repeated measurements on the same blast symptom type 7 and 9 d.p.i. indicated an increase in lesion size and a change from one symptom type (= spectral class) to another e.g., green tissue to chlorotic tissue, grey green tissue to grey tissue, chlorotic tissue to light brown

tissue due to fungal growth (colonization), growth of surface mycelial on the lesion, formation of conidiophores, and production of conidia (Fig. 4.6, Fig. 4.7). The strongest changes in coloration were observed in highly compatible interactions.

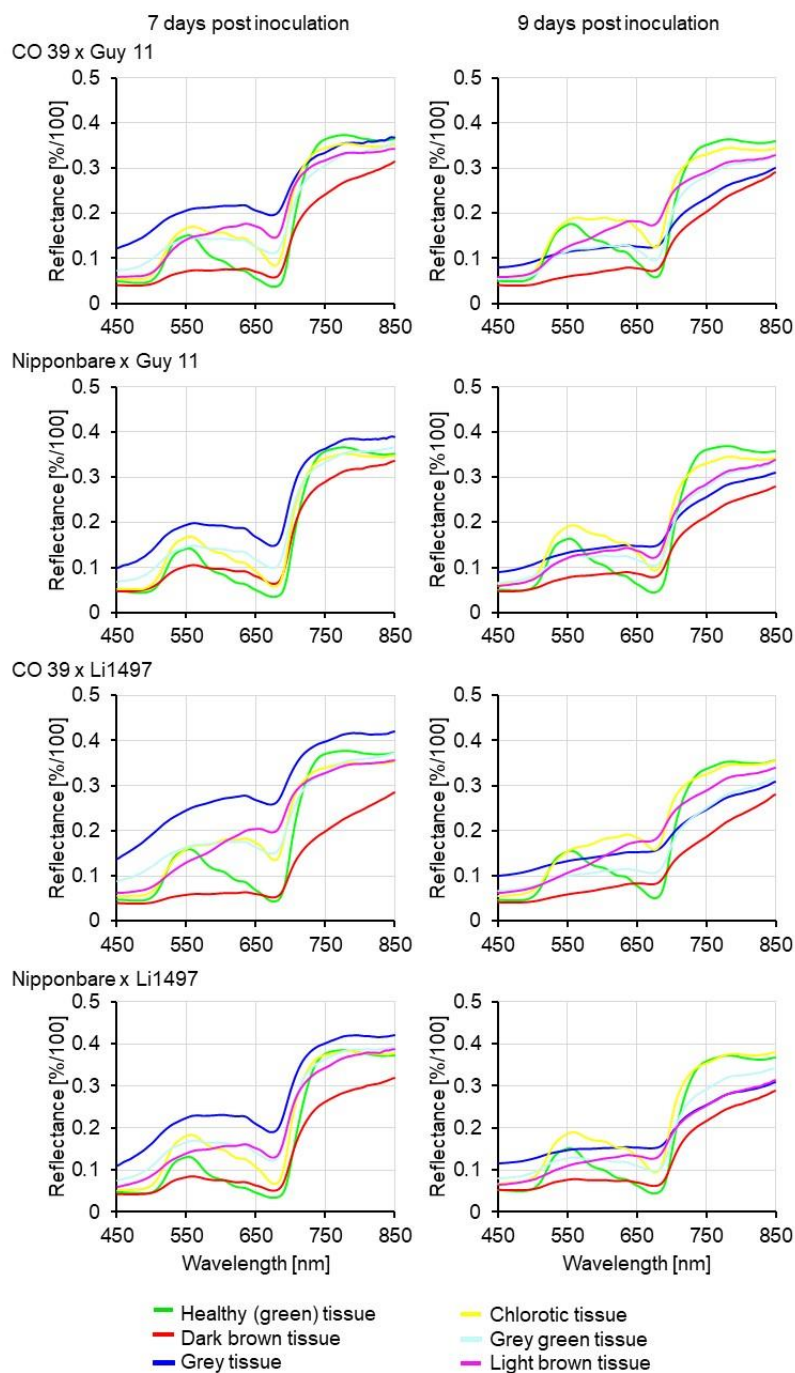


**Fig. 4.5:** Reference spectra of healthy (green) tissue and of blast symptom subareas from leaves of rice genotypes CO 39 and Nipponbare infected with *M. oryzae* isolates Guy 11 and Li1497, respectively. Spectra of healthy tissue and of blast symptom subareas were extracted before (7 d.p.i., left) and 2 days after induction of sporulation (= 9 d.p.i., right).

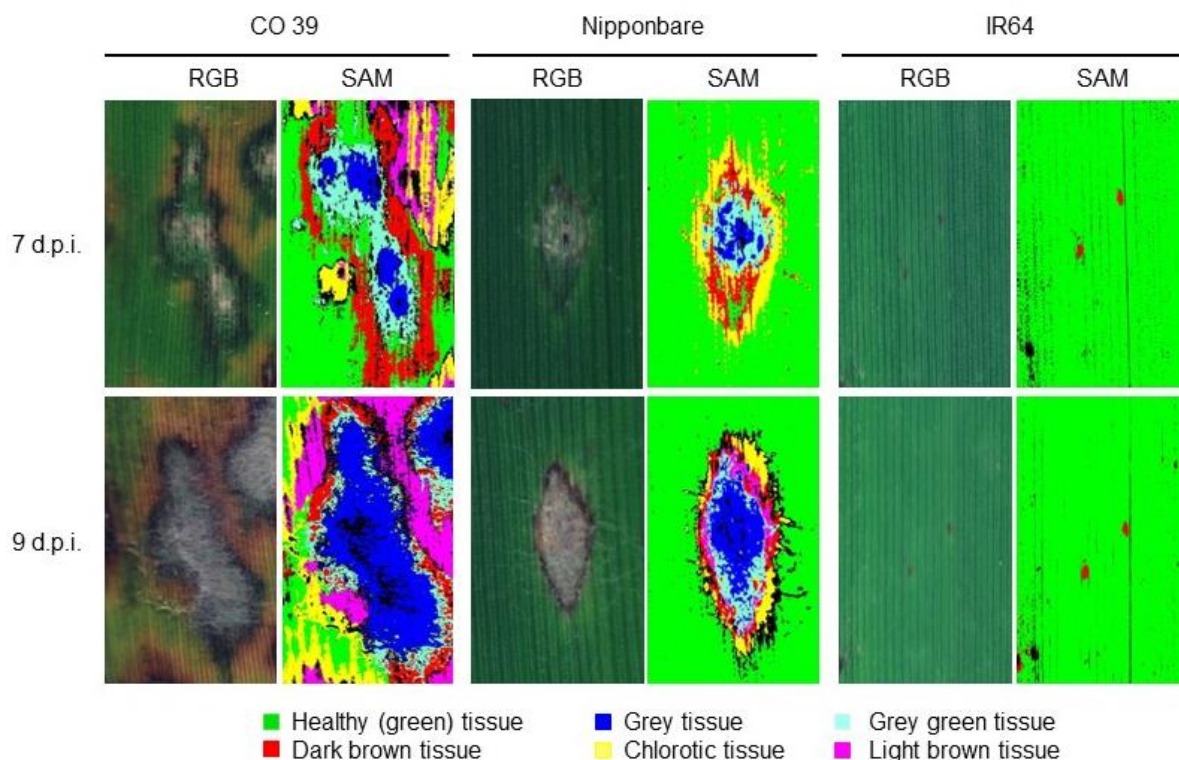


**Fig. 4.6:** Sporulation of *M. oryzae* isolate Guy 11 on leaves of the rice genotypes CO 39, Nipponbare, and IR64 as quantified by hyperspectral imaging. Images illustrate RGB picture and pseudo-color results of spectral angle mapper (SAM) classification of blast lesions before induction of sporulation (7 days post inoculation) and with sporulation (9 d.p.i.) induced by incubation of rice plants under 100% RH for 2 days. Different subareas of blast symptom types were classified for each rice genotype  $\times$  *M. oryzae* interaction.

#### 4.4.5 Effects of *M. oryzae* sporulation on reflectance spectra of blast lesions

The average reflectance spectra of grey tissue from blast infected leaves of rice genotypes CO 39 and Nipponbare were extracted before the induction of sporulation and compared to the reflectance extracted 2 days after induction of sporulation (Fig. 4.8). Compared to the green tissue, the spectral signature of grey tissue was characterized by higher reflectance across the visible (450–700 nm) and near-infrared (700–850 nm) range. After incubating infected rice plants under 100% RH for the induction of sporulation, the formation of aerial mycelia, conidiophores, and conidia by *M. oryzae* on the surface of the grey tissue led to a strong decrease in reflectance across the full spectral range.

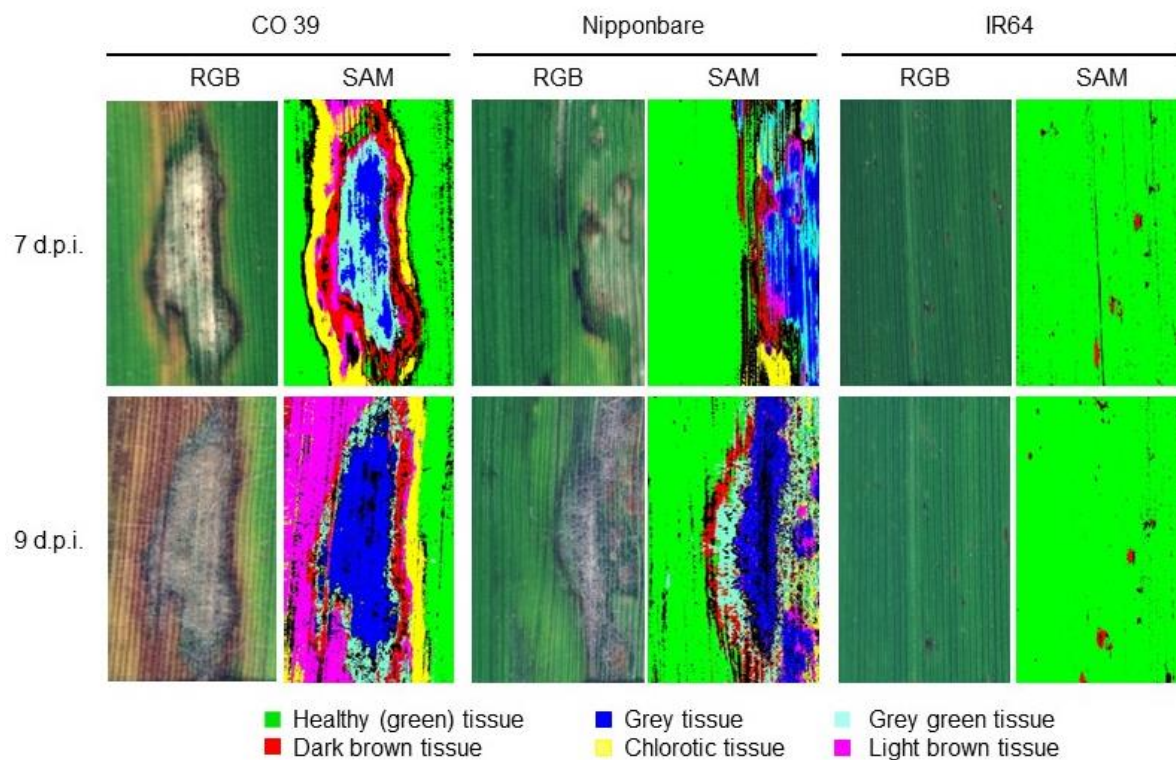


**Fig. 4.7:** Sporulation of *M. oryzae* isolate Li1497 on leaves of the rice genotypes CO 39, Nipponbare, and IR64 as quantified by hyperspectral imaging. Images illustrate RGB picture and pseudo-color results of spectral angle mapper (SAM) classification of blast lesions before induction of sporulation (7 days post inoculation) and with sporulation (9 d.p.i.) induced by incubation of rice plants for 2 days under 100% RH. Different subareas of blast symptom types were classified for each rice genotype  $\times$  *M. oryzae* interaction.

Changes in spectra before and after induction of sporulation were significantly higher for rice genotype CO 39 than for Nipponbare, irrespective of the *M. oryzae* isolate involved (Fig. 4.8) indicating a genotype-specific difference in the spectral characteristics (Fig. 4.8, Fig. 4.9a). The mean value of the area under difference spectrum was highest for the interaction CO 39  $\times$  Li1497 and was significantly ( $P < 0.05$ ) lower for genotype Nipponbare infected by Guy 11 (Fig. 4.9b). The area of grey tissue (i.e., sporulation area) 9 d.p.i., as classified by SAM algorithm ranged from 2,526 to 59,819 pixels, revealing significant differences ( $P < 0.05$ ) between rice genotypes (Fig. 4.9c).

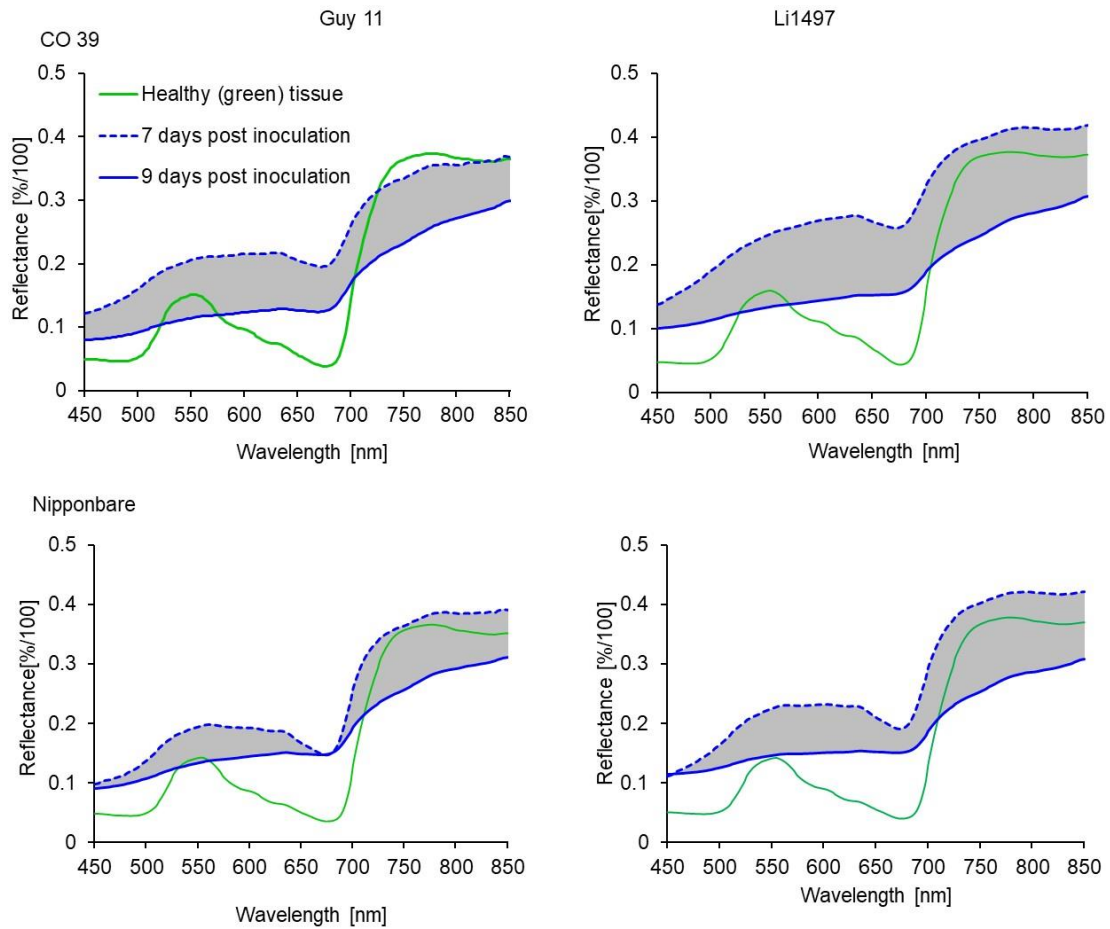


**Fig. 4.8:** Spectral signatures of healthy (green) tissue and grey tissue (sporulating area) of rice genotypes CO 39 and Nipponbare infected with *M. oryzae* isolates Guy 11 and Li1497, respectively. The spectral signatures were extracted before (7 days post inoculation) and with sporulation (9 d.p.i.), ( $n = 8$ ). The shaded area represents the area under difference spectrum for the grey tissue.

The relationship between these spectral differences and the actual *M. oryzae* conidia production was assessed using Pearson correlation analysis. The AUDS values showed a significant, positive correlation to the number of conidia produced per blast lesion and the number of conidia produced per lesion area (Fig. 4.10). For the number of conidia per lesion, the linear relationship ( $R^2 = 0.574$ ;  $r = 0.758$  significantly different from 0,  $P < 0.05$ ) was better than the power function ( $R^2 = 0.535$ ); for the number of conidia per lesion area, the exponential function ( $R^2 = 0.625$ ) was marginally better than the linear function ( $R^2 = 0.617$ ;  $r = 0.785$  significantly different from 0,  $P < 0.05$ ) in describing the relationship to AUDS. When the four host-pathogen interactions were analysed separately, the coefficient of determination for the correlation between AUDS and sporulation per lesion area differed considerably and the slope of the regression lines - range 58x to 257x - indicated to differences in compatibility; cv. Nipponbare limited *M. oryzae* sporulation stronger than CO 39, the sporulation rate of isolate Li1497 was higher than that of Guy 11 (Additional file 3: Fig. A4.3).

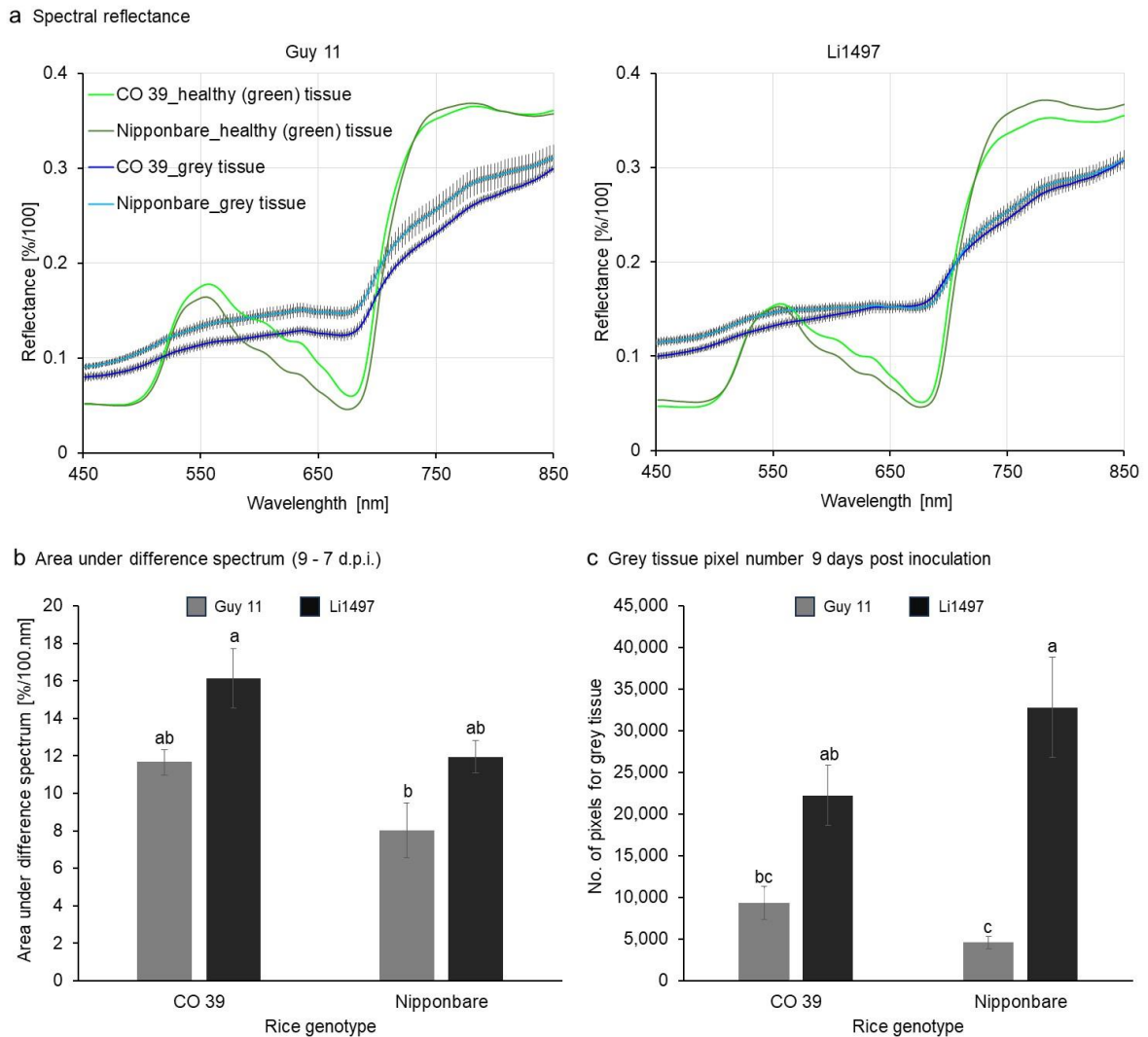


**Fig. 4.9:** (a) Comparison of spectra for healthy (green) tissue and grey tissue (= sporulating area) from rice genotypes CO 39 and Nipponbare infected with *M. oryzae* isolates Guy 11 and Li1497, respectively, 9 days post sporulation. Bars represent standard error of the mean for each waveband ( $n = 8$ ); (b) area under the difference spectrum calculated from spectra taken before (7 d.p.i.) and with sporulation (9 d.p.i.), respectively; (c) Quantitative assessment of the pixels representing grey tissue (= sporulating area) from CO 39 and Nipponbare, 9 days post sporulation. Values with the same letter are not significantly different (Tukey's honestly significant difference test ( $P = 0.05$ ,  $n = 8$  [spectra])). Bars indicate standard error of the mean.

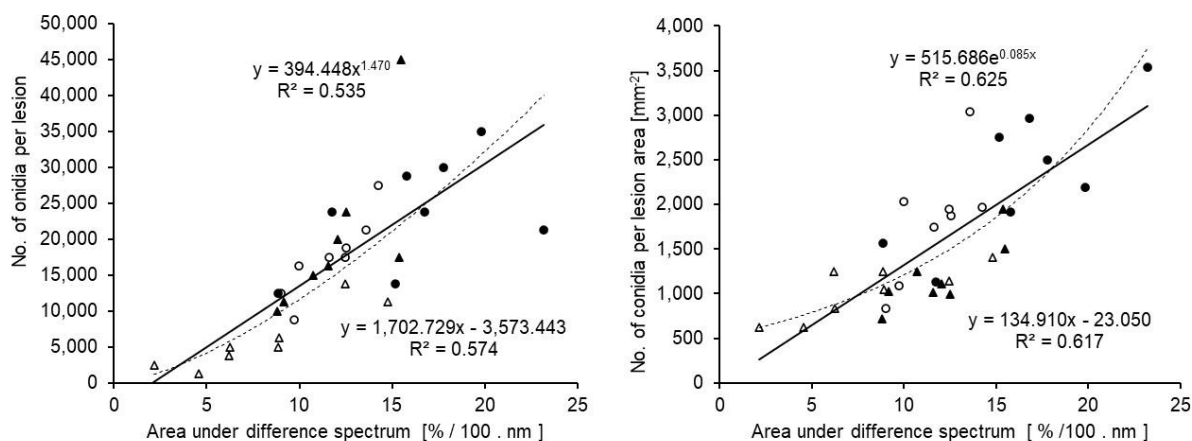


**Fig. 4.10:** Relationship between the area under difference spectrum (AUDS) and the number of *M. oryzae* conidia produced on lesions of two rice genotypes differing in susceptibility to blast. Correlation between AUDS from spectra recorded without (7 d.p.i.) and with (9 d.p.i.) sporulation, respectively, and the counted number of conidia per lesion (left) and the number of conidia per lesion area (right) ( $n = 32$ ). Linear (solid line) and non-linear relationships (dashed line; power function and exponential function, respectively) with the highest coefficients of determination.

#### 4.5 Discussion

This study investigated the potential of HSI to measure the spore production of *M. oryzae* on rice genotypes differing in susceptibility to the blast pathogen. The rate of conidia production per lesion and conidia production per lesion area differed depending on the compatibility between rice genotypes and *M. oryzae* isolates. Resistant genotype IR64 restricted fungal colonization to tiny brown spots and no sporulation was detected, while highly compatible host-pathogen interactions resulted in significantly higher conidia densities than moderately compatible interactions. Significant differences in conidia density of *M. oryzae* on cultivars of varying susceptibility to blast have been reported in rice [10], wheat [46] as well as in other host-pathogen interactions such as the sugar beet–*Cercospora beticola* [37, 47]. Significant differences in the pathogen’s ability to produce conidia on rice genotypes are attributed to the genetic constitution of cultivars [10] and to the interaction between host-pathogen genotypes [41]. Rice genotype Nipponbare infected by *M. oryzae* isolate Guy 11 possessed stable slow-blasting attributes as exhibited by reduced sporulation rate. Thus, by identifying rice genotypes that result in lower fungal sporulation under controlled conditions, breeders can select traits of quantitative disease resistance and develop improved rice varieties with enhanced field - resistance to rice blast.

Sporulation of *M. oryzae* generally occurs under environmental conditions characterized by high RH and leaf wetness [33, 48]. Under such favorable conditions, the pathogen is able to produce an abundance of conidia on rice leaves, reaching hundreds of thousands [1, 6]. Thus, incubation of

susceptible rice plants with typical blast lesions under 100% RH for 2 days combined with alternating periods of darkness and light, lead to the formation of massive mycelium on the surface of leaf blast lesions and the subsequent production of conidiophores with conidia. The mycelium, conidiophores, and conidia collectively contributed to the characteristic grey appearance of sporulating lesions with conidia production typically confined to the central region of blast symptoms as reported in previous studies [49, 50]. The size of this subarea varied among symptoms of a leaf and among rice genotypes [27]. These results suggest that conidia production is spatially restricted and can be influenced by both the size of the grey tissue in the center of leaf blast lesion and the genetic characteristics of the rice plant [32]. Similar observations on *Cercospora beticola* infection of sugar beet have been reported [37].

Mycelial growth of *M. oryzae* is a process essential for both the size of sporulating tissue and the production of conidia, subsequently influencing the patterns and dynamics of disease epidemics [51]. Slow-blasting components such as smaller sporulating lesion areas and low sporulation rate were observed in the interaction between rice genotype Nipponbare and *M. oryzae* isolate Guy 11 as compared to highly compatible interactions, revealing a gene-for-gene specific manner in which minor genes in host genotypes and pathogen isolates operate [19]. Thus, variability in the host-pathogen interactions and genetic diversity among rice plants and pathogen isolates influence the relationship between lesion size and spore production [41, 51]. A substantial increase in blast lesion size on rice leaves within two days of incubation was consistent with observations on *Cercospora* leaf spot on sugar beet [37]. This phenomenon highlights the active mechanisms during fungal colonization, in which the interaction between pathogen and host tissue plays a pivotal role in promoting sporulation. The production of conidia by *M. oryzae* relies on nutrient availability. *M. oryzae* actively exploits the host's resources to fuel its sporulation process, leading to a more extensive and intensified production of conidia [52].

The spectral characterization of green tissue and blast symptom types in this study demonstrated that reflectance spectra of symptom subareas differed from each other in definite regions of the electromagnetic spectrum. Green tissue displayed typical low reflectance in the VIS, a sharp reflectance increase in the red edge inflection point, and a high reflectance plateau in the NIR [27]. Reflectance spectra of healthy leaf tissue of rice genotype CO 39 differed from those of Nipponbare in the VIS and NIR range. The differences in the VIS range may be attributed to differences in pigmentation, e.g., Nipponbare leaves were the greenest and exhibited low reflectance, in contrast to CO 39, which had higher reflectance. Additionally, differences in tissue structure influenced NIR reflectance especially in rice genotypes infected by *M. oryzae* isolate Li1497. The broad and thin leaves of CO 39 were more affected by pathogen colonization than the narrow and thicker leaves of

Nipponbare resulting in a lower NIR reflectance. Different subareas of blast symptoms were associated with changes in reflectance across the full range of the spectrum. The tissue in the center of blast symptoms on rice genotypes CO 39 and Nipponbare at 7 d.p.i. was characterized by an increase in the reflectance over the full range of the spectrum and confirmed an earlier report [27]. On the other hand, the formation of superficial mycelia with conidiophores and conidia on the grey leaf tissue resulted in a reduction of spectral reflectance of this symptom subarea 2 days after the induction of conidiation.

Using separate reference spectra for each image enabled the differentiation of reflectance spectra of the grey tissue before and after sporulation, respectively, across the full spectrum, highlighting distinct spectral characteristics associated with sporulation. Conidia of *M. oryzae* typically develop on conidiophores which usually emerge through stomata but can also breach or directly erupt through the host cuticle from underlying cells of the pathogen [53]. Surface mycelium, conidiophores, and conidia are hyaline and make only a small contribution to the overall spectral reflectance of sporulating lesions. The decreased reflectance of the sporulating leaf area indicates a substantial reduction in the reflectance of the underlying rice tissue due to necrosis and / or tissue damage. The decrease in reflectance is an observable marker for the impact of the pathogen on the host tissue, reflecting the physiological alterations and damage induced during *M. oryzae* colonization of host tissue. In *Cercospora* leaf spot of sugar beet, the sporulation of *C. beticola* reduced the reflectance of lesions over the full range of the spectrum because of the formation of dark- pigmented pseudo stomata and conidiophores [37].

Examining symptom phenotypes may provide valuable insights into the underlying physiology of host-pathogen interactions [54]. The results of SAM classification indicated that the resistant rice genotype IR64 was characterized by small dark brown infection sites without differentiation into distinct zones and colors. The categorization of blast symptoms into different subareas revealed lesions with larger grey centers in highly compatible interactions than in less compatible interactions. Changes in blast symptom composition during the incubation under 100% RH for sporulation resulted from an increase in the size of lesion subareas and a shift from one symptom type to the other. Blast symptoms differ in their spatial and spectral characteristics and the impact of fungal growth and colonization of the leaf tissue during pathogenesis on spectral signatures was correlated with the rate of symptom expansion [27] and as demonstrated here - the production of conidia. However, the spectral differences among rice genotypes made it necessary to use genotype-specific reference spectra of symptom subareas thus limiting the use of general reference spectra (endmembers) in the supervised classification of sporulation structures.

The sporulation of blast lesions is a function of the size of grey tissue in the center of lesions [49] and the limited size of this center is associated with partial resistance to leaf blast [19]. In the present study, the average size of this grey tissue identified and quantified by SAM classification varied between rice genotypes and allowed the assessment of the sporulation area. The area under difference spectrum is a quantitative indicator of the changes in reflectance due to fungal sporulation and characterized genotype CO 39 to be more suitable for *M. oryzae* conidia production than genotype Nipponbare. AUDS values were positively correlated to conidia production per lesion; however, the coefficient of determination was higher for the correlation with conidia production per lesion area. As the exponential equation gave the highest  $R^2$  value, it may be difficult to exactly quantify very high sporulation rates of *M. oryzae* by hyperspectral measurements. However, as the linear relationship had almost the same  $R^2$  value, the spectral difference quantified as AUDS seems to be suitable as a quantitative proxy for fungal spore production and enables an automated assessment of *M. oryzae* sporulation. Moreover, spectral analysis of fungal sporulation was also sensitive enough to characterize differences in the host quality of cultivars and in the aggressiveness of pathogen isolates.

Quantification of *M. oryzae* sporulation on leaf blast symptoms by hyperspectral imaging proved to be challenging, as HSI was not able to differentiate between hyaline mycelium, conidiophore, and conidia. Nonetheless, spectral differences were linked to variations in the number of *M. oryzae* conidia counted under the microscope. It is likely that a rather constant ratio between mycelial mass and number of conidia supports the quantitative assessment of *M. oryzae* sporulation. The coefficient of determination ( $R^2 = 0.625$ ) demonstrates the potential for improvement of the accuracy of automatic assessment of sporulation. Understanding and accounting for variations in the relation between mycelial mass and conidia production are essential for refining the quantification methods of fungal sporulation. The number of conidiophores per unit of area reflects the density of conidia produced by the pathogen, while the area of sporulation indicates the spatial extent of spore production on the leaf surface [20]. Incorporating information from both parameters, the AUDS approach allows for a more precise evaluation of the total number of conidia per blast lesion.

Hyperspectral imaging demonstrated its potential for the quantification of *M. oryzae* sporulation differing among rice genotypes. The high sensitivity of hyperspectral imaging enabled the detection of variation in spectral responses (of grey tissue) during sporulation depending on the rice  $\times$  *M. oryzae* interaction. The integration of an HSI sensor with suitable data processing algorithms offers a more automated approach for the quantification of fungal sporulation. As conidia formation is a crucial step in blast epidemiology, the assessment of the partial resistance factor i.e., sporulation by hyperspectral techniques may improve the phenotyping of crops in breeding for disease resistance.

#### 4.6 References

1. Ebbole DJ. *Magnaporthe* as a model for understanding host-pathogen interactions. *Annu Rev Phytopathol.* 2007;45(1):437–56.
2. Ou S. Rice diseases. In: Rice diseases. 2 nd edition. Commonwealth Mycological Institute Kew, U.K.1985.
3. Dean R, Van Kan JAL, Pretorius ZA, Hammond-Kosack KE, Di Pietro A, Spanu PD, et al. The top 10 fungal pathogens in molecular plant pathology. *Mol Plant Pathol.* 2012;13(4):414–30.
4. Couch BC, Fudal I, Lebrun MH, Tharreau D, Valent B, Van Kim P, et al. Origins of host-specific populations of the blast pathogen *Magnaporthe oryzae* in crop domestication with subsequent expansion of pandemic clones on rice and weeds of rice. *Genetics.* 2005;170:613–30.
5. Yoshida K, Saunders DGO, Mitsuoka C, Natsume S, Kosugi S, Saitoh H, et al. Host specialization of the blast fungus *Magnaporthe oryzae* is associated with dynamic gain and loss of genes linked to transposable elements. *BMC Genomics.* 2016;17:370.
6. Boddy L. Pathogens of autotrophs. The fungi. Academic; 2016. pp. 245–92.
7. Kato H. Rice blast disease. *Pestic Outlook.* 2001;12:23–5.
8. Bonman JM. Durable resistance to rice blast disease - environmental influences. *Euphytica.* 1992;63:115–23.
9. Talbot NJ. On the trail of a cereal killer: exploring the biology of *Magnaporthe grisea*. *Annu Rev Microbiol* 2003;57:177–202.
10. Zaeifi M, Nikkhah MJ, von Tiedemann A, Gohari AM, Aminian H. Disease severity and sporulation potential of *Pyricularia oryzae* in some native rice cultivars in Iran. *Mycol Iran.* 2022;9:41–50.
11. Villareal RL. Some components of slow-blasting resistance in rice. *Phytopathology.* 1981;71:608–11.
12. Miah G, Rafii MY, Ismail MR, Puteh AB, Rahim HA, Asfaliza R, et al. Blast resistance in rice: a review of conventional breeding to molecular approaches. *Mol Biol Rep.* 2013;40:2369–88.
13. Parlevliet JE. Components of resistance that reduce the rate of epidemic development. *Annu Rev Phytopathol.* 1979;17:203–22.
14. Mukherjee A, Mohapatra N, Nayak P. Assessment of partial resistance to rice blast disease. *ORYZA- Int J Rice.* 2018;55:363–82.
15. Mukherjee AK, Mohapatra NK, Nayak P. Identification of slow-blasting rice genotypes through multivariate analysis of disease progress curves. *ARPN J Agric Biol Sci.* 2013;8:125–38.
16. Talukder ZI, Tharreau D, Price AH. Quantitative trait loci analysis suggests that partial resistance to rice blast is mostly determined by race-specific interactions. *New Phytol.* 2004;162:197–209.

17. Vergne E, Grand X, Ballini E, Chalvon V, Saindrenan P, Tharreau D, et al. Preformed expression of defense is a hallmark of partial resistance to rice blast fungal pathogen *Magnaporthe oryzae*. BMC Plant Biol. 2010;10:206.
18. Ou SH. Pathogen variability and host resistance in rice blast disease. Annu Rev Phytopathol. 1980;18:167–87.
19. Roumen EC. Small differential interactions for partial resistance in rice cultivars to virulent isolates of the blast pathogen. Euphytica. 1992;64:143–8.
20. Sakr N. In vitro methodology to assess quantitative resistance in plant-fungus pathosystems. Open Agric J. 2022;17:e187433152210120.
21. Nelson RR. Genetics of horizontal resistance to plant diseases. Annu Rev Phytopathol. 1978;16:359–78.
22. Huang C-M, Liao D, -J., Wu H, -S., Shen W, -C., Chung C. -L. Cyclone-based spore trapping, quantitative real-time polymerase chain reaction and high resolution melting analysis for monitoring airborne inoculum of *Magnaporthe oryzae*. Ann Appl Biol. 2016;169:75–90.
23. Qi L, Jiang Y, Li Z, Ma X, Zheng Z, Wang W. Automatic detection and counting method for spores of rice blast based on micro image processing. Trans Chin Soc Agric Eng. 2015;31:186–93.
24. Xiaolong L, Zhanhong M, Bienvenido F, Feng Q, Haiguang W, Alvarez- Bermejo J, et al. Development of automatic counting system for urediospores of wheat stripe rust based on image processing. Int J Agric Biol Eng. 2017;10:134–43.
25. Wang Y, Mao H, Xu G, Zhang X, Zhang Y. A rapid detection method for fungal spores from greenhouse crops based on CMOS image sensors and diffraction fingerprint feature processing. J Fungi. 2022;8:374.
26. Zhang G, Xu T, Tian Y. Hyperspectral imaging-based classification of rice leaf blast severity over multiple growth stages. Plant Methods. 2022;18:123.
27. Maina AW, Oerke EC. Characterization of rice – *Magnaporthe oryzae* interactions by hyperspectral imaging. Plant Dis. 2023;107:3139–47.
28. Oerke EC, Herzog K, Toepfer R. Hyperspectral phenotyping of the reaction of grapevine genotypes to *Plasmopara viticola*. J Exp Bot. 2016;67:5529–43.
29. Alisaac E, Behmann J, Rathgeb A, Karlovsky P, Dehne HW, Mahlein AK. Assessment of *Fusarium* infection and mycotoxin contamination of wheat kernels and flour using hyperspectral imaging. Toxins. 2019;11:556.
30. Abdulridha J, Ampatzidis Y, Qureshi J, Roberts P. Laboratory and UAV-based identification and classification of tomato yellow leaf curl, bacterial spot, and target spot diseases in tomato utilizing hyperspectral imaging and machine learning. Remote Sens. 2020;12(17):2732.

31. Nguyen C, Sagan V, Maimaitiyiming M, Maimaitijiang M, Bhadra S, Kwasniewski MT. Early detection of plant viral disease using hyperspectral imaging and deep learning. *Sensors*. 2021;21:742.
32. Cruz CD, Valent B. Wheat blast disease: danger on the move. *Trop Plant Pathol*. 2017;42(3):210–22.
33. Shahriar SA, Imtiaz AA, Hossain MB, Husna A, Eaty M, Khatun N. Review: Rice blast disease. *Annu Res Rev Biol*. 2020;50–64.
34. Ustin SL, Jacquemoud S. How the optical properties of leaves modify the absorption and scattering of energy and enhance leaf functionality. In: Cavender-Bares J, Gamon JA, Townsend PA, editors. *Remote sensing of plant biodiversity*. Springer, Cham; 2020. 2020. pp. 349–84.
35. Ren Y, Ye H, Huang W, Ma H, Guo A, Ruan C, et al. A new spectral index for the quantitative identification of yellow rust using fungal spore information. *Big Earth Data*. 2021;5:201–16.
36. Bohnenkamp D, Kuska MT, Mahlein A-K, Behmann J. Hyperspectral signal decomposition and symptom detection of wheat rust disease at the leaf scale using pure fungal spore spectra as reference. *Plant Pathol*. 2019;68:1188–95.
37. Oerke EC, Leucker M, Steiner U. Sensory assessment of *Cercospora beticola* sporulation for phenotyping the partial disease resistance of sugar beet genotypes. *Plant Methods*. 2019;15:133.
38. Hernández I, Gutiérrez S, Ceballos S, Iñíguez R, Barrio I, Tardaguila J. Artificial intelligence and novel sensing technologies for assessing downy mildew in grapevine. *Horticulturae*. 2021;7:103.
39. Zhang X, Song H, Wang Y, Hu L, Wang P, Mao H. Detection of rice fungal spores based on micro-hyperspectral and microfluidic techniques. *Biosensors*. 2023;13:278.
40. Stewart EL, Hagerty CH, Mikaberidze A, Mundt CC, Zhong Z, McDonald BA. An improved method for measuring quantitative resistance to the wheat pathogen *Zymoseptoria tritici* using high-throughput automated image analysis. *Phytopathology*®. 2016;106:782–8.
41. Gallet R, Bonnot F, Milazzo J, Tertois C, Adreit H, Ravigné V, et al. The variety mixture strategy assessed in a G × G experiment with rice and the blast fungus *Magnaporthe oryzae*. *Front Genet*. 2014;4:312.
42. Meier U. Growth stages of mono- and dicotyledonous plants: BBCH Monograph. Verl. Berlin: Blackwell Wiss; 1997.
43. Savitzky Abraham, Golay MJE. Smoothing and differentiation of data by simplified least squares procedures. *Anal Chem*. 1964;36:1627–39.
44. Kruse FA, Heidebrecht KB, Shapiro AT, Barloon PJ, Goetz AFH. The spectral image processing system (SIPS) interactive visualization and analysis of imaging spectrometer data. *Remote Sens Environ*. 1993;44:145–63.

45. Gelfond J, Goros M, Hernandez B, Bokov A. A system for an accountable data analysis process in R. R J. 2018;10:6.
46. Cruz CD, Kiyuna J, Bockus WW, Todd TC, Stack JP, Valent B. *Magnaporthe oryzae* conidia on basal wheat leaves as a potential source of wheat blast inoculum. Plant Pathol. 2015;64:1491–8.
47. Leucker M, Mahlein AK, Steiner U, Oerke EC. Improvement of lesion phenotyping in *Cercospora beticola* –sugar beet interaction by hyperspectral imaging. Phytopathology®. 2016;106(2):177–84.
48. Rajput LS, Sharma T, Madhusudhan P, Sinha P. Effect of temperature on growth and sporulation of rice leaf blast pathogen *Magnaporthe oryzae*. Int J Curr Microbiol Appl Sci. 2017;6:394–401.
49. TeBeest DO, Guerber C, Ditmore M. Rice blast. The plant health instructor. 2007. <https://www.apsnet.org/edcenter/disandpath/fungalasco/pdlessons/Pages/RiceBlast.aspx>. Accessed 3 Aug 2023.
50. Park JY, Jin J, Lee YW, Kang S, Lee YH. Rice blast fungus *Magnaporthe oryzae* infects *Arabidopsis* via a mechanism distinct from that required for the infection of rice. Plant Physiol. 2009;149:474–86.
51. Pinnschmidt H, Bonman J, Kranz J. Lesion development and sporulation of rice blast. J Plant Dis Prot. 1995;102:299–306.
52. Huang P, Cao H, Li Y, Zhu S, Wang J, Wang Q, et al. Melanin promotes spore production in the rice blast fungus *Magnaporthe oryzae*. Front Microbiol. 2022;13:843838.
53. Howard RJ, Valent B. Breaking and entering: host penetration by the fungal rice blast pathogen *Magnaporthe grisea*. Annu Rev Microbiol. 1996;50:491–512.
54. Mutka AM, Bart RS. Image-based phenotyping of plant disease symptoms. Front Plant Sci. 2015;5:734.

## 4.7 Supplementary Material

### Additional file 1

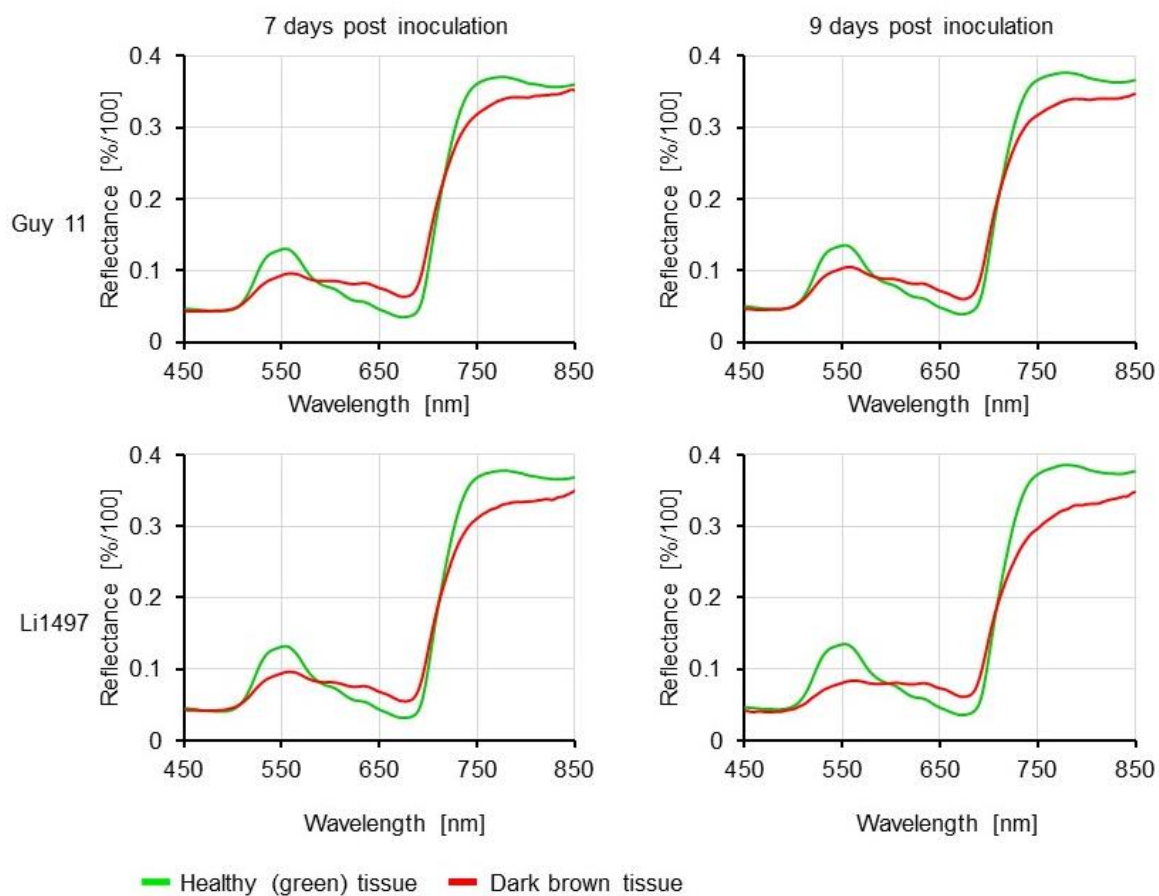


**Fig. A4.1:** Reference spectra of healthy (green) tissue and dark brown spots from leaves of rice genotype IR64 infected with *M. oryzae* isolates Guy 11 and Li1497, respectively. Spectra of green tissue and blast symptom type were extracted before (7 d.p.i.) and 2 days after induction of sporulation (= 9 d.p.i.).

Additional file 2

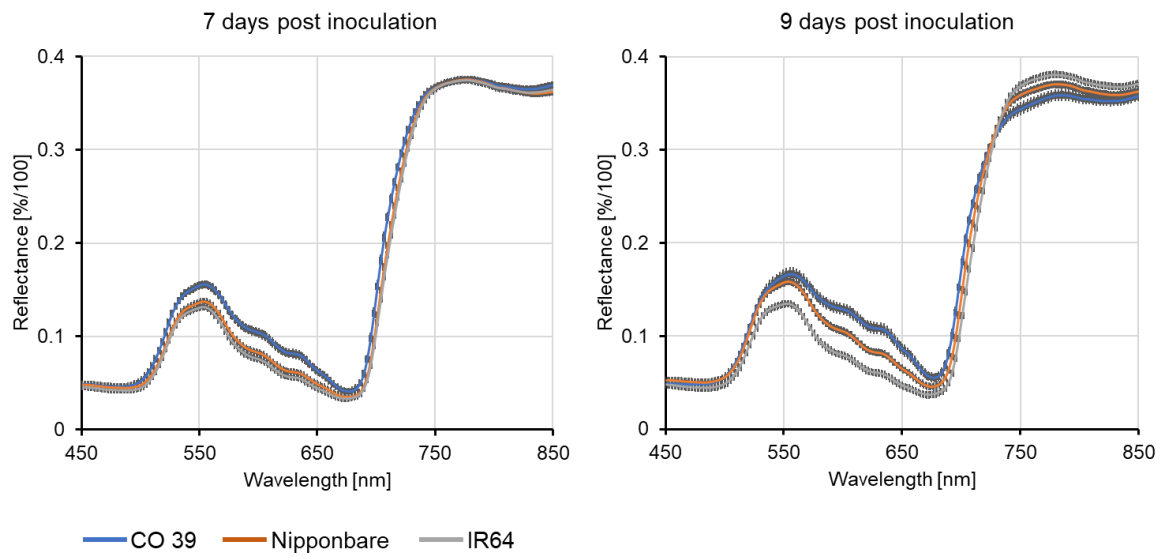


**Fig. A4.2:** Reflectance spectra of healthy (green) tissue of rice genotypes CO 39, Nipponbare and IR64 extracted before (7 d.p.i.) and 2 days after induction of sporulation (= 9 d.p.i.). For each waveband, the bars represent the standard error of the mean (n = 8).

Additional file 3

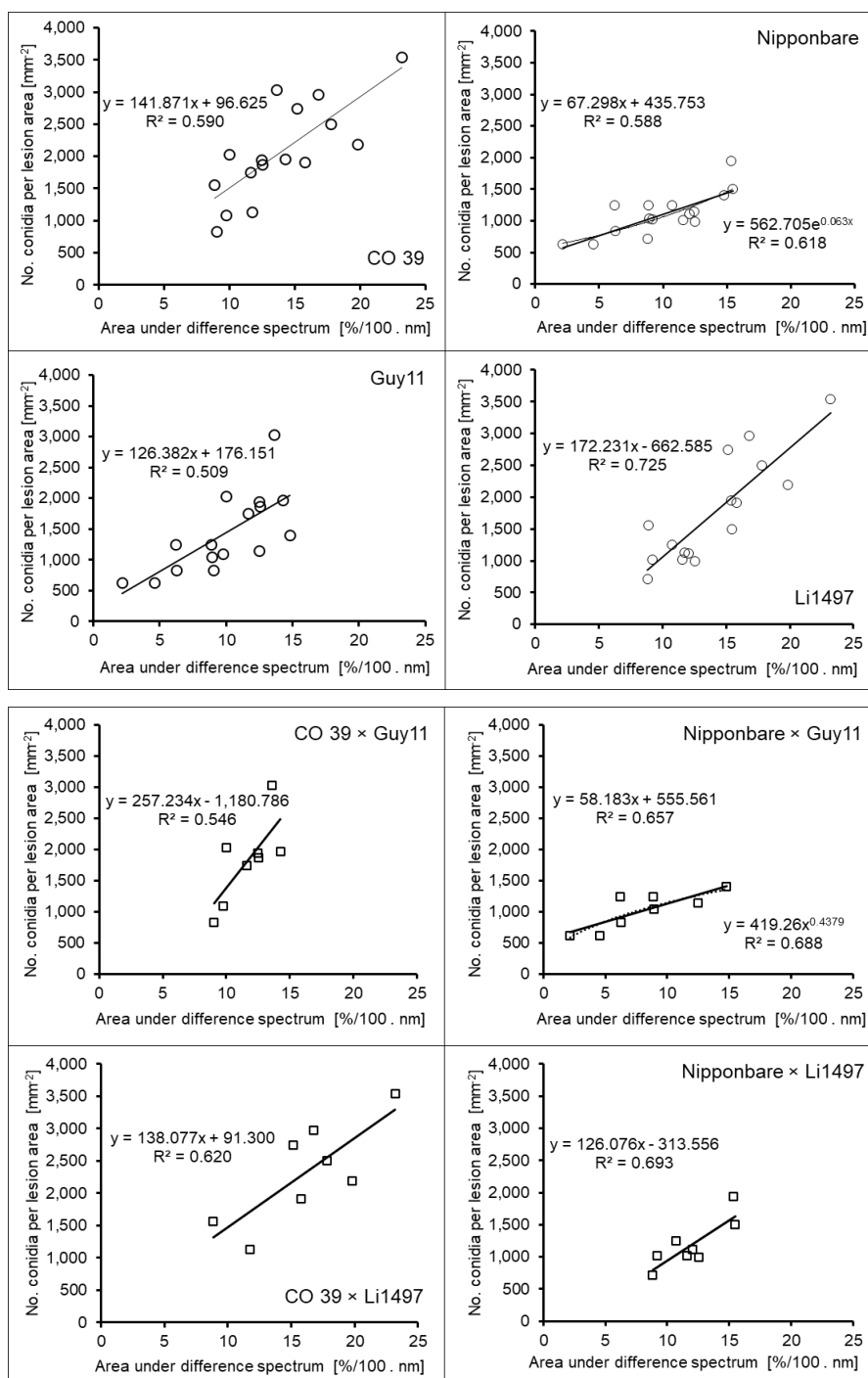


**Fig. A4.3:** Variability in the correlation between spectral data and conidia production by *M. oryzae* depending on the compatibility of the host-pathogen interaction (top two rows individual interactions; bottom two rows interactions depending on host genotype and pathogen genotype). Cv. CO 39 better supported sporulation than cv. Nipponbare; isolate Li1497 was more aggressive than isolate Guy 11.

## 5 General discussion and conclusions

Plant diseases are a major concern in agriculture, as they can significantly affect both the quality and quantity of crop yields, posing a threat to global food production. The key to effective disease assessment and management is an understanding of plant-pathogen interactions, and predisposition of nutritional effects on disease manifestation, and dynamics of disease epidemic. Effective assessment of plant diseases, accurate characterization of resistance reactions, and monitoring of disease occurrences and spread are critical to ensure food production and sustainability (Martinelli et al., 2015).

HSI provides more precise, reproducible, and spatially detailed information on crop plant diseases and nutrient stress in plants. The high-resolution of HSI captures minor changes in plant biochemical and physiological characteristics caused by pathogen attack and disease development (Lowe et al., 2017). The sensitivity of sensors for detecting small disease symptoms is determined by their spatial resolution, which is the minimum size of a pixel or the smallest identifiable symptom (Oerke et al., 2014). A higher spatial resolution allows for the detection of finer details in the observed area, enhancing the sensor's ability to identify and capture small disease symptoms with precision (Lowe et al., 2017). Imaging sensors with a spatial resolution of < 1 mm are well-suited for detection and identification plant diseases (Oerke, 2020). A hyperspectral microscopic approach, offering a high spatial resolution with a pixel size of 7.5  $\mu\text{m}$  and a spectral resolution of 1 nm, enabled the detection of minor spectral changes at both leaf and cellular levels in barley during resistance reactions against powdery mildew (Kuska et al., 2015). The same HSI system has been used successfully to characterize resistance or susceptible reactions of the host to pathogens, which is vital for breeding of disease-resistant plant genotypes (Oerke et al., 2016; Maina and Oerke, 2023). In precision agriculture and crop protection, HSI enables precise site-specific nutritional (Jain et al., 2007) and disease management strategies (West et al., 2010).

In Chapter 2, HSI was used to assess the reactions of five rice genotypes to infection by three *M. oryzae* isolates differing in aggressiveness. Spatial and spectral variability in host-pathogen interactions was observed, with rice genotypes displaying different degrees of susceptibility to *M. oryzae*, resulting in a spectrum of blast phenotypes (Maina and Oerke, 2023). This variability not only manifested within a single leaf but also extended across different rice genotypes, strongly suggesting the presence of gene-for-gene-specific interactions between host and pathogen (Ou, 1980; Maina and Oerke, 2023); a fundamental concept in plant-pathogen interactions that can be further explored and utilized in breeding programs for plant disease resistance. Notably, the variability in lesion manifestation within individual leaves was lower compared to the variations observed among

cultivars. Hubballi et al. (2021) observed differential response of rice genotypes to leaf and neck blast. Different combinations of many resistance genes in the host and many virulence genes in the pathogen combine to produce the observed phenotypic variation in blast symptom occurrence (Ou, 1980; Roumen, 1992).

As a mixture of different infection types highlights the variability in plant tissue reactions to pathogens, thus relying on a single pathogen isolate in disease resistance screening may not be sufficient. In the rice—*M. oryzae* interaction, the reaction type of a host genotype and-pathogen genotype cannot be extrapolated from known H × P interactions because it depends on the highly specific interactions between individual host and pathogen genes. The required high number of pathogen isolates (and H × P interactions to be tested) necessary for an effective screening of new host genotypes makes automation by the use of (imaging) sensors attractive for the selection of resistant genotypes in breeding for disease resistance. The sensor system is objective and available 24/7 and offers a powerful and efficient means to assess thousands of gene-for-gene combinations reliably. The use of HSI is likely to enhance the speed, accuracy, and scale of phenotyping in disease breeding programs.

The high spatial resolution of HSI enabled a detailed assessment of blast symptom subareas on rice leaf surfaces (Maina and Oerke, 2023). The complex and unique patterns of blast symptom types on rice leaves enabled the detection and classification of lesion subareas based on their spectral characteristics across the full range of the spectrum. This high level of detail provides insights into specific host responses and spatial patterns of discrete disease symptoms during the infection (Mutka and Bart, 2014; Zhang et al., 2022). Other studies focused on using the average spectrum to characterize disease symptoms without differentiation into specific subareas. Kuska et al. (2015) used one disease-specific spectrum to characterize disease caused by *Blumeria graminis* f.sp. *hordei* in barley. Bohnenkamp et al. (2021) manually extracted one spectrum per symptom area of individual foliar diseases of wheat. Using the average reflectance spectra of background, infected leaf area, and healthy tissue, Lu et al. (2018) were able to discriminate yellow leaf curl disease in tomato leaves. Metro maps were used to demonstrate disease dynamics as extracted from hyperspectral data, in which the classification of net blotch symptoms on barley leaves (which exhibit high spatial heterogeneity similar to leaf blast symptom) was based on mean archetypal signatures of symptoms at different stages of pathogenesis (Wahabzada et al., 2015).

Spectral signatures of healthy and blast symptom subareas differed, and the spectral characteristics varied as the disease progressed, revealing specific changes in pigments and tissue structure damage caused by pathogen colonization (Maina and Oerke, 2023). The longitudinal data

showed that blast lesions became visible as early as three days post inoculation and disease progression was characterized by an increase in lesion number and size up to seven days (mature symptoms). In contrast to early disease reactions which may be similar and unspecific, reliable disease rating should be done on mature symptoms that provide the most valuable information on compatibility between the host and pathogen. Converse to destructive methods, HSI allows time-series measurements, thus accelerating the characterization of susceptible and resistant plant responses to pathogens (Kuska et al., 2017), and can be valuable for understanding disease resistance dynamics at different stages of pathogenesis.

The complexity of blast symptoms increased with the compatibility of the host-pathogen interaction and the disease stage. The manifestation of leaf blast symptoms during pathogenesis resulted in irregular shape and size of up to 5 tissue types. HSI, specifically utilizing the SAM algorithm, classified and differentiated blast symptoms into subareas of dark brown, grey, chlorotic, grey green, and light brown tissue, allowing for precise mapping of disease symptoms. However, the complex nature of blast symptom complicates the extraction of specific pixel spectra for each subarea. In contrast, Leucker et al. (2016) differentiated lesions on sugar beet genotypes differing in *Cercospora* leaf spot resistance into up to three subareas. The composition of these lesions was linked to the resistance of the genotype, and the margins of the subareas formed a ring-like structure, facilitating the extraction of reflectance spectra. Ashourloo et al. (2014) successfully classified different types of wheat leaf rust symptoms based on their proportions from images taken using an RGB digital camera. In this study, it was apparent that manual labeling of blast symptom subareas was necessary before SAM classification. This time-consuming process is a major drawback in HSI data analysis but an indispensable prerequisite (Kuska et al., 2015). Overcoming this limitation and streamlining the data analysis process will be important for future research.

The sensitivity of HSI permitted the detection of small variations in disease resistance responses that may be missed by visual assessments alone. The ability of HSI to grade the host-pathogen compatibility between rice genotypes and *M. oryzae* isolates is expected to improve phenotyping in breeding programs focused on disease resistance in rice and other crops. The findings in Chapter 2 suggest promising future applications for HSI in plant pathology and plant breeding programs as it can support breeders in selecting the most resistant plant genotypes efficiently. It could support the early detection of diseases and guide timely disease interventions in agricultural practices. However, in practical applications, considerations such as environmental conditions, plant growth stage, 3D crop structure including leaf orientation and shading effects from upper leaf layers, and the timing of disease assessment need attention (Li et al., 2014; Bohnenkamp et al., 2019). In controlled environments like laboratories, it is possible to detect, identify, and quantify plant diseases without

external interferences (Bock et al., 2020). However, in rice-growing fields, especially in flooded areas, rain-fed or irrigated conditions, the use of HSI may face limitations due to challenges in data recording caused by factors such as rainfall, water from irrigation systems, frequent cloud cover, and shadows from other plants. Additionally, for disease control in rice production, the availability of within-season control options (e.g., fungicides) should also be taken into consideration. Nevertheless, utilizing remote sensing to monitor the presence and severity of leaf blast can also serve as a valuable tool for estimating yield losses and assessing rice availability, both at local and regional scales.

One critical factor in rice cultivation is the supply of mineral N, which not only plays a pivotal role in plant growth and development but also has the potential to influence the susceptibility of rice to blast (Huang et al., 2017). An understanding of the relationship between mineral N supply and rice blast is essential for optimizing mineral N application according to crop needs and disease management strategies. In Chapter 3, the influence of mineral N supply on the susceptibility of rice to blast using HSI was investigated. The effect of mineral N application on plant growth, leaf greenness, N content, and spectral reflectance occurred within four days after N application indicating that the N status of plants changed within a short period of time after varying the N supply. The ability of HSI to monitor physiological difference in the N status of rice, suggests that HSI is sensitive enough to detect these small differences within 4 days of mineral N application and could even detect differences in the uptake depending on the cultivar. These responses significantly altered the spectral characteristics of rice leaves, particularly in the VIS and red-edge regions. The sensitivity of HSI allows for quick and precise adjustments in fertilizer application or other interventions to optimize plant growth and yield. It is worth noting that, after recording HSI data, the generated information can be stored for deferred analysis, which may require a considerable amount of time.

Increased mineral N supply resulted in reduced leaf reflectance in the VIS, mainly due to increased chlorophyll content similar to that reported previously (Yao et al., 2015), while the red-edge inflection point (REIP) proved to be a reliable indicator of N supply. Thus, REIP could be used to detect the effect of very small changes in mineral N supply. Likewise, Jain et al. (2007) observed the red edge indices (red edge 750/700 and red edge 740/720) as the most significant in assessing the impact of mineral N rates in potatoes. The difference in reflectance spectra among rice plants at three distinct mineral N rates demonstrates a clear potential for distinguishing between crops subjected to limited N availability from those receiving medium or high mineral N supply (without N overdoses). For two out of three rice genotypes, the effect of mineral N supply on N status and spectral characteristics was more pronounced from low to medium N levels than from medium to high N supply, indicating genotype-specific limitations in N utilization. This suggests that, beyond a certain threshold, additional mineral N may not have much impact on the reflectance spectra of rice leaves.

While increased mineral N availability improved plant performance attributes, high mineral N supply increased rice susceptibility to blast as observed in this study and others (Long et al., 2000; Huang et al., 2017). This could be due to increased N availability for the pathogen as well as amino acid accumulation at the infection site which would all favor the growth of the pathogen (Walters and Bingham, 2007). This increased susceptibility of rice genotypes to blast at high mineral N was manifested by both the increase in number and size of blast symptoms, without the emergence of new lesion types. The impact of mineral N supply on the development of leaf blast symptoms varied among rice—*M. oryzae* interactions, revealing again gene-for-gene-specific interactions. Ballini et al. (2013) observed different types of blast lesions typical of partial resistance on rice leaves under high mineral N supply. High mineral N supply has also been associated with increased susceptibility to *Fusarium* wilt in banana (Orr et al., 2022), while in the spring barley—*Fusarium* head blight (FHB) pathosystem, it has been linked to decreased susceptibility (Hofer et al., 2016). Although not a significant effect, low mineral N supply also increased blast susceptibility in specific rice—*M. oryzae* combinations as discussed in Chapter 3 of this study. Results revealed that some genotypes exhibit better mechanisms to manage nutrient imbalances and pathogen attacks, while others may be more sensitive. Under field conditions, differences in N fertilization may influence the incidence and spread of blast disease not only by direct effects on host plant susceptibility, but also by indirect effects, e.g. panicle density and increased RH within the crop stand (Huang et al., 2017).

The spectral signatures of blast symptom subareas were influenced by rice genotypes, *M. oryzae* isolates, and plant N status. HSI can distinguish incompatible and compatible host-pathogen interactions based on different spectral signatures and spatial patterns (Maina and Oerke, 2023). At the same time, it highlights the dynamics of the high complexity of interactions of plants, pathogens, and nutritional status of plants. The genotype-specific responses to both mineral N application and pathogen infection in rice negate the usefulness of generalizing the effect of mineral N nutrition on disease intensity and symptom expression. It highlights the necessity for tailored approaches to accurately assess and understand these complex interactions. Drawing precise conclusions regarding the exact impact of mineral N on plant-fungal pathogen interactions in the field is, thus, challenging due to the complexity arising from multiple influencing factors, including crop genotype, pathogen genotype, environmental conditions, and cultivation practices.

The differential cultivar response to mineral N indicates that the N status of plant has to be calibrated when using HSI for practical purposes in disease resistance screening within breeding programs and for guiding phytosanitary measures at the field level. The goal should be to provide sufficient mineral N for robust plant growth while avoiding excess N which could promote disease susceptibility. This can be achieved through site-specific and cultivar-specific N management

strategies. Rice plants differ in their greenness and the demand for N / their potential to use N, therefore, exploring how different mineral N application rates affect pathogen infection holds promise for tailored mineral N supply to individual crops using HSI approach.

Plant diseases pose significant threats to crops, and effective mitigation strategies are crucial for agricultural sustainability (Martinelli et al., 2015). Mitigating these diseases involves reducing pathogens' inoculum and use of crop cultivars with genetic diversity for disease resistance. Integrating hyperspectral data into the assessment of pathogens inoculum production could help analyze the spatial (mapping of disease spread), spectral (identification of the disease), and temporal (assess disease progression and patterns over time) dynamics of plant diseases (West et al., 2010; Oerke et al., 2019). Chapter 4 investigated HSI as a non-invasive, non-destructive, and precise method to accurately quantify fungal sporulation, an important component of disease epidemics and partial disease resistance. It focused on how different rice genotypes influence the dynamics of *M. oryzae* sporulation.

Sporulation serves as the initial step in leaf blast epidemic, with conidia playing a crucial role in fungal dissemination, and initiating new infection cycles (Wilson and Talbot, 2009). As a polycyclic disease, the recurring blast infection cycles occur during a growing season between spore germination and production of conidia (Boddy, 2016). The quantity of conidia produced by a pathogen not only determines the inoculum available to infect neighboring plants but also reflects the aggressiveness of the pathogen and the level of host quantitative resistance (Sakr, 2022). The time and amount of sporulation significantly impacts the rate of blast disease development. The conidia are produced in high numbers at night with a single lesion producing over 2000/day (Ebbole, 2007; Boddy, 2016). Decreased spore production is one critical component of quantitative resistance of rice against blast that delays its spread and epidemic development (Villareal et al., 1981). The size of blast lesion influences the quantity of spores produced by *M. oryzae* and contributes to the patterns and dynamics of blast epidemics (Pinnschmidt et al., 1995). However, this relationship may vary because the pathogen sporulates on necrotic tissue unlike in powdery mildew and rust fungi, where the number of spores is directly correlated with the presence of the pathogen (fungal biomass) (Oerke et al., 2019).

The findings of this study revealed that different rice genotypes have distinct effects on fungal colonization and conidia production. The resistant genotype effectively limited fungal colonization resulting in no conidia production. In contrast, susceptible and highly susceptible genotypes enabled rapid fungal colonization and abundant conidia production. In moderately susceptible interaction, slow-blasting components were observed, characterized by smaller sporulating lesion areas and lower sporulation rates. This observation revealed that small differences in the interactions between host

and pathogen genes significantly influence conidia production and subsequent disease spread and severity in the field (Roumen, 1992). This information could be used to develop improved rice varieties with enhanced quantitative resistance to rice blast disease. The influence of environmental conditions (e.g., high RH, alternating period of light and darkness, and leaf wetness) in promoting *M. oryzae* sporulation has been documented (Ebbole, 2007). These conditions influence spatial and temporal changes in plant disease epidemics (West et al., 2010).

HSI provided high spatial and spectral information in the VIS and NIR ranges and detected minor changes associated with fungal conidia production. Previous studies have used HSI data to quantify sporulation by linking spectral changes to conidia production (Oerke et al., 2019; Zhang et al., 2023). In this study, the non-destructive and highly sensitive HSI technique detected spectral modification of the sporulating area (grey tissue), depending on the specific rice–*M. oryzae* interaction. Assessing components of partial resistance e.g., sporulating lesion area and sporulation of pathogens is challenging because they are cumulative and their effects are difficult to separate in the field (Mukherjee et al., 2013). Therefore, combining HSI with supervised classification algorithms to automatically quantify conidia production is a promising approach to assessing the effect of partial resistance on sporulation in controlled environments (Oerke et al., 2019). Formation of hyaline surface mycelium and hyaline conidiophores and conidia is a problem for the quantification of *M. oryzae* sporulation on rice leaves by HSI. In other host-pathogen interactions conidiophores and / or conidia are pigmented and sporulation results in a change of surface color (e.g. *C. beticola* on sugar beet; Oerke et al., 2019).

The SAM algorithm classified different blast symptom subareas - dark brown, grey, grey-green, chlorotic, and light brown tissue without and with sporulation. The size of the grey tissue (associated with sporulation) within blast lesions, as assessed through spectral analysis, varied among rice genotypes, and was restricted to the center of lesions. The magnitude of change in spectral reflectance before and after sporulation was calculated as the area (of grey tissue) under the difference spectrum (AUDS). The method provided information about the spatial distribution of conidia and associated spectral characteristics. A significant and positive correlation was found between AUDS and visual quantification of *M. oryzae* conidia as detailed in Chapter 4. A significant positive correlation between grey surface mycelium (biomass of *M. oryzae*) and the number of conidia produced per lesion area reflects a consistent ratio between the amount of mycelial mass and the number of conidia produced by *M. oryzae* during sporulation. By measuring the mycelial mass, it is possible to predict or estimate the number of conidia produced per lesion area. The ability to distinguish conidia production patterns and dynamics in different rice genotypes is critical to

understanding of host-pathogen interactions, developing effective disease management strategies, and minimizing disease spread.

Different approaches have been used in hyperspectral quantification of fungal sporulation. They include (i) using one representative spectrum per disease symptom without and with sporulation (Oerke et al., 2019), and (ii) using SAM for classification (and quantification) of the sporulating symptom subarea only. In the first method, symptom areas with and without sporulation are manually extracted, and the spectral information for each time of image recording is averaged. The spectral difference of the symptom area before and after sporulation is then calculated as AUDS. This approach does not capture the full range of interactions between the plant and the fungal pathogen. It overlooks spatial variations and localized responses within the leaf associated with conidia production. The second method involves identifying reflectance spectra of different blast symptom subareas without and with sporulation using SAM. The spectra of the symptom subarea where sporulation occurs under favorable environmental conditions (grey tissue; at high RH) are extracted manually, and the AUDS is calculated by computing the spectral differences before and after sporulation. Differences in AUDS characterize differences in the sporulation rate. While this approach is time consuming, it proved essential for understanding the spatial and spectral dynamics of plant-pathogen interactions and dynamics of pathogen reproduction. This approach was used for the first time to assess *M. oryzae* conidia production as an important partial resistance parameter in rice using HSI and depended on the knowledge on the role of the grey tissue of blast lesions for the pathogen's conidia production. The spectral analysis of fungal sporulation was sensitive enough to characterize differences in the host quality of cultivars and in the aggressiveness of pathogen isolates.

The application of HSI in quantifying the sporulation offers a precise approach to advancing crop improvement and may be applied to phenotyping of quantitative resistance of rice to *M. oryzae*. The technique accelerates the development of resistant varieties, increasing the success rate of identifying relevant resistance sources. Precise and rapid identification of rice genotypes with reduced conidia densities by using HSI significantly enhances the efficiency of disease resistance screening within breeding programs. The analysis of spectral changes without and with sporulation allows an understanding of the reproduction of pathogens interacting with different host genotypes. Conidia represents a direct measure of pathogen reproductive output and conidia density represents the epidemic potential of the pathogen on a particular host genotype, thus accurate measurement of conidia production may provide a better indication of a host resistance mechanism (Sakr, 2022). The spatial and spectral data may support decision making for precision agriculture interventions, facilitating site specific responses in disease control. The integration of HSI with advanced data analysis techniques presents a promising avenue for not only mapping of disease spread but also

enabling a more efficient and accurate detection and identification of the presence of fungal pathogens. This integration streamlines the quantification of fungal sporulation aiding in optimization of disease management strategies.

The findings of this study open possibilities for using HSI data for further investigations of disease resistance in the rice—*M. oryzae* pathosystem and other plant-pathogen interactions. To harness the full potential of HSI in plant pathology, it is crucial to optimize specific technical aspects, such as standardized protocols for data extraction, storage, and analysis. One key recommendation is the creation of a comprehensive spectral library encompassing blast symptom types from both resistant and susceptible rice genotypes (representative of the variability of infection types/interaction types) without loss of information. This library will serve as a reference database, facilitating the transferability of spectral information across different rice—*M. oryzae* interactions. In this study, a spectral library was created for each time of image recording and used for classifying disease information of the same image. Despite the time-consuming nature of the approach used in this study, it effectively addressed challenges related to variations in spectral characteristics among different rice genotypes and the different host tissue reactions to pathogen attack and tissue colonization. The use of the recommended generalized spectral library, however, might encounter limitations due to substantial variability in cultivar × isolate interactions. Differences in the spectral reflectance of non-infected leaves among rice genotypes can impact the spectral characteristics of blast symptoms across rice cultivars, complicating the use of a general hyperspectral library for classifying symptom subareas in distinct gene-for-gene interactions. Additionally, differences in the spectral characteristics of blast symptom subareas that look similar when observed with the naked eye limit the application of a generalized hyperspectral library. The risk of too many endmembers in a general spectral library may complicate differentiation among overlapping symptom classes, posing a potential obstacle to accurate classification.

Integrating HSI with microscopy is also essential to understanding spectral reflectance changes that occur at different stages of fungal pathogenesis. Microscopic investigation allows monitoring of pathogen growth during compatible or incompatible interactions between genotypes of rice and *M. oryzae*. Establishing a connection between tissue color (and structure) and the extent of tissue degradation is crucial for comprehensive analysis of leaf blast symptom. The major challenge lies in obtaining detailed information about the different tissue types, encompassing both color and structure, through microscopic observation. This highlights the complexity of studying blast symptoms and emphasizes the need for advanced techniques that can provide a more detailed and accurate characterization of different tissue types that result in a blast symptom. The integrated approach has the potential to significantly advance our understanding of rice blast disease dynamics by offering

valuable insights into the intricate relationships between pathogens and host plants at the microscopic level.

## 6 References

- Abdulridha, J., Batuman, O., and Ampatzidis, Y. (2019). UAV-based remote sensing technique to detect citrus canker disease utilizing hyperspectral imaging and machine learning. *Remote Sensing*, *11*(11), 1373.
- Agrios, G.N. (2005). *Plant Pathology*, 5th edn. San Diego: Academic Press/Elsevier.
- Alisaac, E., Behmann, J., Rathgeb, A., Karlovsky, P., Dehne, H. W., and Mahlein, A. -K. (2019). Assessment of *Fusarium* infection and mycotoxin contamination of wheat kernels and flour using hyperspectral imaging. *Toxins*, *11*, 556.
- Ashkani, S., Rafii, M. Y., Shabanimofrad, M., Miah, G., Sahebi, M., Azizi, P., Tanweer, F. A., Akhtar, M. S., and Nasehi, A. (2015). Molecular breeding strategy and challenges towards improvement of blast disease resistance in rice crop. *Frontiers in Plant Science*, *6*, 886.
- Ashourloo, D., Mobasheri, M.R., and Huete, A. (2014). Developing two spectral disease indices for detection of wheat leaf rust (*Puccinia triticina*). *Remote Sensing*, *6*(6), 4723-4740.
- Ballini, E., Nguyen, T. T. T., and Morel, J. B. (2013). Diversity and genetics of nitrogen-induced susceptibility to the blast fungus in rice and wheat. *Rice*, *6*, 1–13.
- Bock, C. H., Barbedo, J. G., Del Ponte, E. M., Bohnenkamp, D., and Mahlein, A. -K. (2020). From visual estimates to fully automated sensor-based measurements of plant disease severity: status and challenges for improving accuracy. *Phytopathology Research*, *2*(1), 1-30.
- Boddy, L. (2016). Pathogens of autotrophs. Pages 245-292 in: *The Fungi*, 3rd ed. Elsevier Inc, Amsterdam, the Netherlands
- Bohnenkamp, D., Behmann, J., and Mahlein, A.-K. (2019). In-field detection of yellow rust in wheat on the ground canopy and UAV scale. *Remote Sensing*, *11*(21), 2495.
- Bohnenkamp, D., Behmann, J., Paulus, S., Steiner, U., and Mahlein, A.-K. (2021). A hyperspectral library of foliar diseases of wheat. *Phytopathology*, *111*(9), 1583-1593.
- Cheshkova, A.F. (2022). A review of hyperspectral image analysis techniques for plant disease detection and identification. *Vavilov Journal of Genetics and Breeding*, *26*(2), 202-213.
- Couch, B. C., and Kohn, L. M. (2002). A multilocus gene genealogy concordant with host preference indicates segregation of a new species, *Magnaporthe oryzae*, from *M. grisea*. *Mycologia*, *94*(4), 683-693.
- Couch, B. C., Fudal, I., Lebrun, M. H., Tharreau, D., Valent, B., Van Kim, P., Nottéghem, J. L., and Kohn, L. M. (2005). Origins of host-specific populations of the blast pathogen *Magnaporthe oryzae* in crop domestication with subsequent expansion of pandemic clones on rice and weeds of rice. *Genetics*, *170*(2), 613-630.

- Dean, R.A., Talbot, N.J., Ebbole, D.J., Farman, M.L., Mitchell, T.K., Orbach, M.J., Thon, M., Kulkarni, R., Xu, J.R., Pan, H., and Read, N.D. (2005). The genome sequence of the rice blast fungus *Magnaporthe grisea*. *Nature*, 434(7036), 980-986.
- Delalieux, S., Van Aardt, J. A. N., Keulemans, W., Schrevens, E., and Coppin, P. (2007). Detection of biotic stress (*Venturia inaequalis*) in apple trees using hyperspectral data: Non-parametric statistical approaches and physiological implications. *European Journal of Agronomy*, 27(1), 130-143.
- Deng, Y., Ning, Y., Yang, D. L., Zhai, K., Wang, G. L., and He, Z. (2020). Molecular basis of disease resistance and perspectives on breeding strategies for resistance improvement in crops. *Molecular Plant*, 13(10), 1402-1419.
- Dordas, C. (2008). Role of nutrients in controlling plant diseases in sustainable agriculture. A review. *Agronomy for Sustainable Development*, 28, 33-46.
- Ebbole, D. J. (2007). *Magnaporthe* as a model for understanding host-pathogen interactions. *Annual Reviews of Phytopathology*, 45, 437-456.
- Elvanidi, A., Katsoulas, N., Ferentinos, K. P., Bartzanas, T., and Kittas, C. (2018). Hyperspectral machine vision as a tool for water stress severity assessment in soilless tomato crop. *Biosystems Engineering*, 165, 25-35.
- EPPO. (2023). Distribution of *M. oryzae* worldwide. Accessed on 28.11.2023 from <https://gd.eppo.int/taxon/PYRIOR/distribution>.
- FAO. (2023a). Food outlook – Biannual report on global food markets, June 2023. Rome. Accessed 11.12.2023 from <https://www.fao.org/3/cc3020en/cc3020en.pdf>.
- FAO. (2023b). “Rice - Yield (tonnes per hectare)” [dataset]- processed by Our World in Data. Food and Agriculture Organization of the United Nations, “Production: Crops and livestock products” [original data]. Accessed on 25.01.2024 from <https://ourworldindata.org/grapher/rice-yields>.
- Fernandez, J., and Orth, K. (2018). Rise of a cereal killer: The biology of *Magnaporthe oryzae* biotrophic growth. *Trends in Microbiology*, 26(7), 582-597.
- Fukuoka, S., Mizobuchi, R., Saka, N., Ivan, S., Matsumoto, T., Okuno, K., and Yano, M. (2012). A multiple gene complex on rice chromosome 4 is involved in durable resistance to rice blast. *Theoretical and Applied Genetics*, 125, 551-559.
- Fukuoka, S., Yamamoto, S. I., Mizobuchi, R., Yamanouchi, U., Ono, K., Kitazawa, N., Yasuda, N., Fujita, Y., Nguyen, T. T. T., Koizumi, S., Sugimoto, K., Matsumoto, T., and Yano, M. (2014). Multiple functional polymorphisms in a single disease resistance gene in rice enhance durable resistance to blast. *Scientific Reports*, 4(1), 4550.

- Gallet, R., Bonnot, F., Milazzo, J., Tertois, C., Adreit, H., Ravigné, V., Tharreau, D., and Fournier, E. (2014). The variety mixture strategy assessed in a G × G experiment with rice and the blast fungus *Magnaporthe oryzae*. *Frontiers in Genetics*, *4*, 312.
- Girouard, G., Bannari, A., El Harti, A., and Desrochers, A. (2004). Validated spectral angle mapper algorithm for geological mapping: comparative study between QuickBird and Landsat-TM. In *XXth ISPRS Congress, Geo-imagery Bridging Continents* (Vol. 12, pp. 23) Istanbul, Turkey.
- Gitelson, A. A., Kaufman, Y. J., Stark, R., and Rundquist, D. (2002). Novel algorithms for remote estimation of vegetation fraction. *Remote Sensing of Environment*, *80*(1), 76-87.
- Gold, K. M. (2021). Plant disease sensing: studying plant-pathogen interactions at scale. *Msystems*, *6*(6), e01228-21.
- Greer, C. A., and Webster, R. K. (2001). Occurrence, distribution, epidemiology, cultivar reaction, and management of rice blast disease in California. *Plant Disease*, *85*, 1096-1102.
- Hofer, K., Barmeier, G., Schmidhalter, U., Habler, K., Rychlik, M., Hückelhoven, R., and Hess, M. (2016). Effect of nitrogen fertilization on *Fusarium* head blight in spring barley. *Crop Protection*, *88*, 18-27.
- Hoffland, E., Jeger, M.J., and van Beusichem, M.L. (2000). Effect of nitrogen supply rate on disease resistance in tomato depends on the pathogen. *Plant and Soil*, *218*, 239-247.
- Huang, H., Nguyen Thi Thu, T., He, X., Gravot, A., Bernillon, S., Ballini, E., and Morel, J. B. (2017). Increase of fungal pathogenicity and role of plant glutamine in nitrogen-induced susceptibility (NIS) to rice blast. *Frontiers in Plant Science*, *8*, 265.
- Hubballi, M., Pandey, A. K., and Giriappa, R. (2022). Genetic variation of infection degrees to blast disease among rice genotypes. *Journal of Phytopathology*, *170*(2), 107-123.
- IRRI (2013). Standard Evaluation system for rice. International Rice Research Institute, Manila. Accessed on 28.11.2023 from <https://ricepedia.blogspot.com/2018/04/2013-irri-ses-standard-evaluation.html>.
- Jain, N., Ray, S. S., Singh, J. P., and Panigrahy, S. (2007). Use of hyperspectral data to assess the effects of different nitrogen applications on a potato crop. *Precision Agriculture*, *8*, 225-239.
- Jain, P., Singh, P.K., Kapoor, R., Khanna, A., Solanke, A.U., Krishnan, S.G., Singh, A.K., Sharma, V., and Sharma, T.R. (2017). Understanding host-pathogen interactions with expression profiling of NILs carrying rice-blast resistance Pi9 gene. *Frontiers in Plant Science*, *8*, 93.
- Jalalifar, R., Sabouri, A., Mousanejad, S., and Dadras, A.R. (2023). Estimation of genetic parameters and identification of leaf blast-resistant rice RILs using cluster analysis and MGIDI. *Agronomy*, *13*(11), 2730.

- Jones, K., Zhu, J., Jenkinson, C.B., Kim, D.W., Pfeifer, M.A., and Khang, C.H. (2021). Disruption of the interfacial membrane leads to *Magnaporthe oryzae* effector re-location and lifestyle switch during rice blast disease. *Frontiers in Cell and Developmental Biology*, *9*, 681734.
- Kankanala, P., Czymmek, K., and Valent, B. (2007). Roles for rice membrane dynamics and plasmodesmata during biotrophic invasion by the blast fungus. *The Plant Cell*, *19*(2), 706-724.
- Khush, G. S., and Jena, K. (2009). Current status and future prospects for research on blast resistance in rice (*Oryza sativa* L.). In: Wang, G.L., Valent, B. (eds) *Advances in Genetics, Genomics and Control of Rice Blast Disease*. Springer, Dordrecht, pp.1-10.
- Kihoro, J., Bosco, N.J., Murage, H., Ateka, E., and Makihara, D. (2013). Investigating the impact of rice blast disease on the livelihood of the local farmers in greater Mwea region of Kenya. *Springerplus*, *2*, 1-13.
- Krupinsky, J.M., Halvorson, A.D., Tanaka, D.L., and Merrill, S.D. (2007). Nitrogen and tillage effects on wheat leaf spot diseases in the northern great plains. *Agronomy Journal*, *99*(2), 562-569.
- Kruse, F. A., Lefkoff, A. B., Boardman, J. W., Heidebrecht, K. B., Shapiro, A. T., Barloon, P. J., and Goetz, H. A. F. (1993). The spectral image processing system (SIPS)—interactive visualization and analysis of imaging spectrometer data. *Remote Sensing of Environment*, *44*(2-3), 145-163.
- Kuching, S. (2007). The performance of maximum likelihood, spectral angle mapper, neural network and decision tree classifiers in hyperspectral image analysis. *Journal of Computer Science*, *3*(6), 419-423.
- Kuska, M. T., Brugger, A., Thomas, S., Wahabzada, M., Kersting, K., Oerke, E. -C., Steiner, U., and Mahlein, A. -K. (2017). Spectral patterns reveal early resistance reactions of barley against *Blumeria graminis* f. sp. *hordei*. *Phytopathology*, *107*(11), 1388-1398.
- Kuska, M., Wahabzada, M., Leucker, M., Dehne, H. W., Kersting, K., Oerke, E. -C., Steiner, U., and Mahlein, A. -K. (2015). Hyperspectral phenotyping on the microscopic scale: towards automated characterization of plant-pathogen interactions. *Plant Methods*, *11*, 1-15.
- Lecompte, F., Abro, M.A., and Nicot, P.C. (2010). Contrasted responses of *Botrytis cinerea* isolates developing on tomato plants grown under different nitrogen nutrition regimes. *Plant Pathology*, *59*(5), 891-899.
- Leucker, M., Mahlein, A.-K., Steiner, U., and Oerke, E.-C. (2016). Improvement of lesion phenotyping in *Cercospora beticola*–sugar beet interaction by hyperspectral imaging. *Phytopathology*, *106*(2), 177-184.
- Li, L., Zhang, Q., and Huang, D. (2014). A review of imaging techniques for plant phenotyping. *Sensors*, *14*(11), 20078-20111.

- Li, X., Li, R., Wang, M., Liu, Y., Zhang, B. and Zhou, J. (2018). Hyperspectral imaging and their applications in the nondestructive quality assessment of fruits and vegetables. In *Hyperspectral Imaging in Agriculture, Food and Environment*. IntechOpen. pp.27-63.
- Liu, Z.Y., Wu, H.F., and Huang, J.F. (2010). Application of neural networks to discriminate fungal infection levels in rice panicles using hyperspectral reflectance and principal components analysis. *Computers and Electronics in Agriculture*, 72(2), 99-106.
- Long, D. H., Lee, F. N., and TeBeest, D. O. (2000). Effect of nitrogen fertilization on disease progress of rice blast on susceptible and resistant cultivars. *Plant Disease*, 84(4), 403-409.
- Lowe, A., Harrison, N., and French, A. P. (2017). Hyperspectral image analysis techniques for the detection and classification of the early onset of plant disease and stress. *Plant Methods*, 13, 80.
- Lu, J. Z., Zhou, M. C., Gao, Y. W., and Jiang, H. Y. (2018). Using hyperspectral imaging to discriminate yellow leaf curl disease in tomato leaves. *Precision Agriculture*, 19, 379-394.
- Luc, B., Deronde, B., Kempeneers, P., Debruyne, W., and Provoost, S. (2005). Optimized spectral angle mapper classification of spatially heterogeneous dynamic dune vegetation, a case study along the Belgian coastline. In *The 9th International Symposium on Physical Measurements and Signatures in Remote Sensing* (Vol. 1, No. 2). ISPMRS. Beijing.
- Mahlein, A. -K., Kuska, M. T., Thomas, S., Wahabzada, M., Behmann, J., Rascher, U., and Kersting, K. (2019). Quantitative and qualitative phenotyping of disease resistance of crops by hyperspectral sensors: seamless interlocking of phytopathology, sensors, and machine learning is needed! *Current Opinion in Plant Biology*, 50, 156-162.
- Mahlein, A. -K., Steiner, U., Hillnhütter, C., Dehne, H. -W., and Oerke, E. -C. (2012). Hyperspectral imaging for small-scale analysis of symptoms caused by different sugar beet diseases. *Plant Methods*, 8, 3-13.
- Mahlein, A.-K. (2016). Plant disease detection by imaging sensors—parallels and specific demands for precision agriculture and plant phenotyping. *Plant Disease*, 100(2), 241-251.
- Mahlein, A.-K., Rumpf, T., Welke, P., Dehne, H.W., Plümer, L., Steiner, U., and Oerke, E.C. (2013). Development of spectral indices for detecting and identifying plant diseases. *Remote Sensing of Environment*, 128, 21-30.
- Maina, A. W., and Oerke, E. -C. (2023). Characterization of rice – *Magnaporthe oryzae* interactions by hyperspectral imaging. *Plant Disease*, 107(10), 3139-3147.
- Marcel, T.C., Gorguet, B., Ta, M.T., Kohutova, Z., Vels, A., and Niks, R.E. (2008). Isolate specificity of quantitative trait loci for partial resistance of barley to *Puccinia hordei* confirmed in mapping populations and near-isogenic lines. *New Phytologist*, 177(3), 743-755.

- Martinelli, F., Scalenghe, R., Davino, S., Panno, S., Scuderi, G., Ruisi, P., Villa, P., Stroppiana, D., Boschetti, M., Goulart, L. R., and Davis, C. E. (2015). Advanced methods of plant disease detection. A review. *Agronomy for Sustainable Development*, 35, 1-25.
- Martin-Urdiroz, M., Oses-Ruiz, M., Ryder, L. S., and Talbot, N. J. (2016). Investigating the biology of plant infection by the rice blast fungus *Magnaporthe oryzae*. *Fungal Genetics and Biology*, 90, 61-68.
- Maywald, N. J., Francioli, D., Mang, M., and Ludewig, U. (2023). Role of mineral nitrogen nutrition in fungal plant diseases of cereal crops. *Critical Reviews in Plant Sciences*, 42(3), 93-123.
- Mewes, T., Franke, J., and Menz, G. (2011). Spectral requirements on airborne hyperspectral remote sensing data for wheat disease detection. *Precision Agriculture*, 12, 795-812.
- Mishra, P., Asaari, M. S. M., Herrero-Langreo, A., Lohumi, S., Diezma, B., and Scheunders, P. (2017). Close range hyperspectral imaging of plants: A review. *Biosystems Engineering*, 164, 49-67.
- Mukherjee, A. K., Mohapatra, N. K., and Nayak, P. (2013). Identification of slow-blasting rice genotypes through multivariate analysis of components of resistance. *Journal of Agricultural and Biological Science*, 8(2), 125-138.
- Mundt, C. C. (2014). Durable resistance: A key to sustainable management of pathogens and pests. *Infection, Genetics and Evolution*, 27, 446-455.
- Mutka, A. M., and Bart, R. S. (2015). Image-based phenotyping of plant disease symptoms. *Frontiers in Plant Science*, 5, 734.
- Nalley, L., Tsiboe, F., Durand-Morat, A., Shew, A. and Thoma, G. (2016). Economic and environmental impact of rice blast pathogen (*Magnaporthe oryzae*) alleviation in the United States. *PloS One*, 11(12), e0167295.
- Nelson, R., Wiesner-Hanks, T., Wisser, R., and Balint-Kurti, P. (2018). Navigating complexity to breed disease-resistant crops. *Nature Reviews Genetics*, 19(1), 21-33.
- Nutsugah, S.K., Dogbe, W., Twumasi, J.K., Dartey, K., Chipili, J., Sreenivasaprasad, S., and Séré, Y. (2005). Prevalence of rice blast and varietal screening in Ghana. *Journal of Science and Technology*, 25(2), 18-34.
- Oerke, E. -C. (2020). Remote sensing of diseases. *Annual Review of Phytopathology*, 58, 225-252.
- Oerke, E. -C., and Dehne, H. W. (2004). Safeguarding production — losses in major crops and the role of crop protection. *Crop Protection*, 23(4), 275-285.
- Oerke, E. -C., Herzog, K., and Toepfer, R. (2016). Hyperspectral phenotyping of the reaction of grapevine genotypes to *Plasmopara viticola*. *Journal of Experimental Botany*, 67, 5529-5543.

- Oerke, E. -C., Leucker, M., and Steiner, U. (2019). Sensory assessment of *Cercospora beticola* sporulation for phenotyping the partial disease resistance of sugar beet genotypes. *Plant Methods*, 15(1), 1-12.
- Oerke, E.-C., Mahlein, A.-K., and Steiner, U. (2014). Proximal sensing of plant diseases. *Detection and Diagnostics of Plant Pathogens*, pp.55-68.
- Orbach, M.J., Farrall, L., Sweigard, J.A., Chumley, F.G., and Valent B. (2000). A telomeric avirulence gene determines efficacy for the rice blast resistance gene *Pi-ta*. *Plant Cell*, 12, 2019–2032.
- Orr, R., Dennis, P.G., Wong, Y., Browne, D.J., Cooper, M., Birt, H.W., Lapis-Gaza, H.R., Pattison, A.B., and Nelson, P.N. (2022). Nitrogen fertilizer rate but not form affects the severity of *Fusarium* wilt in banana. *Frontiers in Plant Science*, 13, 907819.
- Ou, S. H. (1980). Pathogen variability and host resistance in rice blast disease. *Annual Review of Phytopathology*, 18,167-187.
- Ou, S. H. (1985). Rice diseases, 2nd ed. Commonwealth Mycological Institute, Kew, U.K.
- Paulus, S., and Mahlein, A.-K. (2020). Technical workflows for hyperspectral plant image assessment and processing on the greenhouse and laboratory scale. *GigaScience*, 9(8), p.giaa090.
- Pérez-Roncal, C., López-Maestresalas, A., Lopez-Molina, C., Jarén, C., Urrestarazu, J., Santesteban, L.G., and Arazuri, S. (2020). Hyperspectral imaging to assess the presence of powdery mildew (*Erysiphe necator*) in cv. Carignan Noir grapevine bunches. *Agronomy*, 10(1), 88.
- Pinnschmidt, H.O., Bonman, J.M., and Kranz, J. (1995) Lesion development and sporulation of rice blast. *Journal of Plant Diseases and Protection*, pp. 299-306
- Pu, H., Lin, L., and Sun, D.W. (2019). Principles of hyperspectral microscope imaging techniques and their applications in food quality and safety detection: A review. *Comprehensive Reviews in Food Science and Food Safety*, 18(4), 853-866.
- Rachel, R. (2022). Prevalence of rice blast disease in various countries. *Journal of Plant Pathology and Microbiology*, 13, 645.
- Rant, J.C., Arraiano, L.S., Chabannes, M., and Brown, J.K. (2013). Quantitative trait loci for partial resistance to *Pseudomonas syringae* pv. *maculicola* in *Arabidopsis thaliana*. *Molecular Plant Pathology*, 14(8), 828-837.
- Roman, A., and Ursu, T. (2016). Multispectral satellite imagery and airborne laser scanning techniques for the detection of archaeological vegetation marks. *Landscape archaeology on the northern frontier of the Roman Empire at Porolissum: an interdisciplinary research project*. Cluj-Napoca: Mega Publishing House, pp.141-152.
- Roumen, E. C. (1992). Small differential interactions for partial resistance in rice cultivars to virulent isolates of the blast pathogen. *Euphytica*, 64, 143-148.

- Ryder, L.S., and Talbot, N.J. (2015). Regulation of appressorium development in pathogenic fungi. *Current Opinion in Plant Biology*, 26, 8-13.
- Sakr, N. (2022). Methodology to assess quantitative resistance in plant-fungus pathosystems. *The Open Agriculture Journal*, 17(1).
- Saleh, D., Xu, P., Shen, Y., Li, C., Adreit, H., Milazzo, J., Ravigné, V., Bazin, E., Nottéghem, J.L., Fournier, E., and Tharreau, D. (2012). Sex at the origin: an Asian population of the rice blast fungus *Magnaporthe oryzae* reproduces sexually. *Molecular Ecology*, 21(6), 1330-1344.
- Savitzky, A., and Golay, M.J. (1964). Smoothing and differentiation of data by simplified least squares procedures. *Analytical Chemistry*, 36(8), 1627-1639.
- Séré, Y., Sy, A.A., Sie, M., Akator, S.K., Onasanya, A., Kabore, B., Conde, C.K., Traore, M., and Kiepe, P. (2011). Importance of varietal improvement for blast disease control in Africa. *JIRCAS Working Report*, 70, 77-90.
- Sharma, T. R., Rai, A. K., Gupta, S. K., Vijayan, J., Devanna, B. N., and Ray S. (2012). Rice blast management through host-plant resistance: retrospect and prospects. *Agricultural Research*, 1, 37-52.
- Shoaib, M., Shah, B., Ei-Sappagh, S., Ali, A., Ullah, A., Alenezi, F., Gechev, T., Hussain, T., and Ali, F. (2023). An advanced deep learning models-based plant disease detection: A review of recent research. *Frontiers in Plant Science*, 14, 1158933.
- Sims, D. A., and Gamon, J. A. (2002). Relationships between leaf pigment content and spectral reflectance across a wide range of species, leaf structures and developmental stages. *Remote Sensing of Environment*, 81(2-3), 337-354.
- Skamnioti, P., and Gurr, S.J. (2007). *Magnaporthe grisea* cutinase2 mediates appressorium differentiation and host penetration and is required for full virulence. *The Plant Cell*, 19(8), 2674-2689.
- Sun, Y., Wang, M., Mur, L. A. J., Shen, Q., and Guo, S. (2020). Unraveling the roles of nitrogen nutrition in plant disease defenses. *International Journal of Molecular Sciences*, 21, 572.
- Talbot N. J. (2003). On the trail of a cereal killer: Exploring the biology of *Magnaporthe grisea*. *Annual Review of Phytopathology*, 57, 177-202.
- Talbot, N. J., Ebbole, D. J., and Hamer, J. E. (1993). Identification and characterization of *MPG1*, a gene involved in pathogenicity from the rice blast fungus *Magnaporthe grisea*. *Plant Cell*, 5, 1575-1590.
- Talukder, Z. I., McDonald, A. J., and Price, A. H. (2005). Loci controlling partial resistance to rice blast do not show marked QTL x environment interaction when plant nitrogen status alters disease severity. *New Phytologist*, 168(2), 455-464.

- Talukder, Z. I., Tharreau, D., and Price, A. H. (2004). Quantitative trait loci analysis suggests that partial resistance to rice blast is mostly determined by race-specific interactions. *New Phytologist*, *162*(1), 197-209.
- Tanner, F., Tonn, S., de Wit, J., Van den Ackerveken, G., Berger, B., and Plett, D. (2022). Sensor-based phenotyping of above-ground plant-pathogen interactions. *Plant Methods*, *18*(1), 35.
- TeBeest, D.O., Guerber, C., and Dittmore, M. (2007). Rice blast. The plant health instructor. Accessed 3.08.2023 from <https://www.apsnet.org/edcenter/disandpath/fungalasco/pdlessons/Pages/RiceBlast.aspx>
- Tharreau, D., Fudal, I., Andriantsimialona, D., Santoso, Utami, D., Fournier, E., Lebrun, M.H., and Nottéghem, J.L. (2009). World population structure and migration of the rice blast fungus, *Magnaporthe oryzae*. In *Advances in Genetics, Genomics and Control of Rice Blast Disease* (pp. 209-215). Springer Netherlands.
- Thomas, S., Kuska, M.T., Bohnenkamp, D., Brugger, A., Alisaac, E., Wahabzada, M., Behmann, J., and Mahlein, A.-K. (2018). Benefits of hyperspectral imaging for plant disease detection and plant protection: a technical perspective. *Journal of Plant Diseases and Protection*, *125*, 5-20.
- USDA. (2023). Rice Outlook. Economic research service | Situation and Outlook. Accessed on 14.1.2024 from <https://www.ers.usda.gov/webdocs/outlooks/108111/rcs-23k.pdf?v=8696.8>.
- Ustin, S. L., and Jacquemoud, S. (2020). How the optical properties of leaves modify the absorption and scattering of energy and enhance leaf functionality. *Remote Sensing of Plant Biodiversity*, pp. 349-384.
- Valent, B. (2021). The impact of blast disease: past, present, and future. In: Jacob, S. (eds) *Magnaporthe oryzae. Methods in Molecular Biology*, 2356, 1-18. Humana, New York, NY.
- Villareal, R.L., Nelson, R.R., MacKenzie, D.R., and Coffman, W.R. (1981). Some components of slow-blasting resistance in rice. *Phytopathology*, *71*(6), 608-611.
- Wahabzada, M., Mahlein, A.-K., Bauckhage, C., Steiner, U., Oerke, E.-C., and Kersting, K. (2015). Metro maps of plant disease dynamics—automated mining of differences using hyperspectral images. *Plos one*, *10*(1), p.e0116902.
- Walters, D. R., and Bingham, I. J. (2007). Influence of nutrition on disease development caused by fungal pathogens: implications for plant disease control. *Annals of Applied Biology*, *151*, 307-324.
- Wang, X., Lee, S., Wang, J., Ma, J., Bianco, T., and Jia, Y. (2014). Current advances on genetic resistance to rice blast disease. *Rice-Germplasm, Genetics and Improvement*, pp.195-217.
- West, S. J., Bravo, C., Oberti, R., Moshou, D., Ramon, H., and McCartney, H. A. (2010). Detection of fungal diseases optically and pathogen inoculum by air sampling. In: E.-C. Oerke, R. Gerhards,

- G. Menz and R.A. Sikora, eds., *Precision Crop Protection – The Challenge and Use of Heterogeneity*. Springer, Dordrecht, Netherlands, pp. 135-149.
- Whetton, R.L., Waive, T.W., and Mouazen, A.M. (2018). Hyperspectral measurements of yellow rust and *Fusarium* head blight in cereal crops: Part 2: On-line field measurement. *Biosystems Engineering*, 167, 144-158.
- Wilson, R. A., and Talbot, N. J. (2009). Under pressure: investigating the biology of plant infection by *Magnaporthe oryzae*. *Nature Reviews Microbiology*, 7, 185-195.
- Wu, J., Kou, Y., Bao, J., Li, Y., Tang, M., Zhu, X., Ponaya, A., Xiao, G., Li, J., Li, C., and Song, M.Y. (2015). Comparative genomics identifies the *Magnaporthe oryzae* avirulence effector *AvrPi9* that triggers *Pi9*-mediated blast resistance in rice. *New Phytologist*, 206(4), 1463-1475.
- Yao, X., Huang, Y., Shang, G., Zhou, C., Cheng, T., Tian, Y., Cao, W., and Zhu, Y. (2015). Evaluation of six algorithms to monitor wheat leaf nitrogen concentration. *Remote Sensing*, 7(11), 14939-14966.
- Yoshida, K., Saitoh, H., Fujisawa, S., Kanzaki, H., Matsumura, H., Yoshida, K., Tosa, Y., Chuma, I., Takano, Y., Win, J., and Kamoun, S. (2009). Association genetics reveals three novel avirulence genes from the rice blast fungal pathogen *Magnaporthe oryzae*. *The Plant Cell*, 21(5), 1573-1591.
- Younas, M. U., Wang, G., Du, H., Zhang, Y., Ahmad, I., Rajput, N., Li, M., Feng, Z., Hu, K., Khan, N. U., and Xie, W. (2023). Approaches to reduce rice blast disease using knowledge from host resistance and pathogen pathogenicity. *International Journal of Molecular Sciences*, 24(5), 4985.
- Zhang, G., Xu, T., and Tian, Y. (2022). Hyperspectral imaging-based classification of rice leaf blast severity over multiple growth stages. *Plant Methods*, 18(1), 123.
- Zhang, J. H., and Guo, W. J. (2006). Quantitative retrieval of crop water content under different soil moisture levels. *Agriculture and Hydrology Applications of Remote Sensing SPIE*, 6411, 85-93
- Zhang, J.C., Pu, R.L., Wang, J.H., Huang, W.J., Yuan, L., and Luo, J.H. (2012). Detecting powdery mildew of winter wheat using leaf level hyperspectral measurements. *Computers and Electronics in Agriculture*, 85, 13-23.
- Zhang, N., Yang, G., Pan, Y., Yang, X., Chen, L., and Zhao, C. (2020). A review of advanced technologies and development for hyperspectral-based plant disease detection in the past three decades. *Remote Sensing*, 12(19), 3188.
- Zhang, X., Song, H., Wang, Y., Hu, L., Wang, P., and Mao, H. (2023). Detection of rice fungal spores based on micro-hyperspectral and microfluidic techniques. *Biosensors*, 13(2), 278.

- Zhao, Y. R., Li, X., Yu, K. Q., Cheng, F., and He, Y. (2016). Hyperspectral imaging for determining pigment contents in cucumber leaves in response to angular leaf spot disease. *Scientific Reports*, *6*, 1-9.
- Zheng, Z., Qi, L., Ma, X., Zhu, X., and Wang, W. (2013). Grading method of rice leaf blast using hyperspectral imaging technology. *Transactions of the Chinese Society of Agricultural Engineering*, *29*, 138-144.
- Zhou, J., Yang, Y., Lv, Y., Pu, Q., Li, J., Zhang, Y., Deng, X., Wang, M., Wang, J., and Tao, D. (2022). Interspecific hybridization is an important driving force for origin and diversification of Asian cultivated rice *Oryza sativa* L. *Frontiers in Plant Science*, *13*, 932737.